UNIVERSIDADE ESTADUAL PAULISTA
"JÚLIO DE MESQUITA FILHO"
Câmpus de São José do Rio Preto

Daiane Bortolote Ferreira

Development of technological alternatives for drying and spore extraction of *Metarhizium anisopliae* in biofactories using Solid-State Cultivation on rice

São José do Rio Preto
2025

Daiane Bortolote Ferreira

Development of technological alternatives for drying and spore extraction of Metarhizium anisopliae in biofactories using Solid-State Cultivation on rice

Tese apresentada ao Programa de Pós-Graduação em Alimentos, Nutrição e Engenharia de Alimentos como parte das exigências para a obtenção do título de Doutor em Engenharia e Ciência de Alimentos pelo Instituto de Biociências, Letras e Ciências Exatas, Universidade Estadual Paulista (UNESP), Campus de São José do Rio Preto.

Área de Concentração: Engenharia de Alimentos

Orientador: Prof. Dr. João Cláudio Thoméo

São José do Rio Preto
2025

F383d

Ferreira, Daiane Bortolote

Development of technological alternatives for drying and spore extraction of Metarhizium anisopliae in biofactories using Solid-State Cultivation on rice / Daiane Bortolote Ferreira. -- São José do Rio Preto, 2025

198 p. : il., tabs., fotos

Tese (doutorado) - Universidade Estadual Paulista (UNESP), Instituto de Biociências Letras e Ciências Exatas, São José do Rio Preto

Orientador: João Cláudio Thoméo

1. Tambor. 2. Transferência de massa. 3. Metarhizium anisopliae. 4. Extração. 5. Método de elementos discretos. I. Título.

Sistema de geração automática de fichas catalográficas da Unesp. Dados fornecidos pelo autor(a).

DAIANE BORTOLOTE FERREIRA

Development of technological alternatives for drying and spore extraction of *Metarhizium anisopliae* in biofactories using Solid-State Cultivation on rice

Tese apresentada ao Instituto de Biociências, Letras e Ciências Exatas da Universidade Estadual Paulista "Júlio de Mesquita Filho" para obtenção do título de Doutor em Engenharia e Ciência de Alimentos pelo Programa de Pós-Graduação em Alimentos, Nutrição e Engenharia de Alimentos.

Área de Concentração: Engenharia de Alimentos

Data da defesa: 11/03/2025

Banca Examinadora/Examining Board

Prof. Dr. João Cláudio Thoméo
UNESP - Câmpus de São José do Rio Preto

Profa. Dra. Beatriz Vahan Kilikian
Universidade de São Paulo

Profa. Dra. Cristiane Sanchez Farinas
Empresa Brasileira de Pesquisa Agropecuária

Prof. Dr. Marcos Antônio de Souza Barrozo
Universidade Federal de Uberlândia

To those who always grew up and believed that I would be capable.

ACKNOWLEDGEMENTS

I would like to express my deepest gratitude to my advisor, the distinguished Prof. Dr. João Cláudio Thoméo, for granting me the opportunity to work on a topic that inspires me daily. His exemplary guidance was fundamental to my academic and professional development, and I am immensely grateful for the genuine friendship we have built throughout this journey. I hope this partnership and friendship will last a lifetime.

To my husband, Yago, I dedicate a special thank you. His constant trust in my abilities, even during moments when my own confidence wavered, has been an invaluable foundation. His presence has made this journey lighter, and his ongoing support fuels my courage and determination to pursue my dreams.

To my parents, I express my eternal gratitude. Without the unconditional love, support, and trust they have always offered, this moment would not have been possible. They are the pillars of my life, and their friendship and presence have been essential at every step I have taken. To my sister, for her unconditional love and support, and to my nieces, whose joy and energy brighten my days and inspire me to always move forward.

To my mother-in-law, my heartfelt thanks for being my point of support in São José do Rio Preto. Her generosity and assistance were crucial for me to accomplish this work, and I am deeply grateful for it.

To my colleagues, especially Leda, Maísa, and Ana, I thank you for the daily partnership, the exchange of experiences, and for sharing the challenges and achievements that accompany the life of a researcher in Brazil.

To the distinguished Prof. Evangelos Tsotsas and Prof. Nicole Vorhauer-Huget, my profound gratitude for the warm reception in Magdeburg, where I had a transformative experience for both my academic and professional life.

To the faculty and technical staff of DETA (Department of Food Engineering and Technology), I am grateful for the valuable exchanges of knowledge and experiences that enriched my learning. I am also thankful to Unesp and IBILCE for providing the necessary conditions for this research.

This work was carried out with the support of the Coordination for the Improvement of Higher Education Personnel - Brazil (CAPES) - Funding Code 001. Thus, I cannot fail to thank CAPES for the financial support provided, which was essential for making this study possible.

Finally, to everyone who, directly or indirectly, contributed to this journey, my gratitude is immense. Each of you has played a unique role in my path, and thanks to the support of such

special people, I am now a more accomplished, thankful, and motivated person to keep moving forward.

"How many times, right before dying, does a man feel joy? Is this what they call the dead spark? And is this, then, such a spark?"

Anne Fortier (2010, p. 273)

RESUMO

A busca por alternativas menos agressivas para o controle de pragas tem impulsionado a produção do fungo entomopatogênico *Metarhizium anisopliae*, um biopesticida amplamente utilizado no controle de diversas pragas agrícolas. A produção em escala industrial é realizada por cultivo em estado sólido, utilizando arroz como substrato em embalagens plásticas. No entanto, esse processo enfrenta diversas barreiras tecnológicas, principalmente devido à realização manual de todas as etapas, o que aumenta a frequência de contaminações exógenas. Dentre os desafios que demandam aprimoramento, destacam-se a pré-secagem e a extração de esporos. Tradicionalmente, a secagem ocorre pela abertura das embalagens de cultivo em salas com temperatura controlada, um processo trabalhoso e demorado. Já a extração de esporos é convencionalmente realizada em peneiras vibratórias, resultando em perdas significativas. Esses desafios evidenciam a necessidade de otimização do processo para garantir maior eficiência e viabilidade na produção de *M. anisopliae* em larga escala. Este estudo investiga o uso de um tambor horizontal de 20 cm de diâmetro e 33 cm de comprimento, equipado com duas aletas retas posicionadas longitudinalmente, para a secagem e extração de esporos. A secagem do arroz cozido foi realizada utilizando modos estático e com rotações intermitentes a cada 1 e 24 horas de operação. Para simular a secagem estática, foi empregado um modelo matemático bidimensional baseado no transporte de massa difusivo. No caso do modo com rotações intermitentes, a homogeneização do leito foi investigada por meio de simulações utilizando o Método dos Elementos Discretos (DEM), considerando diferentes níveis de umidade. O modelo matemático previu que seriam necessários 23 dias para reduzir a umidade de 0.667 para 0.250 kg-a/kg-ss a 30°C com fluxo de ar de 50 L/min. No entanto, a introdução de rotações intermitentes reduziu esse tempo em até 97.79%. Simulações DEM, validadas experimentalmente, demonstraram que umidade elevada dificultam a mistura do material, no entanto ao se rotacionar o tambor 11 vezes a 7 rpm atingisse uma boa homogeneização dos leitos. Além disso, observou-se que o número de rotações necessárias para alcançar a homogeneização diminuiu com a redução do diâmetro do tambor e com modificações no formato das aletas, destacando a importância do design do equipamento na otimização do processo. A extração de esporos foi analisada em um tambor com rotação constante, acoplado a um conjunto de ciclones previamente dimensionado. A condição ótima de extração foi determinada variando-se o grau de enchimento do tambor (0.25 e 0.50), a velocidade de rotação (30 e 60 rpm) e o tempo de operação (4 e 8 h). Além disso, simulações DEM foram conduzidas para estimar as trajetórias das partículas, o número e as forças de colisão, parâmetros

inacessíveis experimentalmente. Os resultados confirmaram que a eficiência da extração depende do equilíbrio entre rotação, umidade e forças de colisão. A condição ótima de extração é alcançada ao se rotacionar o tambor com grau de enchimento de 0.50, velocidade de rotação de 30 rpm por 8 horas. De forma geral, as maiores eficiências de extração foram obtidas com o maior tempo de operação (8 h), atribuído à maior redução da umidade das partículas, evidenciando o impacto desse fator na eficiência do desprendimento dos esporos. A força de arrasto necessária para a remoção dos esporos diminui à medida que a umidade das partículas é reduzida, o que também diminui as forças de adesão entre os esporos e o substrato, estimadas entre 1,06x10^{-5} e 3,17x10^{-4} N. As simulações DEM revelaram que, embora 60 rpm aumentassem a frequência e a intensidade das colisões, não resultaram em uma melhora significativa na extração em comparação a 30 rpm. Esse efeito foi atribuído à fragmentação excessiva das partículas e à dissipação de energia em velocidades mais altas, resultando em um movimento menos eficiente para a extração dos esporos. Esses resultados demonstram o potencial dos tambores rotativos para aprimorar os processos de secagem e extração de esporos em biofábricas. A integração de dados experimentais, modelagem matemática e simulações DEM fornece uma compreensão abrangente da dinâmica do processo, contribuindo para o desenvolvimento de soluções escaláveis e econômicas na produção de bioinseticidas.
Palavras–chave: *Metarhizium anisopliae*; secagem; extração; tambor; ciclone; DEM.

ABSTRACT

The search for less aggressive alternatives for pest control has driven the production of the entomopathogenic fungus *Metarhizium anisopliae*, a biopesticide widely used to control various agricultural pests. Industrial-scale production is carried out through solid-state cultivation, using rice as a substrate in plastic packaging. However, this process faces several technological barriers, mainly due to the manual execution of all stages, which increases the frequency of exogenous contamination. Among the challenges requiring improvement, pre-drying and spore extraction stand out. Traditionally, drying occurs by opening the cultivation packages in temperature-controlled rooms, a labor-intensive and time-consuming process. Spore extraction is conventionally performed using vibrating sieves, resulting in significant losses. These challenges highlight the need to optimize the process to ensure greater efficiency and feasibility in the large-scale production of *M. anisopliae*. This study investigates the use of a horizontal drum with a diameter of 20 cm and a length of 33 cm, equipped with two straight longitudinal fins, for drying and spore extraction. The drying of cooked rice was conducted using static modes and intermittent rotations every 1 and 24 hours of operation. To simulate static drying, a two-dimensional mathematical model based on diffusive mass transport was employed. In the case of intermittent rotation, bed homogenization was investigated through simulations using the Discrete Element Method (DEM), considering different moisture levels. The mathematical model predicted that 23 days would be required to reduce moisture from 0.667 to 0.250 kg-w/kg-ds at 30°C with an airflow of 50 L/min. However, the introduction of intermittent rotations reduced this time by up to 97.79%. DEM simulations, experimentally validated, demonstrated that high moisture content hindered material mixing; however, by rotating the drum 11 times at 7 rpm, good bed homogenization was achieved. Additionally, it was observed that the number of rotations required to achieve homogenization decreased with a reduction in drum diameter and modifications to the fin shape, highlighting the importance of equipment design in process optimization. Spore extraction was analyzed in a drum with constant rotation, coupled to a pre-dimensioned cyclone set. The optimal extraction condition was determined by varying the drum filling level (0.25 and 0.50), rotation speed (30 and 60 rpm), and operation time (4 and 8 h). Furthermore, DEM simulations were conducted to estimate particle trajectories, collision numbers, and collision forces—parameters inaccessible experimentally. The results confirmed that extraction efficiency depends on the balance between rotation, moisture, and collision forces. The optimal extraction condition was achieved by rotating the drum with a filling level of 0.50 at a speed of 30 rpm for 8 hours. Overall, the highest extraction efficiencies were obtained with the longest operation time (8 h), attributed to the greater reduction in particle moisture, highlighting the impact of this factor on spore detachment efficiency. The drag force required for spore removal decreased as particle moisture was reduced, which also lowered the adhesion forces between the spores and the substrate, estimated between 1.06×10^{-5} and 3.17×10^{-4} N. DEM simulations revealed that while 60 rpm increased the frequency and intensity of collisions, they did not significantly improve extraction compared to 30 rpm. This effect was attributed to excessive particle fragmentation and energy dissipation at higher speeds, resulting in less efficient movement for spore extraction. These results demonstrate the potential of rotary drums to improve drying and spore extraction processes in biofactories. The integration of experimental data, mathematical modeling, and DEM simulations provides a comprehensive understanding of process dynamics, contributing to the development of scalable and cost-effective solutions in bioinsecticide production.

Keywords: *Metarhizium anisopliae;* drying; extraction; drum; cyclone; DEM.

LIST OF FIGURES

LIST OF TABLES

LIST OF ABBREVIATIONS AND ACRONYMS

AFM	Atomic force microscope
ANOVA	Analysis of variance
CDR	Conidiated rice
CR	Cooked rice
CV	Coefficient of variation
DEM	Discrete element method
EF	Entomopathogenic fungi
MC	Moisture content
MRE	Mean residual error
MSB	Magnetic suspension balance
PDA	Potato dextrose agar
PP	Particle-particle
PW	Particle-wall
RH	Relative humidity
RMSE	Mean square error
RR	Raw rice
SD	Standard deviation
SSC	Solid-state cultivation

LIST OF SYMBOLS

ΔP	Standard error
A_p	Particle reference area
a_w	Water activity
C	Concentration of black pixels in each cell
C_D	Drag coefficients
C_m	Average concentration of black pixels
D	Molecular diffusivity of water vapor in the air
D^*	Cut diameter
D_c	Diameter of the cylindrical section of the cyclone
D_{eff}	Effective mass diffusivity coefficient
D_P	Particle diameter
D_r	Distance traveled by the particle from the launch point to rest
E^*	Equivalent Young's modulus
E_{C1}	Spores restrained in the underflow of the first cyclone
E_{C2}	Spores restrained in the underflow of the second cyclone
$E_{ext,s}$	Extracted spores collected from all the sieves
E_F	Spores restrained in the filter
e_p	Coefficient of restitution
E_{unext}	Non-extracted spores from the residual rice using the drum
$E_{unext,s}$	Non-extracted spores from the residual rice using the shaking sieves
f	Filling degree
$\overline{F}$	Average collision force of the particles.
F_{ad}	Adhesion forces
F_c	Contact force between particles
F_D	Drag forces
F_{max}	Maximum collision force of the particles
F_{min}	Minimum collision force of the particles
F_n	Normal force
F_n^d	Normal damping force
F_t^d	Tangential damping force
Fr	Froude number

$\mathbf{F_t}$	Tangencial force
g	Gravitational acceleration
$\mathbf{G^*}$	Equivalent shear modulus
h	Convective mass transfer coefficient
$\mathbf{h_0}$	Initial height of particle launch
I	Moment of inertia
K	Constant that depends on the cyclone configuration
$\mathbf{K_d}$	Distribution coefficient
l	Half the thickness of the plate
L	Length of the bed
$\mathbf{L_0}$	Surface of the bed
$\mathbf{L_d}$	Length of the drum
$\mathbf{L_l}$	Length of the plate
$\mathbf{L_{rice}}$	Substrate load
$\mathbf{L_t}$	Bottom of the packaging
M	Molar mass of dry air
m*	Equivalent mass
m	Mass of particle
M	Mixing index
N	Number of cells
n	Number of terms in the series
$\mathbf{P_1}$, $\mathbf{P_2}$ **and** $\mathbf{P_3}$	Model parameters to sorption isotherms
$\mathbf{P_{sat}}$	Saturation pressure of water vapor
Q	Air flow rate
r	Radial coordinate
R	Radius of the drum
$\mathbf{R^*}$	Equivalent radius
$\mathbf{R_g}$	Universal gas constant
$\mathbf{R^2}$	Coefficient of determination
$\mathbf{R^2_{adj}}$	Adjusted coefficient of determination
Re	Reynolds number
R	Radius of particle
$\mathbf{S_n}$	Normal stiffness of the nonlinear model

$\mathbf{S_t}$	Tangential stiffness of the nonlinear model
$\mathbf{T}$	Temperature
$\mathbf{t}$	Time
$\mathbf{T_{air}}$	Air temperature
$\mathbf{T_{bed}}$	Bed temperature
$\mathbf{t_d}$	Extraction time using the drum
$\mathbf{t_s}$	Extraction time using the sieves
$\mathbf{T_w}$	Wall temperature
$\mathbf{U_{air}}$	Air humidity
$\bar{\mathbf{v}}$	Average particle velocity
$\mathbf{v}$	Linear velocity
$\mathbf{v_o}$	Velocity before the impact
$\mathbf{v_{max}}$	Maximum velocity of the particles
$\mathbf{v_{min}}$	Minimum velocity of the particles
$\mathbf{v_{air}}$	Air velocity
$\mathbf{v_n}$	Relative normal velocity
$\mathbf{v_r}$	Particle velocity after the collision
$\mathbf{v_t}$	Relative tangential velocity
$\mathbf{w}$	Rotational speed of the drum
$\bar{\mathbf{X}}$	Average mass fraction of water
$\mathbf{X}$	Moisture content of the solids
$\mathbf{X_0}$	Initial moisture content of the solid
$\mathbf{X_{eq}}$	Equilibrium moisture content of the solid
$\mathbf{y}$	Longitudinal coordinate
$\mathbf{z}$	Axial coordinate
$\boldsymbol{\beta}$	Damping coefficient
$\boldsymbol{\delta_n}$	Normal viscoelastic deformation
$\boldsymbol{\delta_t}$	Tangential viscoelastic deformation
$\boldsymbol{\varepsilon}$	Porosity
$\boldsymbol{\eta}$	Individual efficiency
$\boldsymbol{\eta_{col}}$	Useful efficiency using the rotary drum
$\boldsymbol{\eta_{ext,d}}$	Total extraction efficiency using the rotary drum
$\boldsymbol{\eta_{ext,s}}$	Spore extraction efficiency using vibrating sieves

μ	Fluid viscosity
μ_r	Rolling friction coefficient
μ_s	Static friction coefficient
ν	Kinematic viscosity of air
ρ_∞	Density of the air far from the surface.
ρ_{air}	Density of the air
ρ_{bulk}	Bulk density
ρ_{ds}	Dry solid density
ρ_p	Particle density
σ	Standard deviation of pixels
σ_0	Deviations in the fully segregated state
σ_i	Deviation of a mixture at rotation i
σ_r	Deviations in the perfectly mixed state
τ_r	Torque
λ	Tortuosity
φ	Particle angle
Φ	Sphericity
ω_i	Angular velocity
Θ	Static angle of repose
Θ_d	Dynamic resting angle
Θ_s	Critical angle of inclination at which the particles begin to slide

SUMMARY

1. GENERAL INTRODUCTION

1.1 INTRODUCTION

The infastation of insects in plantations and crops results in significant economic losses (Mohamed et al., 2025). Although the use of chemical insecticides is the first solution that comes to mind for farmers, the indiscriminate application of these products leads to severe and long-lasting consequences for the environment and human health. Prolonged use of agrochemicals contributes to soil, watercourse, and food contamination, causing serious diseases in humans and other animals (Mohamed et al., 2025). According to the World Health Organization, approximately 300,000 annual deaths are related to pesticide exposure (Lengai et al., 2020; Sharma et al., 2023). Additionally, excessive use has led to an increase in resistance among target pests, requiring ever-higher concentrations to control their populations (Sharma et al., 2020).

To mitigate these problems, the use of biological control has gained prominence as a sustainable alternative for pest management (Quiroga-Cubides et al., 2025). The biopesticide market has grown sixfold over the past decade (Markets and Markets, 2023), standing out for being harmless to mammals, causing little to no impact on the environment, and being effective, selective, and persistent in the field. The insecticide market generated $13.8 billion in 2023, while the biopesticide market generated $7.6 billion (Kings research, 2024; Spherical Insights and Consulting, 2024). In terms of growth, the insecticide market is expected to grow at an annual rate of 6.45% until 2030, while the biopesticide market is projected to grow at 9.6%. Moreover, the global demand for bioinsecticides specifically derived from entomopathogenic fungi (EF) is rising due to their sustainability benefits. Currently, EF accounts for 10% of the global market for microbiological biocontrol agents (Sabbahi et al., 2022). In Latin America, EF accounts for 60% of the microbial market, with *Metarhizium anisopliae* being the most widely used, followed by *Beauveria bassiana*, which together hold 65% of this market share (Nishi; Sato, 2017).

Despite the significant expansion of the market, increasing production efficiency is essential to enable the widespread adoption and integration of this microorganism in biological control practices (Quiroga-Cubides et al., 2025). The traditional process for producing *M. anisopliae* conidia uses solid-state cultivation (SSC) and employs rice as the substrate, as it provides all the necessary nutrients for the growth of the fungus has a high surface área, and mantains its original structure along the cultivation (Dorta, Arcas, 1998; Kruger et al., 2014). The production process for entomopathogenic fungi faces several technological barriers and involves multiple steps, many of which are performed manually, requiring intensive labor. This dependence increases the frequency of exogenous contaminations (Mishra et al., 2020). Moreover, the lack of proper control over critical variables such as temperature and humidity, along with the absence of standardization in operational procedures, undermines reproducibility, increases production costs, and reduces the effectiveness of the final product. Another critical point is the use of equipment adapted from other processes, such as in the extraction stage, which leads to significant losses (Jaronski; Jackson, 2012; Liu et al., 2015; Mendez-Gonzalez et al., 2018; Velozo et al., 2023).

The production process, designed in the mid-20th century for conidia production using plastic packaging (Jenkins et al., 1998), remains widely used due to its low investment cost and independence from the technological level of the region (Mendez-Gonzales et al., 2025). Among the critical stages of the process, the drying of the cultivation medium and the extraction of spores stand out. Drying is a slow process as it occurs through natural convection, requiring the plastic packaging to be opened to allow moisture removal. Spore extraction, traditionally performed using vibrating sieves, has significant limitations, including substantial spore losses during the process (Mendez-Gonzalez et al., 2018). With the increasing demand for bioinsecticides, it has become necessary to adopt more sophisticated processes that offer greater production capacity and can be more easily industrialized.

Due to its high processing capacity and operational flexibility, the rotary drum is widely used industrially, primarily for drying materials (Tarhan et al., 2010; Delele et al., 2015; Trojosky, 2019; Balakrishnan et al., 2022; Nunes et al., 2024), owing to the intensification of mass transfer provided by the greater gas-solid contact. Furthermore, this equipment allows for significant interaction between the particles, which aids in the detachment of conidia. However, few studies have been published in the literature regarding the use of this equipment for such purposes, with results still inconclusive (Jenkins et al., 1998; Cunha et al., 2020), leaving room for further research in this field. In this context, the rotary drum emerges as a promising alternative, not only for incubation but also for drying and conidia extraction.

Given the high energy demand for drying processes and the high cost of predicting the behavior of granular materials at an industrial scale, simulations and mathematical models are promising tools for forecasting results. The Discrete Element Method (DEM) is widely used to describe the dynamics of granular materials. However, the quality of the DEM model's prediction depends on the selected contact model as well as the input parameters (Machado et al., 2017). DEM has been widely used to describe granular behavior inside rotary drums, providing a robust approach for investigating and modeling drying and extraction phenomena. Previous studies have demonstrated its effectiveness in analyzing particle transport and interaction in rotary systems, enabling the optimization of operational parameters and the design of more efficient equipment (Xu et al., 2010; Liu et al., 2017; Wu et al., 2022; Van Sleeuwen et al., 2024).

In this context, this study aims to enhance the efficiency and quality of the conidia production process of *Metarhizium anisopliae*, promoting technological advancements in the drying and extraction stages through the adoption of a rotary drum. The use of this equipment seeks to optimize mass transfer, accelerate drying, facilitate conidia release, and reduce losses during the process. The results obtained will provide crucial information for the automation of the production process, enabling more precise sizing, greater control of the involved variables, and facilitating the future scaling up of production to meet the growing demand in the bioinsecticide market.

1.2 THESIS OVERVIEW

This thesis addresses technological advancements for biofactories, with an emphasis on the adoption of a horizontal rotary drum for spore drying and extraction. The main focus is on optimizing the pre-drying of conidiated rice and spore extraction stages. In addition to this introductory section, which provides an overview of the entire work, the thesis is divided into seven other chapters.

Section II presents the general objective and specific objectives of the study, establishing the scope of the research. Chapter III provides a detailed review of the solid-state cultivation of *Metarhizium anisopliae* and explores alternatives for process scaling, highlighting challenges and solutions in the industrial context.

In Section IV, an innovative approach to drying rice in a horizontal drum, operating both statically and with intermittent rotations, was investigated. Mass transfer was simulated and experimentally validated, providing insights for process optimization.

Section V addresses the dynamics of mixing rice particles during drying with intermittent rotations. The analysis was conducted using the DEM and supported by experiments, enabling a better understanding of particle behavior correlated with the reduction in particle moisture content during the pre-drying stage.

Section VI examines a new alternative for spore extraction using a horizontal rotating drum coupled with cyclones. The optimal process conditions were determined, and the mechanisms responsible for spore detachment were identified.

In Section VII, the impact of reduced moisture content of conidiated rice particles on movement behavior and the number of particle collisions was assessed, correlating these factors with spore extraction efficiency through DEM.

Finally, Section VIII summarizes the general conclusions of the work, also pointing out perspectives for future research in the development of more efficient biofactories.

1.3 REFERENCES

BALAKRISHNAN, M. et al. Design, development, and evaluation of rotary drum dryer for turmeric rhizomes (*Curcuma longa* L.). **Journal of Food Process Engineering**, v. 45, n. 6, p. e14052, jun. 2022.

CUNHA, L. P. et al. Metarhizium anisopliae conidia production in packed-bed bioreactor using rice as substrate in successive cultivations. **Process Biochemistry**, v. 97, p. 104–111, out. 2020.

DELELE, M. A.; WEIGLER, F.; MELLMANN, J. Advances in the Application of a Rotary Dryer for Drying of Agricultural Products: A Review. **Drying Technology**, v. 33, n. 5, p. 541–558, 4 abr. 2015.

DORTA, B.; ARCAS, J. Sporulation of Metarhizium anisopliae in solid-state fermentation with forced aeration. **Enzyme and Microbial Technology**, v. 23, n. 7–8, p. 501–505, nov. 1998.

JARONSKI, S. T.; JACKSON, M. A. Mass production of entomopathogenic Hypocreales. **Manual of Techniques in Invertebrate Pathology**, p. 255–284, 2012.

JENKINS, N. E. et al. Development of mass production technology for aerial conidia for use as mycopesticides. v. 19, n. 1, 1998.

KINGS RESEARCH. Mercado de Inseticidas: análise por tipo, aplicação e região, previsão 2023-2030. https://www.kingsresearch.com/pt/insecticides-market-1155. (accessed 02 January 2025).

KRUGER, R. D. et al. Solid Substrate Production and Formulation of an Isolate of Metarhizium anisopliae for Biological Control of Stem Bug Tibraca limbativentris. 2014.

LENGAI, G. M. W.; MUTHOMI, Jl W.; MBEGA, E. R. Phytochemical activity and role of botanical pesticides in pest management for sustainable agricultural crop production. **Scientific African**, v. 7, p. e00239, 2020.

LIU, H. et al. Optimised fermentation conditions and improved collection efficiency using dual cyclone equipment to enhance fungal conidia production. **Biocontrol Science and Technology**, v. 25, n. 9, p. 1011–1023, 2 set. 2015.

LIU, X. et al. DEM study on the surface mixing and whole mixing of granular materials in rotary drums. **Powder Technology**, v. 315, p. 438–444, jun. 2017.

MACHADO, M. V. C. et al. Experimental and Numerical Study of Grinding Media Flow in a Ball Mill. **Chemical Engineering & Technology**, v. 40, n. 10, p. 1835–1843, out. 2017.

MARKETS AND MARKETS. Bipesticides by type (bioinsecticides, biofungicides, bionematicides), crop type (cereals & grains, oilseeds & pulses), formulation (liquid and dry), source (microbial, biochemical), mode of application, region – Global forecast to 2028. https://www.marketsandmarkets.com/Market-Reports/bi opesticides-267.html?gad_source=1&gclid=Cj0KCQjw_qexBhCoARIsAFgBles 9LWx4LwQWik7SOomvpwyJ5pwIHVqYMu_XqZGEvHe zQY8qyWLyvDoaAvaFEALw_wcB, 2023 (accessed 13 Apryl 2024).

MENDEZ-GONZALEZ, F.; LOERA, O.; FAVELA-TORRES, E. Conidia production of Metarhizium anisopliae in bags and packed column bioreactors. **Current Biotechnology**, v. 7, n. 1, p. 65–69, 1 mar. 2018.

MÉNDEZ-GONZÁLEZ, F.; BUENROSTRO-FIGUEROA, J. J.; FAVELA-TORRES, E. Solid-State Culture Spore Production of Entomopathogenic Fungi. **The Role of Entomopathogenic Fungi in Agriculture**. CRC Press, p. 321-341, 2025.

MISHRA, J.; DUTTA, V.; ARORA, N. K. Biopesticides in India: technology and sustainability linkages. **3 Biotech**, v. 10, n. 5, p. 210, maio 2020.

MAHMOUD, G. A.; ABD-EL SALAM, A.; AHMED, L. I. Insecticides: Current status, properties, and the biological degradation strategies. **Development in Waste Water Treatment Research and Processes**. Elsevier, p. 45-70, 2025.

NISHI, O.; SATO, H. Species diversity of the entomopathogenic fungi Metarhizium anisopliae and M. flavoviride species complexes isolated from insects in Japan. **Mycoscience**, v. 58, n. 6, p. 472–479, nov. 2017.

NUNES, G.; DUARTE, C. R.; BARROZO, M. A. S. Experimental and numerical study of an alternative technique for fruit processing: Rotary drum with inert bed for acerola pulp dehydration. **Powder Technology**, v. 433, p. 119284, jan. 2024.

QUIROGA-CUBIDES, G. M.; ALVÁREZ, M. I. G.; GARRIGA, L. M. Framework for mass production of entomopathogenic fungi in bioeconomy context. **Fungal Biotechnology**. Academic Press, p. 549-575, 2025.

SABBAHI, R. et al. A global perspective of entomopathogens as microbial biocontrol agents of insect pests. **Journal of Agriculture and Food Research**, v. 10, p. 100376, 2022.

SHARMA, A.; SHARMA, S.; YADAV, P. K. Entomopathogenic fungi and their relevance in sustainable agriculture: A review. **Cogent Food & Agriculture**, v. 9, n. 1, p. 2180857, 31 dez. 2023.

SPHERICAL INSIGHTS & CONSULTING. Mercado Global de Biopesticidas: tamanho, participação e análise de impacto do COVID-19, por tipo de produto, aplicação, fonte, tipo de cultura, forma e região, análise e previsão 2021-2030. https://www.sphericalinsights.com/pt/reports/biopesticides-market (accessed 13 December 2024).

TARHAN, S. et al. Product quality and energy consumption when drying peppermint by rotary drum dryer. **Industrial Crops and Products**, v. 32, n. 3, p. 420–427, nov. 2010.

TROJOSKY, M. Rotary drums for efficient drying and cooling. **Drying Technology**, v. 37, n. 5, p. 632–651, 4 abr. 2019.

VAN SLEEUWEN, R. et al. Efficient DEM modeling of solid flavor particle mixing in a rotary drum. **Powder Technology**, v. 437, p. 119559, mar. 2024.

VELOZO, S. G. M. et al. From the dual cyclone harvest performance of single conidium powder to the effect of Metarhizium anisopliae on the management of Thaumastocoris peregrinus (Hemiptera: Thaumastocoridae). **PLOS ONE**, v. 18, n. 3, p. e0283543, 27 mar. 2023.

WU, W.; CHEN, K.; TSOTSAS, E. Prediction of particle mixing time in a rotary drum by 2D DEM simulations and cross-correlation. **Advanced Powder Technology**, v. 33, n. 4, p. 103512, abr. 2022.

XU, Y. et al. 2D DEM simulation of particle mixing in rotating drum: A parametric study. **Particuology**, v. 8, n. 2, p. 141–149, abr. 2010.

2. OBJECTIVES

2.1 OBJECTIVES

The main objective of this study was to drive technological advancements in biomanufacturing facilities that produce *Metarhizium anisopliae* spores, exploring innovative approaches to the pre-drying and extraction stages by using a horizontal rotary drum.

The specific objectives are as follows:

- Investigate and optimize the pre-drying of rice using a horizontal drum operated under static and intermittent rotation conditions.
- Assess the mixing of cooked rice particles during drying with intermittent rotations in the drum, ensuring process uniformity.
- Determine the coefficients of restitution, rolling friction, and static friction for cooked rice and conidiated rice particles to describe the interactions between particles and between particles and stainless steel.
- Design efficient cyclone for spore collection after extraction in the rotary drum.
- Evaluate spore extraction in a rotary drum.
- Determine the effect of different air flow velocities on the detachment of spores adhered to rice with varying moisture contents.
- Examine the influence of the particle moisture content on the movement regime, particle velocity, and collision frequencies and forces during spore extraction in the rotary drum

3. LITERATURE REVIEW

3.1 BIOINSECTICIDES

Over the past decade, global pesticide use has increased by 20%, reaching a total of 7.2 million tons in 2020 (FAO, 2021; Shattuck et al., 2023), making it the predominant method for pest control over the last 50 years. Although effective, the indiscriminate and reckless use of agrochemicals has led to severe and far-reaching consequences for the environment and human health (Yadav et al., 2022; Shweta; Sood, 2023). According to recent estimates from the World Health Organization, approximately 25 million people suffer from pesticide poisoning annually in developing countries, while about 20,000 deaths related to such exposure are recorded globally (Chakraborty et al., 2023). Furthermore, target pests have become resistant to pesticides, necessitating higher concentrations to control them (Bass et al., 2015; Sharma et al., 2020).

In this context, biopesticides emerge as a promising solution to mitigate these issues while promoting greater sustainability (Marrone, 2023). Currently, the global pesticide market, valued at approximately US$ 56 billion, includes a biopesticide segment estimated between US$ 3 and 5 billion (Marrone, 2023). With a compound annual growth rate of 14.1% (Thalet et al., 2021; Marrone, 2023), biopesticide development is expected to surpass that of chemical pesticides, reaching a market value of US$ 15 billion by 2029 (Chakraborty et al., 2023; Marrone, 2023).

Biopesticides are defined as substances or organisms of natural occurrence used in the control of pests, diseases, and weeds in agricultural and non-agricultural environments (Thakore, 2006; Kenis et al., 2019; Hasan, 2024). In general, they include any organism that compromises the quality, value, or availability of human resources through non-toxic mechanisms (Ramírez-Guzman et al., 2020; Sansinenea, 2021; Seenivasagan; Babalola, 2021). This profile makes them attractive, especially due to their reduced environmental impact, lower toxicity to non-target organisms, and compatibility with sustainable agricultural practices (Kumar; Singh, 2015; Hasan et al., 2024).

One of the main advantages of biopesticides is their specificity. They are designed to target specific pests but also have the ability to control a wide range (Gupta; Dikshit, 2010; Chakraborty et al., 2023). They can be classified into macrobiological, microbiological, and biochemical categories, with microbiological biopesticides derived from microorganisms such as bacteria, fungi, viruses, and nematodes (Glare et al., 2012; Araújo et al., 2019; Hasan, 2024). These, in particular, can be applied in different forms, whether as living organisms, dead organisms, or spores (Mishra et al., 2020; Chakraborty et al., 2023).

With over 750 species isolated in insects and 100 distinct genera, entomopathogenic fungi are the most widely used among microbiological biopesticides due to their ease of propagation and ability to infect pests (Sharma et al., 2023). Among them, *Metarhizium* is of great relevance, as it is effective against more than 200 species of insects and mites (Zimmermann, 1993). There are three species in the genus, namely: *M. flavoviride*, *M. album*, and *M. anisopliae*.

3.2 *Metarhizium anisopliae*

Classified as an acaricide and entomopathogenic, *M. anisopliae* has a transparent (hyaline) mycelium composed of septate cells. These cells are structured with simple or branched hyphae from which conidia originate. The conidia are typically uninucleated, cylindrical, and vary in size, subdivided into two varieties, *minor* and *majus*, based on spore size (Hu, St. Leger, 2002; Arruda et al., 2005; Wang et al., 2016).

The infection process is similar to that of other entomopathogenic fungi and involves conidial attachment to the host surface, followed by germination, penetration, colonization, reproduction, and sporulation (Quintela; McCoy, 1998; Arruda et al., 2005; Fontes, Valadares-Inglis, 2020; Pedrini, 2018). To break through the host's cuticle, *M. anisopliae* secretes enzymes such as proteases, lipases, and chitinases that degrade the primary compounds on the insect's surface, allowing hyphal penetration (Schrank, Vainstein, 2010). The cuticle is predominantly composed of proteins, which play an essential role in host-pathogen interactions, such as proteases and adhesins (Pitarch et al., 2008; Groot et al., 2013; Greenfield et al., 2014).

Firm attachment of the conidia is a determining factor for pathogen success, directly influencing its specificity and virulence (Greenfield et al., 2014). This process occurs in two main stages. The first involves passive adhesion, mediated by a combination of non-specific hydrophobic and electrostatic forces, as well as specific interactions between ligands and adhesin proteins (Holder; Keyhani, 2005; Wang; St. Leger, 2007). In the second stage, the secretion of hydrolytic enzymes occurs. These enzymes are responsible for degrading fungistatic fatty acids, releasing essential nutrients, and facilitating fungal penetration into the cuticle (Peterson et al., 1994; Jarrold et al., 2007). Additionally, the secretion of mucilage helps consolidate fungal attachment to the host surface. Adhesins such as Mad1 and Mad2 play an important role in this process, assisting in the attachment of the fungus to both insect and plant surfaces (Wang; St. Leger, 2007; Leão et al., 2015).

Metarhizium anisopliae has been widely used in the control of various agricultural and veterinary pests. Among its targets are the cattle tick *Rhipicephalus microplus* (Boophilus microplus), stable flies (*Stomoxys calcitrans*), the beetle *Alphitobius diaperinus*, a major poultry pest, bird lice (*Mallophaga*), and larvae of the Asian tiger mosquito (*Aedes albopictus*). In Brazil, *M. anisopliae* is most commonly used for controlling the sugarcane leafhopper and roothopper, *Mahanarva posticata* and *Mahanarva fimbriolata*, respectively.

Currently, more than 3 million hectares of sugarcane are annually treated with *M. anisopliae* spores (Mendez-Gonzalez et al., 2018; Cunha et al., 2020). To achieve efficiency in field application, it is essential to adopt an inundative introduction strategy. This approach requires the application of a concentration of 10^{13} conidia per hectare to achieve a lethality rate of 88.4% against target pests (Schmidt et al., 2007). Therefore, large-scale production of the fungus becomes essential.

Cultivation of *M. anisopliae* requires specific environmental conditions to maximize sporulation and growth. The ideal temperature for fungal development ranges from 25 to 28°C, with temperatures outside this range directly impacting spore production and fungal growth. Additionally, maintaining relative humidity between 70% and 100% is crucial to ensure its high virulence (Dorta; Arcas, 1998; Keyser et al., 2014; Li; Feng, 2009). Traditionally, spores are produced in solid-state culture (SSC), with rice widely used as a substrate.

3.3 RICE

Rice (*Oryza sativa*) is one of the most cultivated and consumed cereals worldwide, serving as a staple food for approximately 60% of the global population (Yadav et al., 2024). Rice grains are predominantly composed of starch, with smaller proportions of proteins, lipids, fibers, and ash (Walter et al., 2008). However, the chemical composition of the grain and its fractions can vary significantly (Zhou et al., 2002). Additionally, nutrients are not uniformly distributed among the different parts of the grain, where the outer layers concentrate higher amounts of proteins, lipids, fibers, minerals, and vitamins, while the center, known as the endosperm, is rich in starch (Walter et al., 2008).

The white rice used in this study undergoes a processing procedure that involves several steps, from harvest to polishing, making it suitable for commercialization and consumption (Riaz et al., 2017). During the polishing process, the outer layers of the grain are removed, resulting in the near-total preservation of the endosperm (Wimberly, 1983). This removal of the outer layers gives white rice superior cooking properties and greater digestibility, making it widely accepted and consumed in various parts of the world.

When rice starch is heated in the presence of sufficient water, the starch granules rupture, releasing amylose and amylopectin. This process, known as gelatinization, results in the formation of a structural network that significantly increases the water retention capacity (Saif et al., 2003; Li et al., 2017). Gelatinization of rice during *M. anisopliae* spore production occurs due to the need for sterilization of the material. This step is essential for minimizing exogenous contamination. As a result, this process increases the surface area of the grains the porosity of the bed, creating more favorable conditions for fungal development (Dorta; Arcas, 1998; Kruger et al., 2014).

3.4 TRADITIONAL PRODUCTION

The mass production of *M. anisopliae* involves the following stages: i) Substrate packaging in plastic bags, ii) Substrate humidification, iii) Sterilization, iv) Cooling, v) Inoculation, vi) Incubation, vii) Pre-drying, viii) Extraction, and ix) Drying of conidia, as shown in Figure 3.1. Concurrently with the main process, inoculum production takes place.

Initially, 300 to 500 g of rice (dry base) are packaged in polypropylene plastic bags and moistened to 0.923 kg-w/kg-ds (kg of water/kg of dry solid) moisture content (Cunha et al., 2020). The bags are sterilized in an autoclave at 121°C for 30 minutes and cooled in climate-controlled rooms. Once they reach room temperature, the rice is inoculated in a laminar flow chamber, adding spore suspension to the substrate until a concentration of 10^7 conidia/g-ds is achieved (Santa et al., 2005). After vigorous manual mixing of the substrate, the bags are placed on shelves for approximately 10 days in a climate-controlled room at 28°C (Mendez-Gonzalez et al., 2018; Cunha et al., 2019, Cunha et al., 2020). After incubation, the bags are opened in a new climate-controlled room at 18°C, where they remain for up to 10 days, allowing the inoculated rice to dry to approximately 0.250 kg-w/kg-ds moisture content (Jenkins et al., 1998). The spores are then extracted from the rice by mechanical agitation in vibrating sieves. The resulting conidia powder is dried in a dehumidifier to approximately 0.099 kg-w/kg-ds or less, taking 3 to 5 days (Jaronski, Jackson, 2012). Finally, the formulation is done by adding adjuvants that aim to increase the product's stability and dissolve it in water for spraying.

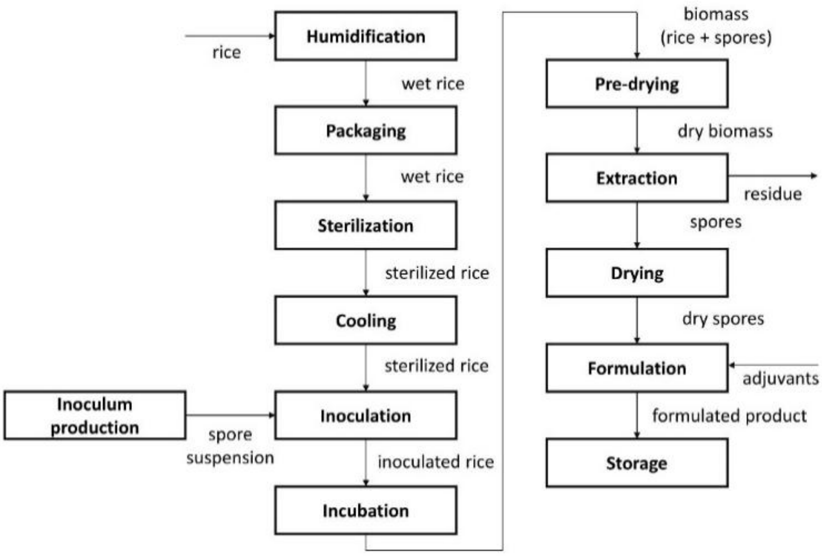

Figure 3.1. Flowchart of the traditional production process of *Metarhizium anisopliae* spores. Source: Ferreira et al. (2023).

This traditional, semi-artisanal process requires extensive labor, which often leads to exogenous contamination and, in many cases, low productivity. The limited control of process variables, such as temperature and humidity, and the lack of standardization in operational procedures make production non-reproducible and expensive, compromising the product's effectiveness (Ferreira et al., 2023). Among the steps that require more technology in the production process are incubation, pre-drying, and spore extraction.

3.4.1 Pre-drying

Pre-drying is a crucial step in the production process of *M. anisopliae* as it facilitates the separation of spores from the substrate during extraction. Additionally, this stage is essential for maximizing storage longevity, particularly when the spores will be used in oil-based or wettable powder formulations (Mascarin; Jaronski, 2016; Sala et al., 2019). However, pre-drying may be omitted if the spores are used within 1 to 2 weeks post-production and applied in an aqueous carrier (Jaronski; Jackson, 2012).

At this stage, the spores should be dried until they reach a moisture content of approximately 0.250 kg-w/kg-ds (Jenkins et al., 1998). At the end of the process, to be incorporated into formulations, spores must have a moisture content below 0.111 kg-w/kg-ds or a water activity (a_w) ≤ 0.3 (Jaronski; Jackson, 2012). Maximum stability, however, is achieved when the moisture content of the spores is further reduced to values between 0.042

and 0.052 kg-w/kg-ds, granting greater tolerance to temperature (Hedgecock et al., 1995; Moore et al., 1996; Mar; Lumyong, 2012). Nonetheless, excessive drying ($a_w > 0.1$) can create operational issues, as it may damage the plasma membrane of conidia during the imbibition process, required for preparing the spray solution (Jaronski, 2014; Faria et al., 2017).

Studies have demonstrated significant beneficial effects of slow drying on the infective propagules of *M. anisopliae*, ensuring high viability when the process is conducted over 5 to 9 days (Hong et al., 2000; Jaronski; Jackson, 2012). Traditionally, drying in biofactories is carried out by opening the packaging or transferring the conidiated rice to trays, allowing the process to occur gradually (Jaronski; Jackson, 2012). However, this traditional method presents significant disadvantages, such as exposing biofactory workers to spores, which should be avoided. Therefore, the use of enclosed and controlled drying systems is preferable, offering greater safety and efficiency to the process (Jaronski; Jackson, 2012).

As a simple alternative, Jaronski and Jackson (2012) suggested transferring the conidiated rice to Kraft paper bags, which provide adequate permeability to ensure efficient drying and contain the spores during the process. However, this approach is slow and semi-controlled, and it generates more waste due to the use of new paper bags. A faster alternative involves drying in plastic boxes transformed into chambers, as illustrated in Figure 3.2. In this method, drying occurs by introducing air into the boxes (Jaronski; Jackson, 2012). While this approach is relatively faster, it still requires large industrial spaces and has limitations, such as the load capacity of the boxes and the inevitable loss of some spores during the process, as the boxes are not completely sealed.

Figure 3.2. Adapted plastic boxes for faster drying of conidiated rice.

Source: Jaronski and Jackson (2012).

For even faster drying, forced convection ovens can be used by distributing conidiated rice on trays (Hong et al., 2000). However, it is essential to monitor the drying air temperature, as this factor significantly impacts the stability of the conidia (Hedgecock et al., 1995). High drying temperatures (T ≥ 40 °C) can harm conidial germination (Hedgecock et al., 1995). A study thoroughly investigated the effect of temperature and drying duration on the quality of *Beauveria bassiana* conidia. In this study, Li and Liu (2009) evaluated seven temperatures between 28 and 35°C and observed that rapid drying (5 h) at 35°C did not affect conidial viability. However, the effects of temperature and drying speed on the quality of *M. anisopliae* spores remain poorly understood, though it is believed to be more severe since *B. bassiana* is a more resilient fungus (Sala et al., 2019). Additionally, optimizing the drying temperature may positively impact conidial viability because it directly influences trehalose accumulation (Liu; Liu, 2009). Trehalose plays a protective role in cells, helping to mitigate stress effects, such as those faced by conidia when applied to soil (Liu; Liu, 2009).

Since drying is a critical step in producing high-quality *M. anisopliae* spores, finding a faster, more efficient, and controlled alternative that reduces industrial space and labor remains a significant challenge. One potential solution is the use of equipment like the rotary drum, widely used in the food, chemical, and pharmaceutical industries for similar purposes (Delele et al., 2015; Trojosky, 2019; Balakrishnan et al., 2022; Nunes et al., 2024).

3.4.2 Extraction of spores

In general, fungal spore-based bioinsecticides can be marketed in various forms, such as wettable powders, granules, concentrated suspensions, and emulsifiable oils (Michereff Filho et al., 2009). Among these options, wettable powders are the most commercially available due to their ease of preparation, storage, and transportation. Therefore, achieving an efficient spore extraction process is essential to meet production demands.

The traditional process for extracting *M. anisopliae* spores remains rudimentary, with few studies proposing effective alternatives for large-scale production. The simplest method involves mechanical sieving using a vibratory shaker (Jaronski; Jackson, 2012). Typically, two sieves are used, with the upper sieve having a maximum mesh opening of 0.125 mm (Jenkins et al., 1998; Jaronski; Jackson, 2012). The sieves are agitated for 20 to 25 minutes, or until most of the conidial powder is separated from the rice. This process has a recovery efficiency of 60% to 90%, not accounting for spores lost during operation, which can represent up to 25% of the total produced (Jenkins et al., 1998; Jaronski; Jackson, 2012; Oligos Biotec, 2023). In addition to significant environmental losses, this method is only effective for small-scale operations and requires intensive labor for conidial collection.

To simplify and reduce losses during the process, studies have proposed combining mechanical agitation with vacuum collection of the conidia. A device developed by Dan Johnson (Jaronski, Jackson, 2012) utilizes a vacuum cyclone system coupled with a cement mixer, as illustrated in Figure 3.3. The rotation of the cement mixer detaches the conidia from the substrate, which are then rapidly collected by the vacuum system (Jaronski, Jackson, 2012). Another adaptation was presented by Jenkins et al. (1998), who employed a household dryer connected to a fan, generating negative pressure to attract conidia and other fine particles, which are collected in a set of four cyclones. However, these adaptations present several limitations for industrial-scale application, such as capacity restrictions, efficiency issues, and operational safety challenges.

Figure 3.3. Extraction equipment using a concrete mixer developed.
Source: Jaronski and Jackson (2012).

The use of cyclones for spore collection offers several advantages, such as the elimination of large particles, separation of high-quality spores, increased safety for operators, ease of storage, and high productivity (Velozo et al., 2023). An example of this technology is the Mycoharvester1 system (Mycoharvester Company, UK), which utilizes dual cyclone technology integrated with a fluidized bed to separate pure conidia from the substrate. This equipment achieves an extraction efficiency of 85% of the conidia present in rice, and compared to the traditional sieve extraction method, it shows superior performance (Liu et al., 2015; Velozo et al., 2023).

Despite the high yield, the system has significant limitations. It processes only 150 g of conidiated rice at a time, with a collection time of up to 24 hours (Velozo et al., 2023). Furthermore, the high cost of the equipment is a considerable barrier to its large-scale application, limiting its use to smaller operations or those with greater investment capacity (Jaronski, Jackson, 2012).

In search of a viable alternative for scaling up, with a simple and low-cost design, Cunha et al. (2020) proposed a spore extraction system using a rotary drum coupled to a cyclone. This method achieved a collection efficiency of 61% of the spores after 12 hours of rotation. However, the author explored few of the variables in the extraction process, such as rotation speed, optimal time, and the relationship between the drum's loading capacity and collection efficiency, which limits the optimization and applicability of the system in large-scale industrial operations.

3.5 ROTARY DRUM

Rotary drum dryers have been used in the industry for many decades, playing a crucial role in the manufacturing and processing of various granular materials, whether free-flowing or cohesive in nature (Karali et al., 2016). These devices are employed in drying, cooling, calcination, granulation, and coating processes (Trojosky, 2019). A rotary drum consists of an elongated cylinder, which may be slightly inclined and rotate around its axis. The solid material and processing gas pass through and interact within the drum, specifically in the area transported by the gas flow, which can operate in either co-current or counter-current flow regimes (Krokida et al., 2007).

The use of rotary drums offers significant advantages for various processes, including solid-state cultivation. During fermentation, the continuous mixing of the substrate reduces temperature gradients and promotes efficient heat transfer to the equipment walls. Additionally, it enables the uniform addition of water or nutrients throughout the fermentation process, improving the control of the reaction environment (Schutyser et al., 2003). In static systems, desiccation can lead to channel formation within the substrate, compromising the process even before water activity reaches critical levels (Weber et al., 2002).

Mixing in the drum plays a crucial role in mitigating the adverse effects of evaporation, ensuring the homogeneous distribution of added water. Studies by Nagel et al. (2002)

demonstrate that, in systems with paddle mixers continuously agitated and cooled by evaporation, spraying water as a fine mist over the bed significantly increased the fermentation rate. However, it is essential that both the substrate and the fungus can withstand the shear forces generated by the mixing process (Schutyser et al., 2003).

In solid-state cultivation, the use of rotary drums has been less explored. Van Breukelen (2010) evaluated the cultivation of *Metarhizium anisopliae* in rotary drums and observed that, after 50 hours of cultivation, there was a drastic reduction in CO_2 production, associated with a halt in fungal growth. This was attributed to potential damage to the aerial mycelium caused by the shear forces generated during mixing. Despite this single study, the use of drums in solid-state fermentation presents significant potential, especially if operational conditions are optimized to minimize damage to the mycelium.

In addition to the advantages during the incubation stage, rotary drums are widely used industrially for material drying (Delele et al., 2015; Trojosky, 2019; Balakrishnan et al., 2022; Nunes et al., 2024). Their versatility is one of the main reasons for their popularity, standing out compared to other drying technologies. During operation, the movement of solid particles within the drum plays a crucial role in mass transfer efficiency. This movement prevents clumping, improves evaporation, and promotes more uniform and faster drying. As a result, rotary drums offer high efficiency, making them ideal for large-scale applications and various types of materials.

3.6 MOVING REGIME IN ROTARY DRUMS

The movement of particulate materials in rotary drums, such as glass beads, steel cylinders, fertilizer pellets, coffee beans, and others (Mellmann, 2001; Santos et al., 2013; Resende et al., 2017; Brandão et al., 2020; Berkinova et al., 2024), is widely described by the classification proposed by Mellmann (2001). In this study, Mellmann presents a comprehensive review of the six identifiable granular flow regimes in particulate systems, which are used to describe particle movement in rotary drums. These regimes depend on operational variables, such as rotation speed, the coefficient of friction on the drum wall, and the degree of filling, as illustrated in Figure 3.4.

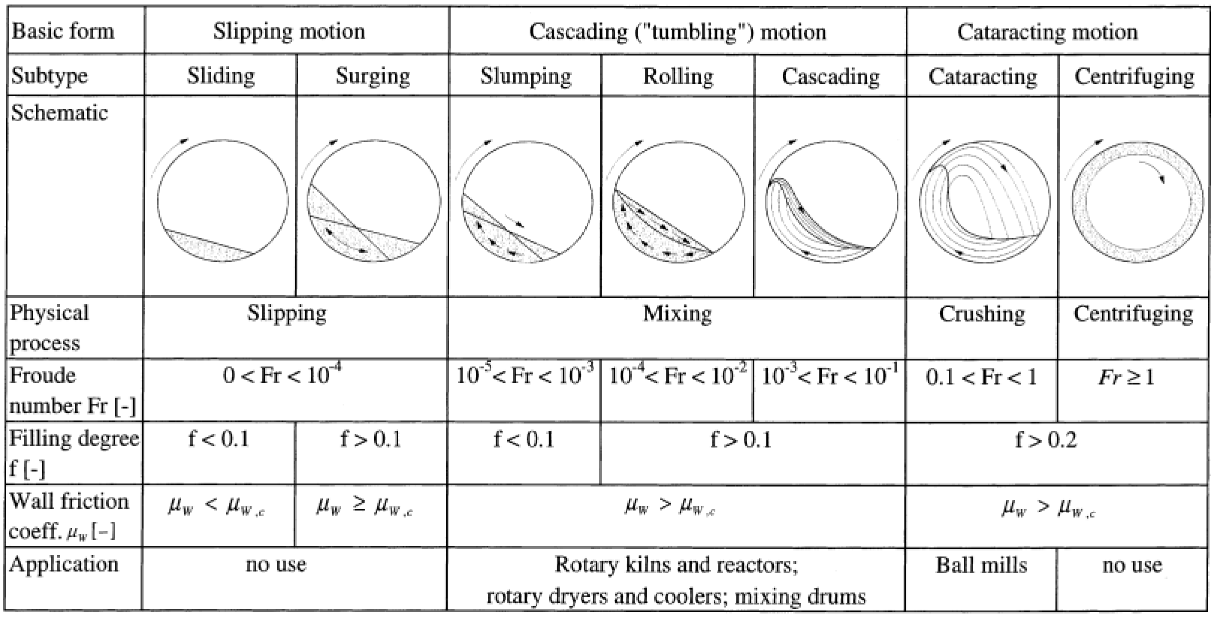

Basic form	Slipping motion		Cascading ("tumbling") motion			Cataracting motion	
Subtype	Sliding	Surging	Slumping	Rolling	Cascading	Cataracting	Centrifuging
Schematic							
Physical process	Slipping		Mixing			Crushing	Centrifuging
Froude number Fr [-]	$0 < Fr < 10^{-4}$		$10^{-5} < Fr < 10^{-3}$	$10^{-4} < Fr < 10^{-2}$	$10^{-3} < Fr < 10^{-1}$	$0.1 < Fr < 1$	$Fr \geq 1$
Filling degree f [-]	$f < 0.1$	$f > 0.1$	$f < 0.1$	$f > 0.1$		$f > 0.2$	
Wall friction coeff. μ_w [-]	$\mu_w < \mu_{w,c}$	$\mu_w \geq \mu_{w,c}$	$\mu_w > \mu_{w,c}$			$\mu_w > \mu_{w,c}$	
Application	no use		Rotary kilns and reactors; rotary dryers and coolers; mixing drums			Ball mills	no use

Figure 3.4. Forms of transverse motion of solids in rotating cylinders.

Source: Mellmann (2001).

The most common characterization of particle flow in rotary drums is based on the Froude number (Fr), which expresses the ratio between inertial forces and gravitational forces in the particle bed, as defined in Eq. (3.1). The Froude number, combined with the drum's degree of filling, allows the prediction of granular flow regimes. However, the material's intrinsic properties, such as shape, density, and friction, also have a significant influence (Mellmann, 2001).

$$Fr = \frac{w^2 R}{g} \tag{3.1}$$

where w is the rotational speed of the drum, R is the radius of the drum (m) and g is the gravitational acceleration (m/s^2).

Grajales et al. (2012) conducted a specific study on the movement regime of pre-gelatinized rice particles in a rotary drum. The results indicated that regions of higher movement occur near the drum wall and on the surface of the bed, typical characteristics of cascading and rolling sub-type regimes. These findings highlight the basic granular behavior in rotary drum systems and demonstrate the importance of operational control in achieving efficiency in processing particulate materials.

3.7 MIXING

Mixing efficiency in rotary drums is influenced by various factors, such as the degree of filling, mixing time, component concentration, equipment geometry, and the presence of lifters. Industrial mixing operations typically operate within the rolling and cascading regimes. Recent studies, such as those by Jiang et al. (2023), have shown that mixing quality improves with increasing rotational speed, as long as particle flow remains within the rolling or cascading regimes. However, higher speeds can reduce mixing efficiency due to the transition into the cataracting regime. Grajales et al. (2012) conducted a study on the mixing of pre-gelatinized rice particles in a rotary drum, where tracer techniques and image analysis were employed to evaluate the radial homogeneity of the bed mixture. The study revealed that the homogenization of rice particles was independent of the drum's rotational speed.

The degree of filling plays a crucial role in particle flow performance. High filling levels restrict the spatial distribution of particles, delaying the transition to higher flow regimes at increased speeds. Conversely, low filling levels favor particle distribution along the drum walls, promoting the occurrence of the centrifuging regime at lower rotational speeds (Louati et al., 2017).

Material properties, such as particle size and density, also significantly impact segregation in granular systems (Gray, 2017; Jiang et al., 2018). Segregation primarily occurs through percolation, where smaller particles pass through the interstices of larger particles, or due to density differences, where denser particles accumulate at the bottom of the active layer (Ottino; Lueptow, 2008). In this context, smaller and heavier particles tend to form a central core within the bed, while larger and lighter particles remain on the surface.

Particle mixing in rotary drums predominantly occurs in the radial direction, controlled by diffusion and convection processes. Convection, associated with the macro-scale movement of particle groups, is influenced by the degree of filling. Lifters play a key role in the efficiency of rotary drums by altering particle velocity fields and interfering with convection and diffusion processes in the active layer (Zhou et al., 2016). Their main function is to create a cascading pattern in particle movement, facilitating transport and discharge along the drum's rotation.

3.8 DISCRETE ELEMENT METHOD

In the Discrete Element Method (DEM) simulation approach, interactions between particles, as well as between particles and surfaces, are modeled to predict the behavior of granular beds in various equipment. The effectiveness of DEM is directly linked to the quality of the contact model used and the proper selection of input parameters. These parameters include the intrinsic properties of particles and the characteristics of their interactions. However, obtaining precise measurements of these parameters remains a significant challenge, making calibration a common practice for determining optimal DEM input values. The calibration approach is widely employed due to the difficulties associated with directly measuring physical parameters, which often lack reliable procedures to adequately represent real-world conditions (González-Montellano et al., 2011).

DEM models are generally classified into two main categories: rigid sphere models and soft sphere models. Soft sphere models, also known as non-linear Hertz-Mindlin models, are particularly suited for systems with a high concentration of granular particles and interactions involving prolonged contact periods. This model is extensively used in simulations of processes that require detailed contact force analysis, such as in dense mixtures (Kloss et al., 2012). Table 3.1 presents the fundamental equations of the non-linear Hertz-Mindlin formulation, detailing the mathematical principles underlying this model. This formulation is widely recognized for its ability to realistically represent contact phenomena, providing accurate predictions of granular bed behavior under various operational conditions.

Several intrinsic particle properties are difficult to measure, such as instantaneous velocity and shear forces acting on the material. However, some of these properties can be predicted using mathematical tools, such as the DEM approach. In DEM-based simulations, material parameters such as shear modulus, Poisson's ratio, and density, along with surface interaction properties such as restitution coefficients, static friction, and dynamic friction, are used as input parameters. These parameters influence the calculations of collision models, determining the orientation and velocity of particles after impacts. Therefore, a detailed study of each of these factors is essential for simulation accuracy, and they will be addressed in this section. Improper definition of these parameters may result in inaccurate simulations or, in some cases, physically inconsistent predictions.

The DEM approach has been widely used to simulate the behavior of particles in rotary drums, enabling detailed analysis of phenomena such as granular transport, mixing, segregation, impact, and particle wear (Orefice & Khinast, 2017; Jayasundara; Zhu, 2022; Hadi et al., 2024; Van Sleeuwen et al., 2024). Simulations predict granular flow patterns and optimize drying efficiency in industrial processes (Armir et al., 2019; Li et al., 2023). These simulations provide a solid foundation for optimizing the design and operational conditions of rotary drums in various industrial applications.

Table 3.1. Fundamental equations of the non-linear Hertz-Mindlin. F_n and F_t are the normal and tangential forces, respectively; F_n^d and F_t^d are the normal and tangential damping forces, respectively; E*, G*, R*, and m* are the Young's modulus, shear modulus, radius, and equivalent mass, respectively; δ_n and δ_t are the normal and tangential viscoelastic deformations, respectively; v_n and v_t are the normal and tangential relative velocities, respectively; S_n and S_t are the normal and tangential stiffness of the nonlinear model, respectively; and e_p is the coefficient of restitution.

Normal force	$F_n = \frac{4}{3} E^* \sqrt{R^*} \delta_n^{3/2}$	(3.1)
Normal damping force	$F_n^d = -2\sqrt{\frac{5}{6}} \beta \sqrt{S_n m^*} v_n$	(3.2)
Normal stiffness	$S_n = 2E^* \sqrt{R^* \delta_n}$	(3.3)
Damping coefficient	$\beta = \frac{\ln e_p}{\ln^2 e_p + \pi^2}$	(3.4)
Tangential force	$F_t = -\delta_t S_t$	(3.5)
Tangential damping force	$F_t^d = -2\sqrt{\frac{5}{6}} \beta \sqrt{S_t m^*} v_t$	(3.6)
Tangential stiffness	$S_t = 8G^* \sqrt{R^* \delta_n}$	(3.7)

3.9 REFERENCES

ARAÚJO, I. S. et al. Perspectivas atuais da utilização de bioinseticidas em Spodoptera frugiperda (Lepidoptera: Noctuidae). **Revista Brasileira de Meio Ambiente**, v. 7, n. 3, 2019.

ARRUDA, W. Caracterização molecular e morfofisiológica de diferentes isolados do fungo entomopatogênico Metarhizium anisopliae e análise morfológica do processo de infecção em Boophilus microplus. 2005.

BALAKRISHNAN, M. et al. Design, development, and evaluation of rotary drum dryer for turmeric rhizomes (*Curcuma longa* L.). **Journal of Food Process Engineering**, v. 45, n. 6, p. e14052, jun. 2022.

BASS, C. et al. The global status of insect resistance to neonicotinoid insecticides. **Pesticide Biochemistry and Physiology**, v. 121, p. 78–87, jun. 2015.

BERKINOVA, Z. et al. Estimation of the effect of rotational speed on flow and mixing quality of particles with different shapes in a rotary drum. **Computational Particle Mechanics**, 5 out. 2024.

BRANDÃO, R. J. et al. A systematic evaluation of DEM input parameters measurement and calibration. **Powder Technology**, v. 448, p. 120157, dez. 2024.

cuCHAKRABORTY, N. et al. Biopesticide Consumption in India: Insights into the Current Trends. **Agriculture**, v. 13, n. 3, p. 557, 24 fev. 2023.

CUNHA, L. P. et al. Production of conidia of the entomopathogenic fungus Metarhizium anisopliae ICB 425 in a tray bioreactor. **Bioprocess and Biosystems Engineering**, v. 42, n. 11, p. 1757–1768, nov. 2019.

CUNHA, L. P. et al. Metarhizium anisopliae conidia production in packed-bed bioreactor using rice as substrate in successive cultivations. **Process Biochemistry**, v. 97, p. 104–111, out. 2020.

DE GROOT, P. W. J. et al. Adhesins in Human Fungal Pathogens: Glue with Plenty of Stick. **Eukaryotic Cell**, v. 12, n. 4, p. 470–481, abr. 2013.

DELELE, M. A.; WEIGLER, F.; MELLMANN, J. Advances in the Application of a Rotary Dryer for Drying of Agricultural Products: A Review. **Drying Technology**, v. 33, n. 5, p. 541–558, 4 abr. 2015.

DORTA, B.; ARCAS, J. Sporulation of Metarhizium anisopliae in solid-state fermentation with forced aeration. **Enzyme and Microbial Technology**, v. 23, n. 7–8, p. 501–505, nov. 1998.

FAO. **Guide to the classical biological control of insect pests in planted and natural forests**. Rome: Food and Agriculture Organization of the United Nations, 2021.

FARIA, M.; HAJEK, A. E.; WRAIGHT, S. P. Imbibitional damage in conidia of the entomopathogenic fungi Beauveria bassiana, Metarhizium acridum, and Metarhizium anisopliae. **Biological Control**, v. 51, n. 3, p. 346–354, dez. 2009.

FERREIRA, D. B.; MENDES, F. B.; THOMÉO, J. C. Assessment of the Techno-Economic Feasibility of Semicontinuous Production of *Metarhizium anisopliae* Spores. **Industrial & Engineering Chemistry Research**, v. 62, n. 43, p. 17385–17393, 1 nov. 2023.

FONTES, E. M. G.; VALADARES-INGLIS, M. C. Controle biológico de pragas da agricultura. 2020.

GLARE, T. et al. Have biopesticides come of age? **Trends in Biotechnology**, v. 30, n. 5, p. 250–258, maio 2012.

GONZÁLEZ-MONTELLANO, C. et al. Validation and experimental calibration of 3D discrete element models for the simulation of the discharge flow in silos. **Chemical Engineering Science**, v. 66, n. 21, p. 5116–5126, nov. 2011.

GRAJALES, L. M. et al. Mixing and motion of rice particles in a rotating drum. **Powder Technology**, v. 222, p. 167–175, maio 2012.

GRAY, J. M. N. T. Particle Segregation in Dense Granular Flows. **Annual Review of Fluid Mechanics**, v. 50, n. 1, p. 407–433, 5 jan. 2018.

GREENFIELD, B. P. J. et al. Conidia of the insect pathogenic fungus, *Metarhizium anisopliae*, fail to adhere to mosquito larval cuticle. **Royal Society Open Science**, v. 1, n. 2, p. 140193, out. 2014.

GUPTA, S.; DIKSHIT, A. K. Biopesticides: An ecofriendly approach for pest control. **Journal of Biopesticides**, v. 3, n. Special Issue, p. 186, 2010.

HADI, A. et al. DEM modelling of segregation in granular materials: a review. **KONA Powder and Particle Journal**, v. 41, p. 78-107, 2024.

HASAN, A. et al. Role of Plant Growth Promoting Rhizobacteria (PGPR) as a Plant Growth Enhancer for Sustainable Agriculture: A Review. **Bacteria**, v. 3, n. 2, p. 59–75, 1 abr. 2024.

HEDGECOCK, S. et al. Influence of Moisture Content on Temperature Tolerance and Storage of Metarhizium flavoviride Conidia in an Oil Formulation. **Biocontrol Science and Technology**, v. 5, n. 3, p. 371–378, set. 1995.

HOLDER, D. J.; KEYHANI, N. O. Adhesion of the Entomopathogenic Fungus *Beauveria* (*Cordyceps*) *bassiana* to Substrata. **Applied and Environmental Microbiology**, v. 71, n. 9, p. 5260–5266, set. 2005.

HU, G.; ST. LEGER, R. J. Field Studies Using a Recombinant Mycoinsecticide (*Metarhizium anisopliae*) Reveal that It Is Rhizosphere Competent. **Applied and Environmental Microbiology**, v. 68, n. 12, p. 6383–6387, dez. 2002.

JARONSKI, S. T. Mass Production of Entomopathogenic Fungi: State of the Art. **Mass Production of Beneficial Organisms,** p. 357–413, 2014.
JARONSKI, S. T.; JACKSON, M. A. Mass production of entomopathogenic Hypocreales. **Manual of Techniques in Invertebrate Pathology**, p. 255–284, 2012.
JARROLD, S. L. et al. The contribution of surface waxes to pre-penetration growth of an entomopathogenic fungus on host cuticle. **Mycological Research**, v. 111, n. 2, p. 240–249, fev. 2007.
JAYASUNDARA, C. T.; ZHU, H. P. Impact energy of particles in ball mills based on DEM simulations and data-driven approach. **Powder Technology**, v. 395, p. 226-234, 2022.
JENKINS, N. E. et al. Development of mass production technology for aerial conidia for use as mycopesticides. v. 19, n. 1, 1998.
JIANG, C. et al. DEM modelling and analysis of the mixing characteristics of sphere-cylinder granular mixture in a rotating drum. **Powder Technology**, v. 426, p. 118653, ago. 2023.
JIANG, Y.-J. et al. Influence of particle-size segregation on the impact of dry granular flow. **Powder Technology**, v. 340, p. 39–51, dez. 2018.
KARALI, M. A. et al. Comparison of image analysis methods to determine the optimum loading of flighted rotary drums. **Powder Technology**, v. 291, p. 147-153, 2016.
KLOSS, C. et al. Models, algorithms and validation for opensource DEM and CFD-DEM. **Progress in Computational Fluid Dynamics, An International Journal**, v. 12, n. 2/3, p. 140, 2012.
KROKIDA, M.; MARINOS-KOURIS, D.; MUJUMDAR, A. S. Rotary drying. **Handbook of Industrial Drying**, v. 1, p. 151-172, 2007.
KRUGER, R. D. et al. Solid Substrate Production and Formulation of an Isolate of Metarhizium anisopliae for Biological Control of Stem Bug Tibraca limbativentris. 2014.
KUMAR, S.; SINGH, A. Biopesticides: Present Status and the Future Prospects. **Journal of Fertilizers & Pesticides**, v. 06, n. 02, 2015.
LEÃO, M. P. C. et al. Differential expression of the pr1A gene in Metarhizium anisopliae and Metarhizium acridum across different culture conditions and during pathogenesis. **Genetics and Molecular Biology**, v. 38, n. 1, p. 86–92, mar. 2015.
LI, H. et al. The molecular structural features controlling stickiness in cooked rice, a major palatability determinant. **Scientific Reports**, v. 7, n. 1, p. 43713, 6 mar. 2017.
LI, J.; FENG, M.-G. Intraspecific tolerance of Metarhizium anisopliae conidia to the upper thermal limits of summer with a description of a quantitative assay system. **Mycological Research**, v. 113, n. 1, p. 93–99, jan. 2009.
LI, G. et al. Numerical investigation on thermal drying process of sludges based on CFD-DEM. **Industrial & Engineering Chemistry Research**, v. 62, n. 42, p. 16990-17007, 2023.
LIU, C.-P.; LIU, S.-D. Low-Temperature Spray Drying for the Microencapsulation of the Fungus *Beauveria bassiana*. **Drying Technology**, v. 27, n. 6, p. 747–753, 4 jun. 2009.
LIU, H. et al. Optimised fermentation conditions and improved collection efficiency using dual cyclone equipment to enhance fungal conidia production. **Biocontrol Science and Technology**, v. 25, n. 9, p. 1011–1023, 2 set. 2015.
LOUATI, H.; OULAHNA, D.; DE RYCK, A. Effect of the particle size and the liquid content on the shear behaviour of wet granular material. **Powder Technology**, v. 315, p. 398–409, jun. 2017.
MARRONE, P. G. Status of the biopesticide market and prospects for new bioherbicides. **Pest Management Science**, v. 80, n. 1, p. 81–86, jan. 2024.
MASCARIN, G. M.; JARONSKI, S. T. The production and uses of Beauveria bassiana as a microbial insecticide. **World Journal of Microbiology and Biotechnology**, v. 32, n. 11, p. 177, nov. 2016.

MELLMANN, J. The transverse motion of solids in rotating cylinders—forms of motion and transition behavior. **Powder Technology**, v. 118, n. 3, p. 251–270, ago. 2001.

MICHEREFF FILHO, M. et al. Micoinseticidas e micoacaricidas no brasil: como estamos após quatro décadas? **Arquivos do Instituto Biológico**, v. 76, n. 4, p. 769–779, dez. 2009.

MISHRA, J.; DUTTA, V.; ARORA, N. K. Biopesticides in India: technology and sustainability linkages. **3 Biotech**, v. 10, n. 5, p. 210, maio 2020.

MOORE, D. et al. Effects of Moisture Content and Temperature on Storage of Metarhizium flavoviride Conidia. **Biocontrol Science and Technology**, v. 6, n. 1, p. 51–62, mar. 1996.

NAGEL, F.-J. J. I. et al. Temperature control in a continuously mixed bioreactor for solid-state fermentation. **Biotechnology & Bioengineering**, v. 72, n. 2, p. 219–230, 20 jan. 2001.

NUNES, G.; DUARTE, C. R.; BARROZO, M. A. S. Experimental and numerical study of an alternative technique for fruit processing: Rotary drum with inert bed for acerola pulp dehydration. **Powder Technology**, v. 433, p. 119284, jan. 2024.

OLIGOS BIOTEC. Personal Information. 2023.

OTTINO, J. M.; LUEPTOW, R. M. On mixing and demixing. **Science**, v. 319, n. 5865, p. 912-913, 2008.

OREFICE, L.; KHINAST, J. G. DEM study of granular transport in partially filled horizontal screw conveyors. **Powder Technology**, v. 305, p. 347-356, 2017.

PATERSON, I. C. et al. Partial characterization of specific inducers of a cuticle-degrading protease from the insect pathogenic fungus Metarhizium anisopliae. **Microbiology**, v. 140, n. 11, p. 3153-3159, 1994.

PEDRINI, N. Molecular interactions between entomopathogenic fungi (Hypocreales) and their insect host: Perspectives from stressful cuticle and hemolymph battlefields and the potential of dual RNA sequencing for future studies. **Fungal Biology**, v. 122, n. 6, p. 538–545, jun. 2018.

PITARCH, A.; NOMBELA, C.; GIL, C. Cell Wall Fractionation for Yeast and Fungal Proteomics. Em: POSCH, A. (Ed.). **2D PAGE: Sample Preparation and Fractionation**. Methods in Molecular Biology™. Totowa, NJ: Humana Press, v. 425, p. 217–239, 2008.

QUINTELA, E. D.; MCCOY, C. W. Conidial Attachment of Metarhizium anisopliae and Beauveria bassiana to the Larval Cuticle of Diaprepes abbreviatus(Coleoptera: Curculionidae) Treated with Imidacloprid. **Journal of Invertebrate Pathology**, v. 72, n. 3, p. 220–230, nov. 1998.

RAMÍREZ-GUZMÁN, N. et al. Significant Advances in Biopesticide Production: Strategies for High-Density Bio-Inoculant Cultivation. **Microbial Services in Restoration Ecology**, p. 1–11, 2020.

RESENDE, I. A. et al. An experimental analysis of coffee beans dynamics in a rotary drum. **The Canadian Journal of Chemical Engineering**, v. 95, n. 12, p. 2239–2248, dez. 2017.

RIAZ, M.; ISMAIL, T.; AKHTAR, S. Harvesting, Threshing, Processing, and Products of Rice. Em: CHAUHAN, B. S.; JABRAN, K.; MAHAJAN, G. (Eds.). **Rice Production Worldwide**. Cham: Springer International Publishing, p. 419–453, 2017.

SAIF, S. M. H.; LAN, Y.; SWEAT, V. E. Gelatinization Properties of Rice Flour. **International Journal of Food Properties**, v. 6, n. 3, p. 531–542, 10 jan. 2003.

SALA, A. et al. Rice husk as a source for fungal biopesticide production by solid-state fermentation using B. bassiana and T. harzianum. **Bioresource Technology**, v. 296, p. 122322, jan. 2019.

SANSINENEA, E. Application of biofertilizers: Current worldwide status. **Biofertilizers**. Woodhead Publishing, p. 183-190, 2021.

SANTOS, D. A. et al. Experimental and CFD study of the hydrodynamic behavior in a rotating drum. **Powder Technology**, v. 250, p. 52–62, dez. 2013.

SCHMIDT, F. G. V. et al. Metodologia de aplicação do fungo Metarhizium anisopliae var. acridum para o controle do gafanhoto Rhammatocerus schistocercoides em campo. 2007.

SCHRANK, A.; VAINSTEIN, M. H. Metarhizium anisopliae enzymes and toxins. **Toxicon**, v. 56, n. 7, p. 1267–1274, dez. 2010.
SCHUTYSER, M. A. I. et al. Heat and water transfer in a rotating drum containing solid substrate particles. **Biotechnology and Bioengineering**, v. 82, n. 5, p. 552–563, 5 jun. 2003a.
SCHUTYSER, M. A. I. et al. Substrate aggregation due to aerial hyphae during discontinuously mixed solid-state fermentation with *Aspergillus oryzae*: Experiments and modeling. **Biotechnology and Bioengineering**, v. 83, n. 5, p. 503–513, 5 set. 2003b.
SEENIVASAGAN, R.; BABALOLA, O. O. Utilization of Microbial Consortia as Biofertilizers and Biopesticides for the Production of Feasible Agricultural Product. **Biology**, v. 10, n. 11, p. 1111, 28 out. 2021.
SHARMA, A. et al. Global trends in pesticides: A looming threat and viable alternatives. **Ecotoxicology and Environmental Safety**, v. 201, p. 110812, set. 2020.
SHARMA, A.; SHARMA, S.; YADAV, P. K. Entomopathogenic fungi and their relevance in sustainable agriculture: A review. **Cogent Food & Agriculture**, v. 9, n. 1, p. 2180857, 31 dez. 2023.
SHATTUCK, A. et al. Global pesticide use and trade database (GloPUT): New estimates show pesticide use trends in low-income countries substantially underestimated. **Global Environmental Change**, v. 81, p. 102693, jul. 2023.
SHWETA; SOOD, S. A review on nanotechnological advancements in tomato: a model plant. The Journal of Horticultural Science and Biotechnology, v. 98, n. 5, p. 563-579, 2023
THAKORE, Y. The biopesticide market for global agricultural use. **Industrial Biotechnology**, v. 2, n. 3, p. 194-208, 2006.
THALER, E. A.; LARSEN, I. J.; YU, Q. The extent of soil loss across the US Corn Belt. **Proceedings of the National Academy of Sciences**, v. 118, n. 8, p. e1922375118, 23 fev. 2021.
TROJOSKY, M. Rotary drums for efficient drying and cooling. **Drying Technology**, v. 37, n. 5, p. 632–651, 4 abr. 2019.
VAN BREUKELEN, F. R. et al. Bioreactor and substrate selection for solid-state cultivation of the malaria mosquito control agent Metarhizium anisopliae. **Process Biochemistry**, v. 46, n. 3, p. 751–757, mar. 2011.
VAN SLEEUWEN, R. et al. Efficient DEM modeling of solid flavor particle mixing in a rotary drum. **Powder Technology**, v. 437, p. 119559, 2024.
VELOZO, S. G. M. et al. From the dual cyclone harvest performance of single conidium powder to the effect of Metarhizium anisopliae on the management of Thaumastocoris peregrinus (Hemiptera: Thaumastocoridae). **PLOS ONE**, v. 18, n. 3, p. e0283543, 27 mar. 2023.
WALTER, M.; MARCHEZAN, E.; AVILA, L. A. D. Arroz: composição e características nutricionais. **Ciência Rural**, v. 38, n. 4, p. 1184–1192, ago. 2008.
WANG, C.; ST LEGER, R. J. The MAD1 Adhesin of *Metarhizium anisopliae* Links Adhesion with Blastospore Production and Virulence to Insects, and the MAD2 Adhesin Enables Attachment to Plants. **Eukaryotic Cell**, v. 6, n. 5, p. 808–816, maio 2007.
WANG, J. B.; ST. LEGER, R. J.; WANG, C. Advances in Genomics of Entomopathogenic Fungi. **Advances in Genetics**, v. 94, p. 67–105, 2016.
WIMBERLY, J. E. Technical handbook for the paddy rice postharvest industry in developing countries. **Int. Rice Res. Inst.**, 1983.
YADAV, G. P. et al. A comprehensive review on instant rice: Preparation methodology, characterization, and quality attributes. **Food Chemistry Advances**, v. 4, p. 100581, jun. 2024.
YADAV, R.; SINGH, S.; SINGH, A. N. Biopesticides: Current status and future prospects. 2022.
ZHOU, Z. et al. Composition and functional properties of rice. **International Journal of Food Science & Technology**, v. 37, n. 8, p. 849–868, dez. 2002.

ZHOU, Z. et al. Enhancing mixing of cohesive particles by baffles in a rotary drum. **Particuology**, v. 25, p. 104–110, abr. 2016.

ZIMMERMANN, G. The entomopathogenic fungus *Metarhizium anisopliae* and its potential as a biocontrol agent. **Pesticide Science**, v. 37, n. 4, p. 375–379, jan. 1993.

4. SIMULATION OF STATIC DRYING AND DRYING WITH INTERMITTENT ROTATIONS IN A HORIZONTAL DRUM OF RICE USED IN THE CULTIVATION OF *Metarhizium anisopliae*

*Published chapter: FERREIRA, D. B.; TADA, É. F. R.; THOMÉO, J. C. Simulation of static drying and drying with intermittent rotations in a horizontal drum of rice used in the cultivation of Metarhizium anisopliae. **Chemical Engineering and Processing-Process Intensification**, v. 209, p. 110169, 2025.

ABSTRACT

The drying of rice inoculated with *Metarhizium anisopliae*, traditionally carried out in the industry by opening the cultivation plastic packages in climate-controlled rooms, faces significant limitations regarding process productivity and scaling up. This study presents an innovative approach for the technological enhancement of rice drying, utilizing a horizontal drum partially filled and operating both statically and with intermittent rotations. A two-dimensional mathematical model considering purely diffusive mass transport was employed to simulate static drying. The results indicated that 23 days are required to reach a moisture content of 0.250 kg of water per kg of dry mass, with air flowing at 50 L/min in the drum headspace and at a temperature of 30°C. The intermittent operation mode was carried out by rotating the drum at every 24 h and every 1 h and a reduction of 82.61% and 97.79%, respectively, were observed compared to the purely static operation mode. The mathematical models agreed with the experimental data, confirming their effectiveness in predicting moisture profiles and enabling scale-up studies.

Keywords: drying; *Metarhizium anisopliae*; cooked rice; mathematical model; drum.

4.1. INTRODUCTION

The generalized use of synthetic pesticides worldwide, which reached 7.2 million tons in 2020 (Shattuck et al., 2023), has serious and far-reaching consequences for the environment and human health. With the prolonged and indiscriminate use of chemical insecticides, over 800 pest species now exhibit resistance to one or more of these agents (ARPD, 2024). Driven by the need to manage pest resistance and achieve more sustainable production, farmers have been seeking alternative (Marrone, 2024), and biopesticides present themselves as an option, being harmless to mammals while effective and selective against target pests.

The biopesticide market has grown sixfold in the last decade, with an annual expansion rate of 13.6% (Markets and Markets, 2024). In 2023, this market reached USD 6.7 billion, and it is projected to grow to USD 13.9 billion by 2028 (Marrone, 2024). Brazil is considered to have the largest biological pest control program for agricultural pests, with a predominant use of entomopathogenic fungi, particularly of the genera *Metarhizium* and *Beauveria*. The fungus *Metarhizium anisopliae*, effective against more than 200 insect species, is widely used in pest control in crops and pastures, especially in sugarcane cultivation (Mascarin et al., 2019; Fontes, 2020). In the 2021-2022 season, 52% of the sugarcane area, totaling 4.74 million hectares, was treated with bioproducts in Brazil (Marrone, 2024).

The traditional process for producing conidia of *M. anisopliae* adopts solid-state cultivation (SSC) using rice as a substrate and incubating it in plastic packages (Jenkins et al., 1998; Mascarin et al., 2019) The process involves a series of steps, namely moisturization, sterilization, and inoculation of the substrate, incubation, pre-drying of the cultivated medium, extraction, and drying of spores. All of these steps are performed manually, requiring extensive labor, which reduces productivity and increases the incidence of exogenous contamination. Among the various steps that demand substantial improvement in the production process is the pre-drying of the material after SSC. This step is crucial to ensure proper spore separation during extraction and to maximize storage duration, especially in solid formulations containing aerial conidia. To enable the application of wettable powders, the conidia must be in a dormant state, which prolongs their viability, achieved through the drying process (Horaczek et al., 2004; Faria et al., 2009). Generally, drying occurs by opening the plastic packages or placing the cultivated medium in trays in a controlled-humidity environment, lasting from 3 to 5 days (Hong et al., 2000; Jaronski; Jackson, 2012). Therefore, performing drying in a closed system under controlled conditions is preferable to reduce the duration of this step and ensure the quality of the biological agent (Jaronski; Jackson, 2012).

Grain drying can be accomplished using various types of dryers, including fluidized bed (Özbey et al., 2005; Luthra; Sadaka, 2021), pneumatic (Bunyawanichakul et al., 2007), microwave (Gunasekaran, 1990; Behera et al., 2021; Silva et al., 2021), solar (Zomorodian et al., 2007; Chavan et al., 2021), fixed bed (Li et al., 2023), and rotary drum dryers (Behere et al., 2021). However, many of these systems operate at high temperatures, which adversely affects the stability of fungal conidia (Hedgecock et al., 1995). In contrast, rotary drum drying is suitable for many heat-sensitive products (Islam et al., 2007). In this context, using a horizontal drum for the drying operation emerges as a promising solution due to its high processing capacity, energy efficiency, simple design, and control alternatives (Tang et al., 2003; Yi et al., 2020). Using a static drum allows drying to occur slowly, ensuring the high viability of the conidia (Jaronski; Jackson, 2012). On the other hand, static systems can result in channeling and total loss of process control, even before the water activity is reduced to a critical level (Weber et al., 2022). Thus, mixing the particles during operation can prevent this adverse effect (Schutyser et al., 2003).

In a broader context, the drum bioreactor could consolidate multiple stages of the process into a single piece of equipment, such as substrate preparation and sterilization, inoculation, incubation (Van Breukelen et al., 2011), drying, and spore extraction (Jenkins et al., 1998; Cunha et al., 2020). The SSC process in a drum bioreactor is complex, involving microbial tolerance to agitation, particle movement and heat and mass transfer. Due to this complexity, it is common to study the phenomena individually. Agitation in drum bioreactors can be continuous or intermittent, playing a crucial role in bed uniformity, gas exchange, and heat removal (Brand et al., 2010; Mitchell; Krieger, 2019).

Metarhizium anisopliae exhibits low tolerance to intense agitation, requiring movement to be carefully controlled in specific periods and conditions to minimize damage to the microorganism (Schutyser et al., 2003; Canedo et al., 2022). The choice of the agitation regime is directly influenced by the characteristics of the substrates used and the agitation conditions adopted (Grajales et al., 2012). Furthermore, agitation plays a crucial role in heat transfer, as heat accumulation affects fungal development (Schutyser et al., 2003; Tada et al., 2020). The static operation also faces challenges related to mass transfer, especially when the filling degree is high (Lin et al., 2013; Rodríguez-Jasso et al., 2013; Da Silva et al., 2024).

Considering that the drying process typically requires a significant amount of energy and the increasing use of computational methods to describe material drying (Loncar; Pezo, 2024), simulations emerge as a promising alternative for predicting changes in moisture profiles in horizontal drums. Tada *et al*. (2020) presents a model that describes mass transport in a horizontally rotating drum partially filled with sugarcane bagasse. This model, assuming an isothermal environment and air flow parallel to the free surface of the particles, demonstrated satisfactory agreement with experimental results in predicting the moisture profile of the bed. This study aims to achieve efficient and controlled drying of rice colonized by *M. anisopliae*. To this end, the drying of rice in a partially filled horizontal drum with intermittent rotations was simulated and experimentally validated. Thus, the work presents an effective alternative to replacing traditional rice drying methods in biomanufacturing facilities, aiming to enhance process productivity.

4.2. MATERIALS AND METHODS

4.2.1. Particle

Long-grain rice (*Oryza sativa*) purchased from the local market was used in all trials. The rice was placed in plastic bags and moistened with distilled water until reaching a moisture content of 0.667 kg of water per kg of dry solid (kg-water/kg-dry solid), equivalent to the moisture level achieved after the cultivation of *Metarhizium anisopliae*, a stage that precedes the drying of the substrate. After moistening, the rice was sterilized in an autoclave at 120ºC for 30 minutes and then cooled to room temperature. The material was kept in a sterile environment for 10 days, simulating the fungus incubation period in bioproduction facilities (Dorta; Arcas, 1998; Li; Feng, 2009; Cunha et al., 2020). In this study, to better understand the effect of particle movement and mass transfer, uncultivated rice was used, which will be identified as cooked rice (CR), because there is little information in the literature about particle movement in rice covered by a layer of mycelium. The drying experiments were conducted with cooked rice, assuming that its hygroscopic characteristics are similar to those of cultivated rice (CDR).

4.2.2. Solid-State Cultivation of the fungus *Metarhizium anisopliae* in plastic packaging

To determine the impact of drying temperature on spore quality, the spores were produced through solid-state cultivation in polypropylene plastic packaging, using long-grain rice as a substrate. The fungal strain *Metarhizium anisopliae* IBCB 425, kindly provided by the Biological Institute of São Paulo, was used in all experiments. The plastic packages, equipped with short PVC tubes (5 cm internal diameter) sealed with cotton plugs to allow gas exchange while preventing contamination, were loaded with 400 g (dry basis) of rice. After hydration and autoclaving at 121°C for 30 minutes, the substrate was cooled under a laminar flow hood and inoculated with a spore suspension, followed by thorough manual mixing. Cultivation was carried out for 10 days in a climate chamber at 28°C, following established protocols (Dorta; Arcas, 1998; Li; Feng, 2009; Cunha et al., 2020).

4.2.3. Drying of conidiated rice in a climatic chamber

The drying of conidiated rice after SSC was performed in a DBO chamber, using temperatures of 20, 30, 40, 50, 60, and 70°C. For this purpose, 500 g-ds of conidiated rice were distributed on aluminum trays and kept in the chambers until reaching a moisture content of 0.250 kg-w/kg-ds. The moisture content was verified using a halogen moisture analyzer, model MB45 (Ohaus, Parsippany, USA), and all operations were conducted in duplicate.

4.2.4. Determination of Spore Viability

To evaluate spore viability, a suspension was prepared by performing liquid extraction of spores from the dried solid material. The liquid extraction was conducted by adding 10 mL/g-ds of Tween 80 solution (0.1% v/v) to the conidiated rice, followed by reciprocal shaking in a thermostatic bath at 120 cycles per minute for 50 minutes.

The spores were inoculated by drop plating (15 μL) onto Petri dishes containing Potato-Dextrose-Agar (PDA) medium and dried in a laminar flow chamber for 15 minutes (Lopes et al., 2013). The plates were incubated in a DBO chamber at 28°C for 18 hours, and the experiments were performed in triplicate. To determine the concentration of viable spores, germination was assessed after incubation via direct microscopic observation at 40x magnification. Viable spores were identified as those with germ tubes longer than the diameter of an ungerminated spore.

4.2.5. Determination of Fungus Virulence

To evaluate the influence of drying temperature on the virulence of the fungus, *Zophobas morio* larvae, measuring 0.04 m, were used. The assays were conducted by immersing the larvae in suspensions containing 10^8 conidia/mL. As a control, the larvae were immersed only in a Tween 80 (0.1% v/v) solution, and a blank was established where the larvae were not immersed in any liquid. The larvae were placed in plastic boxes with filter paper at the bottom to absorb excess suspension and covered with screens allowing for natural ventilation.

The assays were performed in triplicate, each containing fifteen larvae. The treatments were kept in a climatic chamber at 28°C for 15 days, during which the larvae were fed fresh vegetables (replaced every 2 days). The number of larval deaths was monitored daily, following the protocols described by Potrich et al. (2007) and Oreste et al. (2012).

4.2.6. Experimental determination of effective mass diffusivity

The effective mass diffusivity coefficient (D_{eff}) of water in the rice bed was experimentally determined in a tray dryer with forced air convection parallel to the surface of the bed. Air was supplied by a fan and heated by an electrical resistance bank with automatic power control to maintain the temperature at the dryer inlet at 60, 70, and 80ºC. A rectangular acrylic box with dimensions 0.20 m in length, 0.20 m in width, and 0.02 m in height was filled (ρ_{bulk} = 850 kg/m^3) with cooked rice (CR) and placed in the drying chamber. Metal screens with 0.003 m openings were placed at the top and bottom of the box to contain the particles, and air flowed parallel to the surfaces at 2 m/s. Drying kinetics were obtained by weighing the rectangular box every 10 minutes. The experiments were performed in triplicate.

The diffusion coefficient was estimated using the classical Fickian model (Crank, 1976), using the analytical solution for an semi-infinite plate, considering twelve terms of the series, according to Eq. (4.1) and adjusting to the experimental kinetics using the coefficient of determination (R^2) as the optimization criterion. The geometry of the rectangular box was considered as a semi-infinite flat plate with unidirectional mass flow. The statistical sensitivity of the effective diffusion coefficient to temperature variations was verified through an analysis of variance (ANOVA) at a 5% significance level, and the comparison between means was performed using the Tukey test via Excel®.

$$\frac{\bar{X} - X_{eq}}{X_0 - X_{eq}} = \frac{8}{\pi^2} \sum \frac{1}{(2n+1)^2} \exp\left[- \frac{(2n+1)^2 \, \pi^2 \, D_{eff} \, t}{4l^2}\right] \tag{4.1}$$

where $\bar{X}$ is the average mass fraction of water at a time t, X_0 is the initial moisture content of the solid, X_{eq} is the equilibrium moisture content of the solid, n is the number of terms in the series, l is half the thickness of the plate.

The equilibrium moisture content (X_{eq}) was determined by subjecting a known quantity of particles to drying in dry air at a flow rate of 50 L/min. For this purpose, a short cylinder with an internal diameter of 2.54 cm and a length of 4 cm, made of polyvinyl chloride, was filled. The test was stopped when no variation in moisture content was detected.

4.2.7. Experimental determination of sorption isotherms

To determine the sorption isotherms of cooked rice (CR) and conidiated rice (CDR), the static gravimetric method was used, as described by Spiess and Wolf (1983). Samples of 0.001 kg of rice were placed individually in containers where the relative humidity (RH) of the air was controlled by saturated saline solutions. The containers were kept in a climate chamber at the temperatures described in Table 4.1. The water activity (a_w) of the saline solutions at the temperatures of interest was determined using the Aw Sprint analyzer (Novasina, Lachen, Switzerland). The samples were weighed to a constant weight on an analytical balance, and all experiments were conducted in triplicate. Special care was taken to avoid contamination. To this end, the saline solutions were sterilized in an autoclave at 121ºC for 25 minutes, and the other operations were carried out in a laminar flow chamber. Special precautions were taken to prevent fungal development from interfering with the experimental results. To achieve this, the spores present in the conidiated rice were inactivated in a laminar flow chamber through direct exposure to UV light for 48 hours. The effectiveness of the inactivation was confirmed by spore germination tests, as described in Section 4.2.4.

Table 4.1. Water activity provided by the saline solutions and temperatures used to obtain the sorption isotherms of cooked rice.

Temperature	20ºC	30ºC	40ºC
Salt		**a_w**	
LiCl	0.113	0.111	0.108
CH_3COOK	0.227	0.222	0.216
$MgCl_2$	0.324	0.321	0.318
K_2CO_3	0.440	0.438	0.437
$NaNO_2$	0.561	0.555	0.548
NaCl	0.730	0.728	0.726
NaBr	0.753	0.748	0.744

The models fitted to the experimental data are presented in Table 4.2, and the Non-Linear Least Squares method was applied to estimate the parameters. The commercial software Origin 9.0 (Microcal Software Inc., Massachusetts, USA) was used for the fitting, employing the Levenberg-Marquardt algorithm to optimize the search for the minimum of the residual quadratic function.

Table 4.2. Models employed to describe the sorption isotherms.

Model	**Equation**	
Peleg (1993)	$X_{eq} = P_1\, a_w^{P_2} + P_3\, a_w^{P_4}$	(4.2)
GAB	$X_{eq} = \dfrac{P_1\, P_2\, P_3\, a_w}{(1 - P_2\, a_w)[1 + (P_3 - 1)P_2\, a_w]}$	(4.3)
Liwicki (1998)	$X_{eq} = \dfrac{P_1}{(1 - a_w)^{P_2}} - \dfrac{P_1}{1 + a_w^{P_3}}$	(4.4)
Oswin (1946)	$X_{eq} = P_1 \left(\dfrac{a_w}{1 - a_w}\right)^{P_2}$	(4.5)
Halsey (1948)	$X_{eq} = \left(\dfrac{-P_1}{\ln(a_w)}\right)^{1/P_2}$	(4.6)

Notes: (*) Extracted from Lewicki (1998); P_1, P_2 and P_3 model parameters.

4.2.8. Mathematical model of mass transfer

4.2.8.1.Model for partially filled horizontal drum

The schematic diagram of the partially filled horizontal drum with wet rice particles is presented in Figure 4.1. A two-dimensional, single-phase, isothermal mass balance based on Fick's Diffusion Law, as proposed by Tada *et al*. (2020) and described in Eq. (4.7), was adopted. In this model, no angular variation of water concentration was considered, as the radial coordinate was expressed as a function of the angular coordinate. The assumption of negligible axial moisture dispersion made by Tada *et al*. (2020) was also adopted in this study, as presented in Eq. (4.8). This assumption was made due to the high airflow used in the headspace.

$$\frac{\partial X}{\partial t} = D_{eff} \left[\frac{1}{r} \frac{\partial}{\partial r} \left(r \frac{\partial X}{\partial r}\right) + \frac{\partial^2 X}{\partial z^2}\right] \tag{4.7}$$

$$\frac{\partial X}{\partial t} = D_{eff} \left[\frac{1}{r} \frac{\partial}{\partial r} \left(r \frac{\partial X}{\partial r}\right)\right] \tag{4.8}$$

where X is the moisture content of the solids, r, and z are the radial and axial coordinates, respectively, and t is the time.

The initial and boundary conditions are presented in Eqs. (4.9) – (4.11). In these equations, the radial position $r_{i(\Theta)}$ refers to the bed surface, where a convective boundary condition is assumed due to the airflow in the headspace parallel to the surface. The radial position r = R refers to the drum wall, which is assumed to be impermeable. In the drying simulation with intermittent rotations, the final moisture content of a previous drying cycle is the initial moisture content (X_o) of the next drying cycle, considering that the rotations promote the homogenization of the moisture profile throughout the material.

$$t = 0, \qquad X = X_0 \tag{4.9}$$

$$r = r_{i(\theta)}, \qquad \rho_{ds} D_{eff} \frac{\partial X}{\partial r} = h K_d (X - X_{eq}) \tag{4.10}$$

$$r = R, \qquad D_{eff} \frac{\partial X}{\partial r} = 0 \tag{4.11}$$

where ρ_{ds} is the dry solid density, h is the convective mass transfer coefficient between the bed surface and the air flowing in the headspace, K_d is the distribution coefficient and X_{eq} is the equilibrium moisture content of the solid under the thermodynamic conditions of the air, determined through the established sorption isotherms.

The coefficient h was calculated using Eqs. (4.12) – (4.16) by analogy with the correlations of Gnielinski (1975), while the distribution coefficient was calculated using Eq. (4.17) assuming that the air is an ideal gas.

$$h = \frac{Sh\, D}{L} \tag{4.12}$$

$$Sh = \sqrt{Sh_{lam}^2 + Sh_{turb}^2} \tag{4.13}$$

$$Sh_{lam} = 0{,}664\, Re^{1/2}\, Sc^{1/3} \tag{4.14}$$

$$Sh_{turb} = \frac{0{,}037\ Re^{0{,}8}\ Sc}{1 + 2{,}433\ Re^{-0{,}1}\ (Sc^{2/3} - 1)} \tag{4.15}$$

$$Sc = \frac{\nu}{D} \tag{4.16}$$

$$K_d = \frac{M}{R_g\ T}\frac{P_{sat}}{a_w} \tag{4.17}$$

where D é is the molecular diffusivity of water vapor in the air, L is the length of the bed, ν is the kinematic viscosity of air, M is the molar mass of dry air, P_{sat} is the saturation pressure of water vapor; R_g is the universal gas constant; T is the temperature and a_w is the water activity.

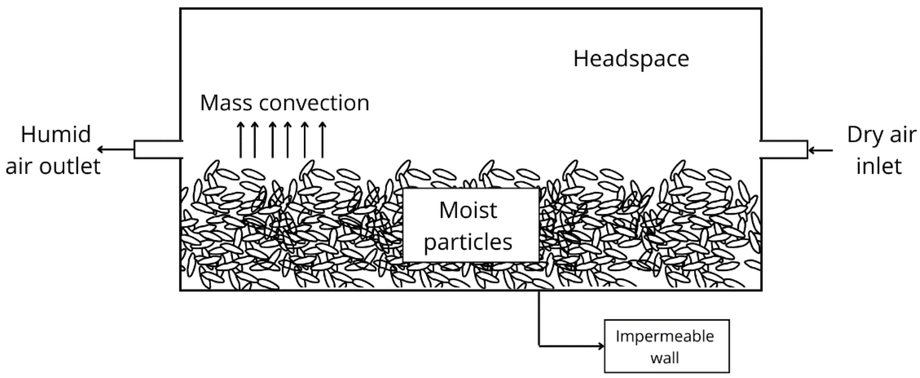

(a)

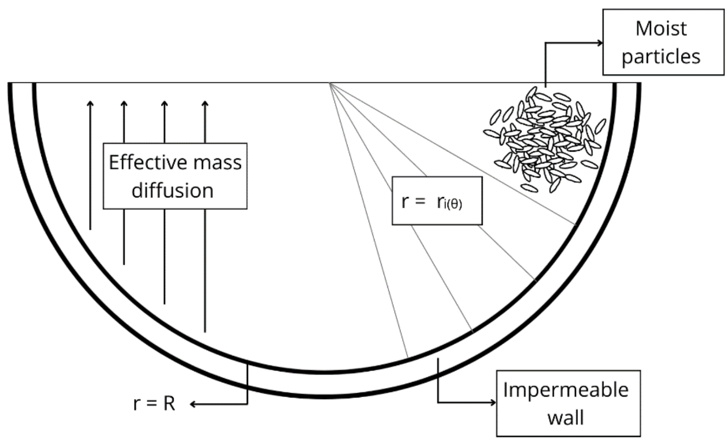

(b)

Figure 4.1. Schematic diagram of the mass transfer mechanisms (a-front view; b-side view).

4.2.8.2.Model for polypropylene plastic packaging

Figure 4.2 presents the schematic diagram of a representative plastic packaging used in industrial applications. The diffusive model applied to this geometry is described by the following equation, for which unidimensional Cartesian geometry was assumed:

$$\frac{\partial X}{\partial t} = D_{eff} \frac{\partial^2 X}{\partial y^2} \tag{4.18}$$

where y is the longitudinal coordinate.

The initial condition for solving Eq. (4.18) is similar to Eq. (4.9), while the boundary conditions are presented in Eq. (4.19) and (4.20). In these equations, the longitudinal position L_0 refers to the surface of the bed and the longitudinal position y = L_t refers to the bottom of the packaging, which is assumed to be impermeable.

$$y = L_0, \qquad \rho_{ds} D_{eff} \frac{\partial X}{\partial y} = hK(X - X_{eq}) \tag{4.19}$$

$$y = L_t, \qquad D_{eff} \frac{\partial X}{\partial y} = 0 \tag{4.20}$$

The coefficient h was calculated using Eqs. (4.21) and (4.22) for mass transfer by natural convection on a flat plate (Goldstein et al., 1975). The parameters adopted in this simulation were kept consistent with those found in traditional drying processes carried out in biofactories.

$$Ra = \frac{g\,(\rho_{air} - \rho_\infty)\,{L_l}^3}{\rho_\infty\,\nu^2}\,Sc \tag{4.21}$$

$$Sh = 0.54\ Ra^{1/4} \tag{4.22}$$

where g is the acceleration due to gravity; L_l is the length of the plate; ρ_{air} is the density of the air near the surface; ρ_∞ is the density of the air far from the surface.

(a) (b)

Figure 4.2. (a) Plastic packaging during the drying process; (b) Diagram of mass transfer on a flat plate with the conditions adopted in the mathematical model.

4.2.9. Experimental setup for drying in the horizontal drum

The mass transfer was conducted in a jacketed horizontal drum made of stainless steel with an internal diameter of 0.20 m and a length of 0.33 m, as shown in Figure 4.3. The experiments were conducted exclusively with cooked rice. The drum wall temperature was maintained at the drying temperature of 30ºC by circulating water through the jacket, which was supplied by a thermostatic bath. Air was continuously fed into the drum, also at the drying temperature, through a 0.01 m diameter tube fixed to the front lid, 0.01 m above the surface of the bed, while air exhaust was done through an identical tube at the same position on the opposite lid. The air was supplied by a radial compressor and its flow rate was measured and controlled by a rotameter. The air was dried, and its temperature was controlled by percolating it through a bed of dry silica beads placed inside a jacketed tube, whose wall was maintained at the drying temperature by water flowing through the jacket. The airflow was considered uniform and parallel to the bed surface, with a flow rate of 50 L/min. The relative humidity and temperature of the air were measured using a digital thermo-hygrometer MTH-1362 (Minipa Inc., Houston, USA). The CR load was 2 kg, corresponding to a drum filling degree of 0.50.

Two drying strategies were adopted: keeping the drum static throughout the process, rotating the drum intermittently. For the second strategy, two alternatives were used: rotating the drum every hour (CONDITION A) and rotating the drum every 24 hours (CONDITION B). At each rotation event, the drum was rotated 11 times using a roller system (PHD Equipment, Brazil) at 7 rpm, following the recommendation of Grajales *et al*. (2012) to ensure complete mixing of the particles.. To obtain local information on the moisture content of the solid, two positions within the bed were chosen for sampling: the bed surface and 0.05 m below the surface, identified as the bed center. Samples were collected at the axial position 0.15 m from the air inlet lid. A collector was used to sample particles from the bed center. Samples of 0.001 kg were taken every hour during the first 5 hours of static drying. For the intermittent rotation drying, sampling was performed before and after the rotation events until the bed moisture reached 0.250 kg-w/kg-ds. The moisture content of the particles was determined using an infrared moisture analyzer.

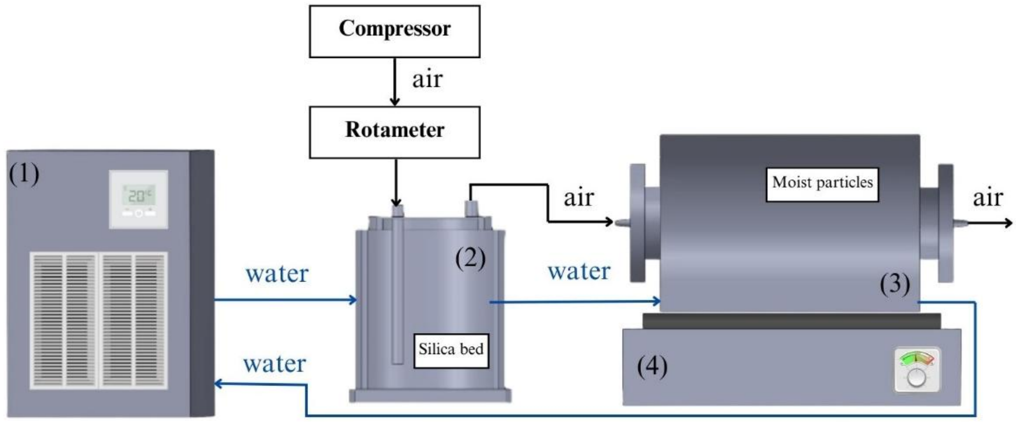

Figure 4.3. Experimental setup for static drying and intermittent rotations of rice in a partially filled horizontal drum: (1 - thermostatic bath; 2 - air drying column; 3 - drum; and 4 - rollers for rotation).

4.2.10. Experimental setup for drying in plastic packaging

The plastic packages containing CR particles was placed individually in containers maintained in climatic chambers at 30ºC. The packages had dimensions of 0.10 m in length, 0.05 m in width, and 0.03 m in height, and held 0.400 kg of CR. The relative humidity inside the containers was controlled by a NaCl saline solution, providing a_w = 0.728. Samples were taken from the surface and the bottom of the bed every 24 hours. The moisture content of the particles was determined using the MB45 moisture analyzer.

4.3. RESULTS AND DISCUSSION

4.3.1. Viability and virulence of spores in relation to drying temperature

The influence of drying temperature on spore viability and virulence is presented in Table 4.3. It is observed that as the drying temperature increases to levels above 40ºC, the number of viable and virulent spores decreases, demonstrating a negative impact of temperature on these parameters.

Table 4.3. Spore viability and virulence of spores dried at different temperatures.

Temperature (ºC)	Viable spores	*Zophobas morio* mortality
20	96.22% ± 1.39%[a]	86.67% ± 0.71%[b]
30	96.00% ± 1.76%[a]	88.89% ± 0.50%[a]
40	92.67% ± 1.76%[a]	84.44% ± 0.16%[b]
50	80.22% ± 0.77%[b]	71.11% ± 0.28%[c]
60	72.67% ± 1.33%[c]	58.78% ± 0.45%[d]
70	70.22% ± 4.44%[c]	55.56% ± 2.24%[d]

(*) means followed by the same lowercase letters in the same column do not differ significantly according to Tukey's test at the 95% confidence level.

Through the Tukey test, it is observed that regarding the viability of the spores, the temperatures of 20, 30, and 40ºC do not differ significantly. However, regarding mortality, the temperature of 30ºC presents marginally higher results.

To ensure the quality of commercial products based on pure spores, it is recommended that they have a minimum viability of 80% (Alves; Faria, 2010). Additionally, these products should cause at least 85% to 90% mortality of the target pests when applied (Schmidt et al., 2007). Therefore, using viability and virulence as parameters for ensuring the quality of the material obtained, it is observed that only temperatures between 20 and 40ºC are adequate for the operation. Hedgecock et al. (1995) reported similar results, as drying temperatures above 40ºC caused an adverse effect on the germination of *M. flavoviride* conidia. For this reason, a temperature of 30ºC was adopted in the simulations and in the validations of all the drying processes presented further.

4.3.2. Experimental determination of the effective mass diffusion coefficient

The drying kinetics and the D_{eff} coefficients obtained from fitting the solution of the second Fick's Law are presented in Table 4.4, with $R^2 = 0.98$. A gradual increase of 10ºC in the drying temperature resulted in a 40-minute reduction in the time to reach equilibrium. Similar results are described by Luangmalawat *et al*. (2007) during the drying of cooked jasmine rice at 60 and 80ºC, requiring 220 and 120 minutes, respectively.

Table 4.4. Comparison of D_{eff} values with literature values.

Temperature (ºC)	D_{eff} (m^2/s)	SD	Material	Reference
60ºC	1.00×10^{-8a}	5.23×10^{-12}	Cooked rice	Present study
	8.90×10^{-11}	-	Cooked rice	Crank (1976)
	4.83×10^{-11}	-	Cooked rice	Spiess; Wolf (1983)
70ºC	1.33×10^{-8b}	5.77×10^{-11}	Cooked rice	Present study
	7.09×10^{-11}	-	Cooked rice	Spiess; Wolf (1983)
	7.60×10^{-10}		Uncooked rice	Gnielinski (1975)
80ºC	1.75×10^{-8c}	9.75×10^{-11}	Cooked rice	Present study
	1.39×10^{-10}	-	Cooked rice	Crank (1976)
	1.02×10^{-10}	-	Cooked rice	Spiess; Wolf (1983)

(*) means followed by the same lowercase letters are not significantly different according to the Tukey test at the 95% confidence level; SD – Standard deviation.

It is observed that the drying temperature has a significant influence on the obtained D_{eff} values, with higher temperatures resulting in higher coefficients. A similar behavior was observed by Ramesh (2003) and Luangmalawat *et al*. (2007) for the drying of cooked rice particles. The dependence of D_{eff} on temperature was well described by Arrhenius-type relationships, as presented in Eq. (4.22), with $R^2 = 0.98$. This equation represents the variation of the D_{eff} parameter with temperature and has been widely reported in the literature (Elbert et al., 2001; Iguaz et al., 2003; Mukhopadhyay et al., 2019).

$$D_{eff} = 1.89 \cdot 10^{-4} * \exp\left(-27265.03/R_g \cdot T\right) \quad (4.22)$$

The diffusion coefficients obtained in this study exceed many of the values found in the literature for rice grains. However, it is crucial to consider the significant role that changes in the physical structure of the grains caused by sterilization play in moisture transport (Elbert et al. 2001), as changes in the structure and composition of foods are accompanied by changes in water transport mechanisms (Yi et al., 2020). Rice grains are primarily composed of starch, which is a glucose polymer (Yadav et al., 2024). Cooking rice grains causes starch gelatinization, forming a structural network capable of increasing water retention capacity (Goldstein et al., 1975). Gelatinization is highly dependent on temperature and vapor pressure, which are elevated during the sterilization process (Ramesh et al., 2003; Li; Feng, 2009). Conversely, cooking causes the grains to swell and consequently increase the pore size (Bakshi; Singh, 1980; Piyawanitpong et al., 2018). This expansion facilitates mass transfer, resulting in lower D_{eff} values compared to raw grains. Lin (1993) found coefficients ranging from 10^{-8} to 10^{-10} m²/s for cooked white rice, operating at temperatures between 48 and 85ºC. The higher value found is justified by the ease of removing moisture retained in large pores compared to small pores (Le et al., 2020). Piyawanitpong *et al*. (2018) demonstrate that the starch granules in black rice undergo structural changes with thermal treatment, transitioning from crystalline to amorphous due to gelatinization, and consequently exhibit pore expansion and changes in roughness (Rordprapat et al., 2005).

The differences between the experimental setup and procedures presented here and those reported in the literature make the comparison between the D_{eff} values ineffective. It must also be considered that different varieties of rice and different methods of cooking the grains can affect the results (Khatoon; Prakash, 2006). Another aspect to be considered is modeling. In this work, a pseudo-homogeneous approach was assumed for a thin flat plate of rice grains, using the unidimensional analytical solution of the second Fick's law, with air flowing parallel to both surfaces and ignoring particle shrinking. For instance, Luangmalawat *et al*. (2007) adopt air flow perpendicular to the bed surface, while Ramesh (2003) does not provide complete information on the direction of airflow, compromising comparison. Additionally, Luangmalawat *et al*. (2007) applied the pseudo-homogeneous approach to a single particle, which they assumed to be spherical, although the experimental procedure was carried out for a bed of particles, a common practice in the literature (Lu; Siebenmorgen, 1992; Alves Pereira et al., 2020). Therefore, considering a bed of moist grains, the order of D_{eff} here obtained (10^{-8}) is consistent, as it was expected that it to be higher than the values observed for a single particle.

4.3.3. Sorption Isotherms

The sorption isotherms obtained for cooked rice and conidiated rice are presented in Figure 4.4, along with the fitting provided by the GAB model. The sorption isotherms exhibit the typical sigmoid shape of type II, according to the BET classification (Brunauer et al., 1938). The equilibrium moisture content of a material such as rice generally increases with rising relative humidity at a constant temperature (Chen et al., 1993). Minimal dependence of the equilibrium moisture content on the applied temperatures can be observed. The results obtained for both materials were similar, indicating that the action of *M. anisopliae* during cultivation had little impact on the sorption behavior of rice. Thus, the hygroscopic properties determined for CR can also be applied to CDR. The determined parameters and their respective statistics are presented in Table 4.5, with the model fitting performed using a single dataset that combined all data from the various temperatures employed.

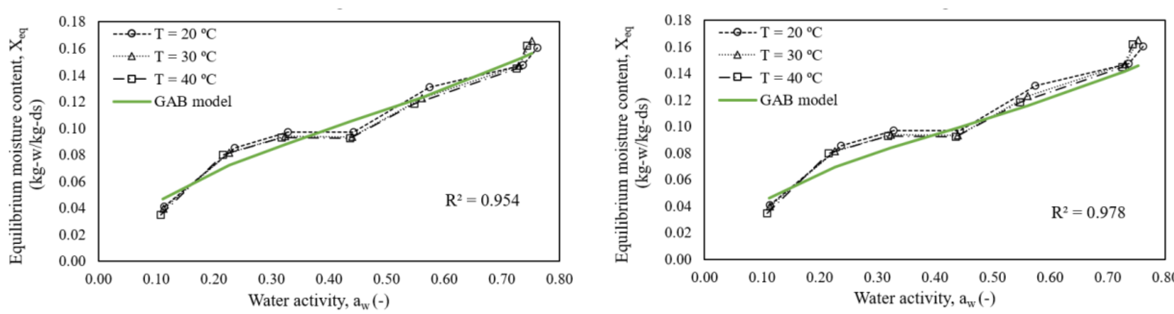

(a) (b)

Figure 4.4. Sorption isotherm of (a) cooked rice and (b) conidiated rice following type II BET classification. Little dependence of X_{eq} on the temperature (T) is noticed. The model GAB provided the best fit.

It can be observed from the coefficients of determination that all the models considered provided a good fit, regardless of the number of parameters. In contrast, Siripatrawan and Jantawat (2006) assumed that a model is considered adequate if the mean residual error (MRE) is less than 10. The GAB model exhibited a high R^2 and the lowest MRE among the tested models. This model is semi-empirical and represents the multilayer adsorption phenomenon, considering various properties of water and its interactions with the medium where it is adsorbed, and it is capable of accurately describing isotherms up to an a_w of 0.90 (Spiess; Wolf, 1983). The GAB equation is used as a standard in Europe and is recommended for describing water sorption in foods (Wolf et al., 1985).

Although many studies in the literature present sorption isotherms for various rice varieties, most of them use grains that have not undergone any treatment, especially thermal treatment (Gencturk et al., 1986; Reddy; Chakraverty, 2004; Iguaz et al., 2007; Oikonomopoulou et al., 2011; Bingol et al., 2012). The GAB model has been chosen by several researchers to model the sorption isotherm of rice (Gencturk et al., 1986; Reddy; Chakraverty, 2004; Iguaz et al., 2007; Oikonomopoulou et al., 2011). Ramesh (2003) established the isotherms for parboiled rice and fitted them to the GAB (R^2 = 0.97) and Halsey (R^2 = 0.99) models. Both models provided good fits. However, only the GAB model showed a reduced mean relative percentage error (MRE = 2.58%). Therefore, the GAB model was chosen to continue this work.

Table 4.5. Estimated parameters for the sorption isotherm models.

Model	**P**		**ΔP**	**CV**	**R^2 adj**	**MRE (%)**
Cooked rice						
Peleg	P_1	6.592	36.997	561.241	0.952	9.199
	P_2	21.208	20.669	97.459		
	P_3	0.169	0.010	5.917		
	P_4	0.577	0.059	10.225		
GAB	P_1	0.098	0.016	16.327	0.954	9.055
	P_2	0.579	0.094	16.235		
	P_3	11.673	3.080	26.386		
Lewicki	P_1	-0.053	0.006	-11.321	0.955	8.688
	P_2	-8.686	2.900	-33.387		
	P_3	-1.933	0.210	-10.864		
Oswin	P_1	0.109	0.002	1.835	0.940	11.680
	P_2	0.340	0.022	6.471		
Halsey	P_1	0.006	0.002	33.333	0.912	14.138
	P_2	2.083	0.157	7.537		
Conidated rice						
Peleg	P_1	0.477	1.428	299.080	0.977	5.326
	P_2	12.053	10.944	90.802		
	P_3	0.154	0.007	4.645		
	P_4	0.539	0.041	7.626		
GAB	P_1	0.091	0.009	10.159	0.978	5.274
	P_2	0.575	0.060	10.378		
	P_3	13.173	2.326	17.653		
Lewicki	P_1	-0.051	0.003	-6.659	0.978	5.090
	P_2	-9.241	2.009	-21.741		
	P_3	-1.867	0.134	-7.187		
Oswin	P_1	0.103	0.002	1.490	0.965	7.117
	P_2	0.326	0.002	4.772		
Halsey	P_1	0.005	0.001	29.550	0.937	10.042
	P_2	2.168	0.136	6.251		

ΔP - standard error; CV - coefficient of variation; R^2 adj - adjusted coefficient of determination; MRE - mean relative percentage error.

4.3.4. Simulations of mass transfer in a plastic package

Drying in traditional biomanufacturing facilities occurs in rooms with controlled relative humidity and temperature (Jenkins et al., 1998; Ibrahim et al., 2015). However, drying conditions vary among production units. Generally, the drying process of the cultivated medium is lengthy, and control alternatives are inadequate because the packages are placed on shelves in climate-controlled rooms, with a single room potentially containing over 300 kg of rice with the cultivation process still ongoing. Alternatively, colonized rice is placed on trays to facilitate the drying process. In facilities with more technological resources, the water activity of the medium is measured, and the drying phase is completed when the water activity of the medium is equal to or less than 0.40 (Bateman, 2007; Jaronski; Jackson, 2012). Thus, simulation is essential for improving the process and enhancing the product.

The parameters used in the mass transfer simulations for a flat plate are presented in Table 4.6. The model simulates the drying of cooked rice in plastic packaging placed in a climate-controlled room at 30 °C with a relative humidity of 70%. Mass transport occurs only through the surface of the bed due to the water concentration gradient established between the ambient air and the particle bed. Figure 4.5 shows the simulated moisture content distribution for the cooked rice bed.

Table 4.6. Simulation conditions for the packaging.

Symbol	Description	Values
L_t	Layer thickness	0.03 m
L_l	Layer length	0.10 m
T_{bed}	Bed temperature	30ºC
T_{air}	Air temperature	30ºC
T_w	Wall temperature	30ºC
RH	Relative humidity	70 %
X_0	Initial solid moisture content	0.667 kg-w/kg-ds
X_{eq}	Equilibrium solid moisture content	0.126 kg-w/kg-ds
D_{eff}	Effective mass diffusivity of water	3.788×10^{-9} m^2/s
h	Bed-to-headspace mass transfer coefficient	3.400×10^{-5} m/s
K	Distribution coefficient	0.264 kg-ds/m^3
D	Molecular diffusivity of the water in the air	2.205×10^{-5} m^2/s
ν	Air kinematic viscosity	1.516×10^{-5} m^2/s
ρ_{air}	Air density	1.164 kg/m^3

Cultivated rice must be dried to approximately 0.250 kg-w/kg-ds of moisture so that the spores can be extracted (Jenkins et al., 1998). In the simulations, to achieve this moisture level in the last layer of particles on the plate, 8 days of drying are required. Studies demonstrate a substantial beneficial effect of slow drying of infective propagules, maintaining high viability when dried for 5 to 9 days, as done in traditional biomanufacturing facilities (Hong et al., 2000; Jaronski; Jackson, 2012). However, it should be noted that the drying is only slow for the CR particles located at the bottom of the packaging. The grain drying process can be divided into two distinct phases: a constant rate drying period and one or more periods of decreasing drying rate (Sahni et al., 2012). In the first stage, free water weakly bound to the saturated surface of the grain is evaporated through a convective mechanism. Subsequently, when the surface is no longer saturated, surface water needs to be replenished by the water inside the grain, and the diffusive mechanism starts to dominate the process, leading to the decreasing drying rate period (Sahni et al., 2012; Yi et al., 2020).

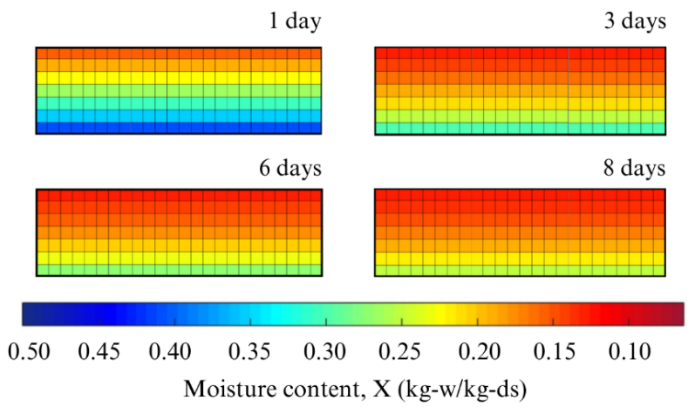

Figure 4.5. Simulated moisture profiles for the drying of cooked rice in plastic packaging approximated to a flat plate with a thickness of 0.03 m (RH = 70%; T = 30 °C).

In Figure 4.6, the average moisture content of the particle bed during the eight-day process is presented. At the end of drying, the particles have an average moisture content of 0.221 kg-w/kg-ds. It is observed that by the third day, the average moisture is 0.248 kg-w/kg-ds, which is below the desired 0.250 kg-w/kg-ds, potentially allowing for early termination of the process, provided that the particles are periodically mixed to achieve uniform moisture throughout the bed. However, mixing these particles in plastic packaging would cause several inconveniences. Opening the packages by employees to initiate the drying process inevitably releases particulate material into the air, which can lead to respiratory issues, especially if proper protective measures are not adopted. This highlights the need for more controlled and safer drying methods for the workers.

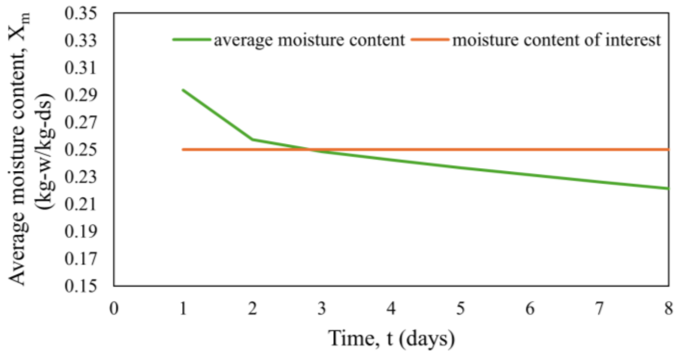

Figure 4.6. The simulated average moisture content of the cooked rice bed during drying in plastic packaging, assuming a flat plate configuration with a thickness of 0.03 m (RH = 70%; T = 30 °C).

4.3.5. Simulation of mass transfer in a horizontal drum

4.3.5.1.Static operation

The conditions and parameters used in the static drying simulations in a horizontal drum are presented in Table 4.7. Figure 4.7 shows the simulated moisture content distribution in the drum partially filled with cooked rice after 23 days of drying when the last layer of particles reaches the final desired moisture content of 0.250 kg-w/kg-ds. With a fill degree of 0.50, the thickness of the grain layer equals the drum radius, which is 0.10 m. Mass transport occurs only through the surface of the bed, as the air flowing in the headspace is the only driving force for water removal, with the drum wall considered impermeable. Inside the bed, transport is purely diffusive, controlled by the low value of the effective diffusion coefficient. Figure 4.8 shows the average moisture contents of the bed as a function of time.

After 23 days of drying, the particles in direct contact with the airflow have a moisture content of 0.069 kg-w/kg-ds, while the particles located in a 0.03 m thick layer from the free surface have an average moisture content of 0.084 kg-w/kg-ds. In contrast, the particles situated between the center and the bottom of the bed have an average moisture content of 0.119 kg-w/kg-ds. Mass transfer occurs exclusively at the surface, between the air and the top layer of grains, in a region known as the drying zone (Moore et al., 1996). Given the high flow rate of dry air, the moisture gradient within the bed is intense, drastically reducing the moisture content of the particles in the upper layers.

Table 4.7. Conditions and parameters used for mass transfer simulations in a partially filled horizontal drum.

Symbol	Description	Values
f	Filling degree	0.50
R	Radius of the drum	0.10 m
L_d	Length of the drum	0.33 m
T_{bed}	Bed temperature	30ºC
T_{air}	Air temperature	30ºC
T_w	Drum-wall temperature	30ºC
U_{air}	Air humidity	15 % (b.u.)
X_0	Initial solid moisture content	0.667 kg-w/kg-ds
X_{eq}	Equilibrium solid moisture content	0.056 kg-w/kg-ds
D_{eff}	Effective diffusivity of water in rice bed	$3.788x10^{-9}$ m^2/s
Q	Air flow rate	50 L/min
h	Bed-to-headspace mass transfer coefficient	$5.580x10^{-4}$ m/s
K	Distribution coefficient	0.266 $kg-ds/m^3$

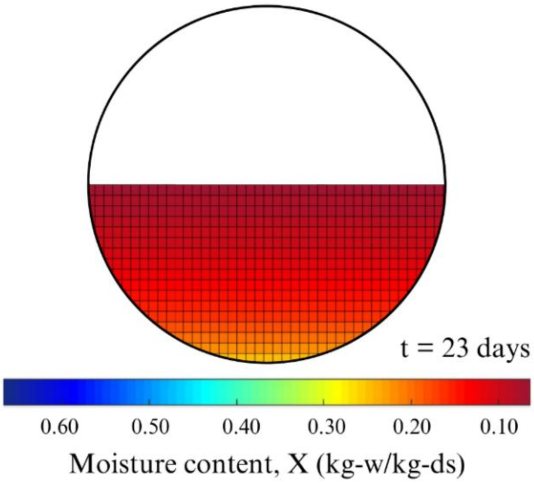

Figure 4.7. Simulated moisture distribution of cooked rice after 23 days of drying in a partially filled static horizontal drum (RH = 15%; T = 30 °C; Q = 50 L/min).

The maximum stability of spores desired for storage is achieved when the moisture content is between 0.042 and 0.052 kg-w/kg-ds, providing greater temperature tolerance (Hedgecock et al., 1995; Moore et al., 1996; Mar et al., 2012). However, excessive drying, resulting in water activity below 0.10, may compromise conidial quality due to damage to the plasma membrane during the subsequent soaking stage for spray preparation (Faria et al., 2009; Jaronski, 2014). It is crucial to highlight that after the drying stage of the cultivated medium, the material will be sent for extraction in the industries. Subsequently, the spores undergo a second drying stage, as they must have a moisture content below 0.111 kg-w/kg-ds or a water activity lower than 0.30 to be stored under freezing conditions. Finally, the spores are mixed with other ingredients to formulate the product known as wettable dry powder (Jaronski; Jackson, 2012). Therefore, the moisture gradient of the particles at the end of static drying can result in excessively dry spores at the end of the production process.

Another negative aspect is the long drying time. Figure 4.8 shows that the static drying process results in particles with an average moisture content lower than desired at the end of the drying process. This occurs due to the moisture gradient between particle layers, as the drying process is only completed when the last layer of particles reaches a moisture content of 0.250 kg-w/kg-ds. It is noted that after eight days of static drying, the average moisture content of the bed reaches 0.250 kg-w/kg-ds, as desired. During this period, the last layer of particles in the drum still has a moisture content of 0.379 kg-w/kg-ds. Alternatively, the drum could be rotated to homogenize the particles and enhance mass transfer, as will be discussed in the next section.

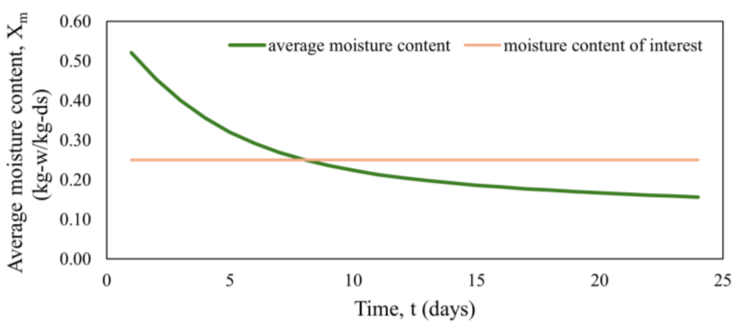

Figure 4.8. Simulated average moisture content of the cooked rice bed during static drying in a partially filled horizontal drum (RH = 15%; T = 30 °C; Q = 50 L/min).

4.3.5.2. Operation with intermittent rotations

The conditions and parameters used in the simulations of drying in a horizontal drum with intermittent rotations are presented in Table 4.7. Figure 4.9 illustrates the simulated moisture content profile in the drum partially filled with cooked rice, rotating every 1 hour of static drying (CONDITION A), while Figure 4.10 shows the simulated profile with the drum rotating every 24 hours (CONDITION B). It is observed that to achieve the desired moisture content for all particles, 16 and 97 hours are required for CONDITION A and CONDITION B, respectively.

Intermittent rotations are effective in reducing drying time, as rotation allows for the homogenization of the particle bed after a period of static drying. This homogenization repositions wetter particles to the surface, where the driving force of drying occurs. Additionally, it places wet and dry particles side by side, promoting mass transfer within the bed. Thus, both drying mechanisms, convection, and diffusion, are enhanced. Compared to completely static drying in the drum, intermittent rotations reduce drying time by 97.10% and 82.61% for CONDITION A and CONDITION B, respectively. However, the effects of drying speed on the quality of the propagules, an important commercial aspect that will determine the effectiveness of the product in the field, are still not well understood. Hong *et al*. (2000) compared the impacts of slow and rapid drying of basmati rice on the shelf life of infective propagules from *M. flavoviride*. The authors observed that rapidly dried conidia had a shorter shelf life compared to those dried slowly. However, the reduction in shelf life was slight and did not discourage the use of rapid drying.

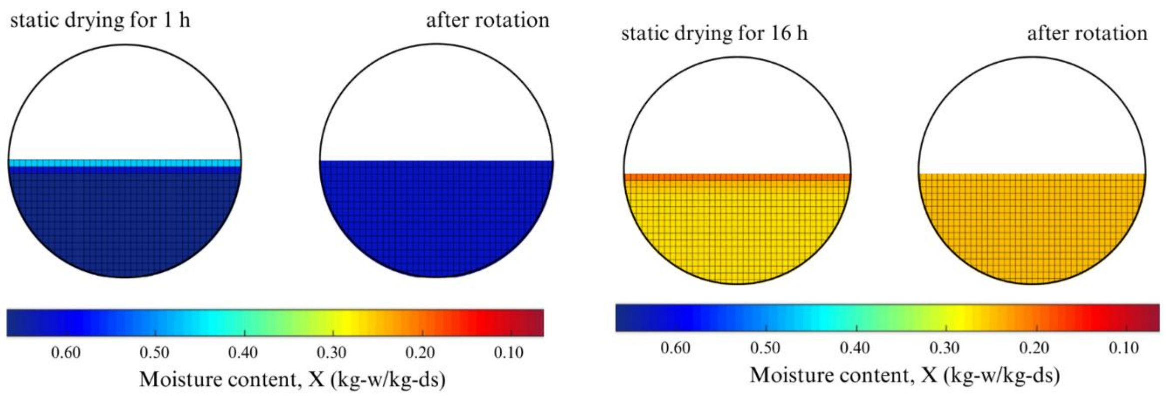

(a) (b)

Figure 4.9. Simulated moisture content distribution for the drying of cooked rice in a partially filled horizontal drum with rotations every 1 hour (CONDITION A) (a - after the first hour of drying; b - at the end of the process) (RH = 15%; T = 30 °C; Q = 50 L/min).

Figure 4.11 shows that both intermittent drying processes resulted in particles with an average moisture content equal to the desired level at the end of the drying process, differing only in the final processing time. This reduces the drying time compared to plastic packaging and prevents the formation of excessively dry particles that could compromise spore quality, in addition to facilitating the standardization of subsequent stages (extraction and spore drying).

If only the pre-drying stage is considered, the use of the drum is valuable, as it might reduce the drying time of the cultivated medium by up to 95%. Additionally, since spore extraction can be performed with the same equipment, this represents a significant improvement to the process. If all steps, except for spore drying, could be conducted in the drum bioreactor, it would represent a major innovation in the process.

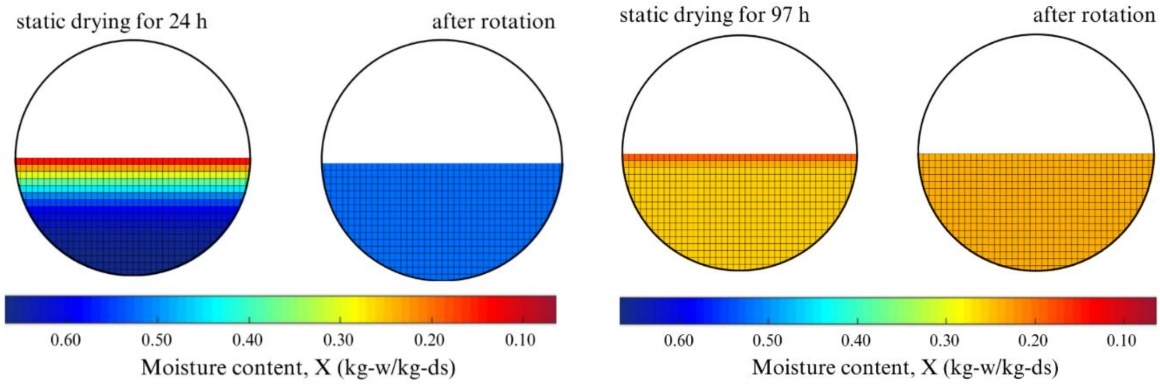

(a) (b)

Figure 4.10. Simulated moisture content distribution for the drying of cooked rice in a partially filled horizontal drum with rotations every 24 hours (CONDITION B) (a - after the first 24 hours of drying; b - at the end of the process) (RH = 15%; T = 30 °C; Q = 50 L/min).

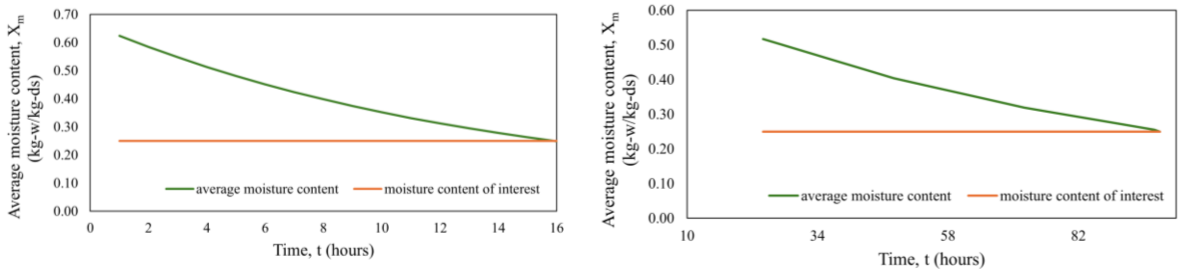

(a) (b)

Figure 4.11. Simulated average moisture content of the cooked rice bed during drying in a partially filled horizontal drum with rotations (a – CONDITION A; b – CONDITION B) (RH = 15%; T = 30 °C; Q = 50 L/min).

4.3.6. Model experimental validation

Figures 4.12 – 4.15 present simulated and experimental data for beds of cooked rice when dried in plastic packaging and in a horizontal drum with and without rotations. Two positions within the bed were chosen for comparison in the drum: at the free surface and the center of the bed, 0.05 m from the surface, as indicated in the Figures. For experiments in the horizontal drum with rotations, in addition to these measurements, moisture content was determined at the center of the bed after particle homogenization.

The proposed model provides a good representation of the actual drying behavior of cooked rice in plastic packaging and in a horizontal drum with rotations every 1 and 24 hours. The same can be said for the static horizontal drum drying system, noting that samples were only collected during the first 5 hours of the process. Overall, the agreement between experimental and simulated results is supported by the high determination coefficients and root of the mean square error (RMSE) values found. The results collected for the surface show the greatest variation, which is justified by the larger moisture gradient in this zone compared to the center or bottom of the particle bed. Tada *et al*. (2020) demonstrated a good fit of this model when applied to experimental data from beds of silica gel and sugarcane bagasse with low and high airflow rates in the headspace.

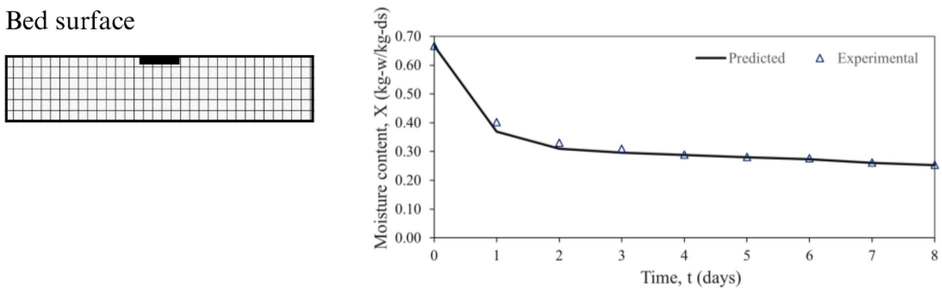

(a) R^2 = 0.982; RMSE = 0.027 kg-w/kg-ds

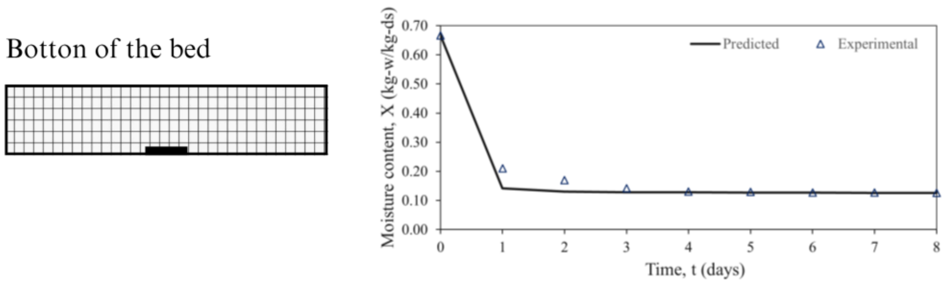

(b) R^2 = 0.991; RMSE = 0.014 kg-w/kg-ds

Figure 4.12. Experimental validation of the moisture content predicted by the model for the drying of cooked rice in plastic packaging (a - at the surface; b - at the bottom of the bed, y = 0,03 m).

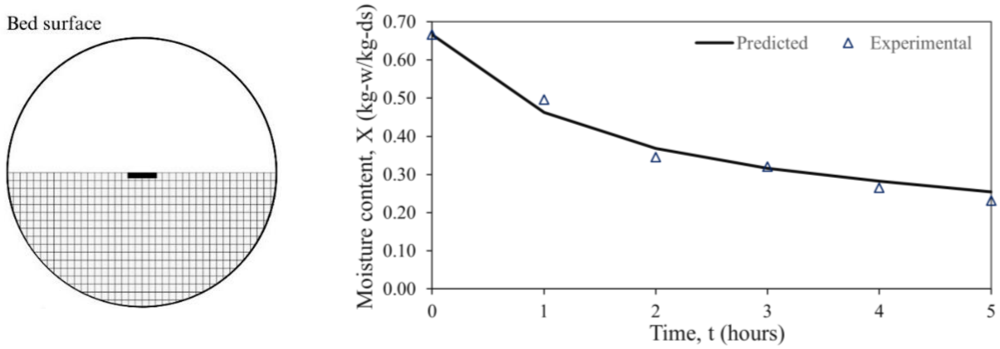

(a) $R^2 = 0.982$; RMSE = 0.020 kg-w/kg-ds

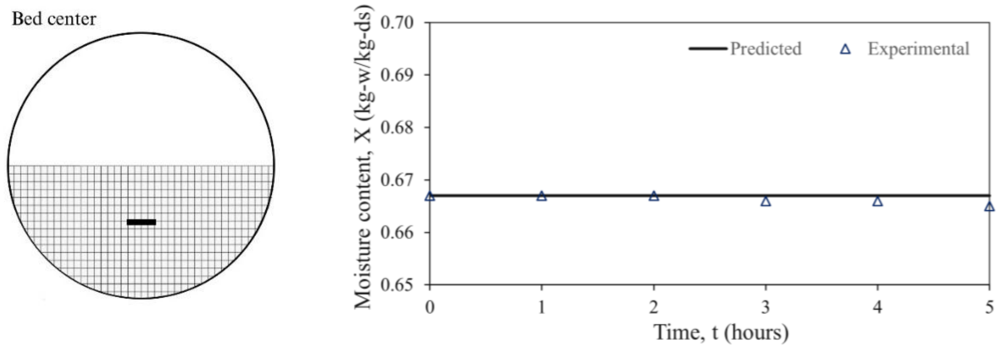

(b) $R^2 = 1$; RMSE = 0.001 kg-w/kg-ds

Figure 4.13. Experimental validation of the moisture content predicted by the model for static drying of cooked rice in a partially filled horizontal drum (a - at the surface; b - at the center of the bed, r = 0.05 m).

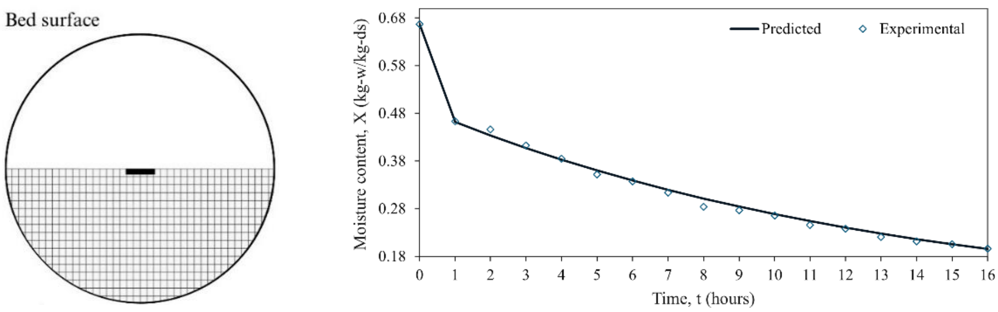

(a) $R^2 = 0.995$; RMSE = 0.007 kg-w/kg-ds

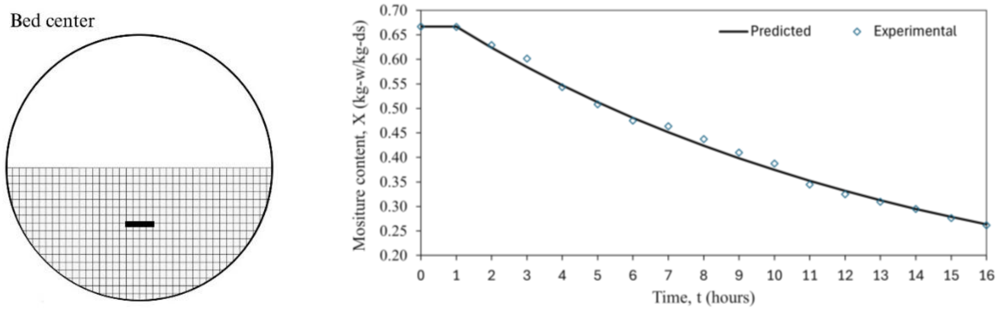

(b) $R^2 = 0.995$; RMSE = 0.008 kg-w/kg-ds

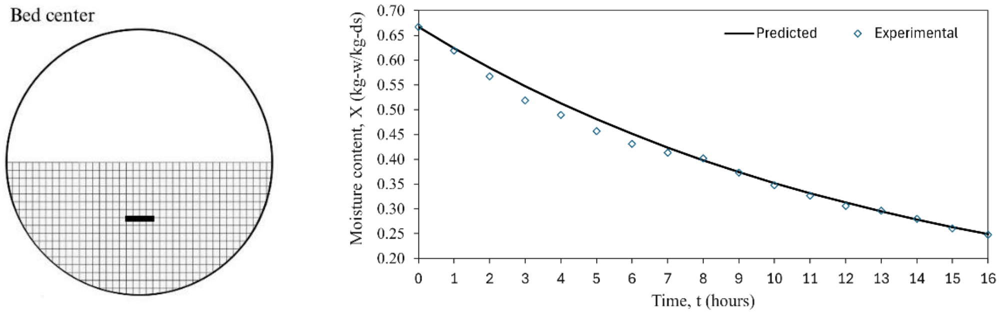

(c) $R^2 = 0.995$; RMSE = 0.013 kg-w/kg-ds

Figure 4.14. Experimental validation of the moisture contents predicted by the model for drying cooked rice in a partially filled horizontal drum with rotations every 1 hour (CONDITION A) (a - at the surface; b - at the center of the bed; c - at the center of the bed after rotation with homogenized moisture profile).

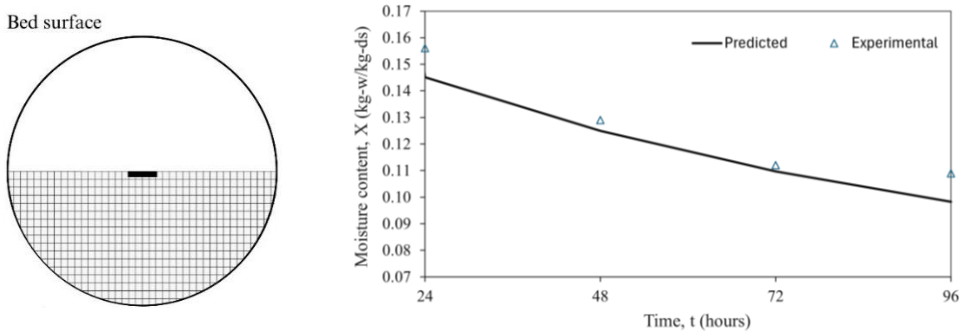

(a) R^2 = 0.938; RMSE = 0.007 kg-w/kg-ds

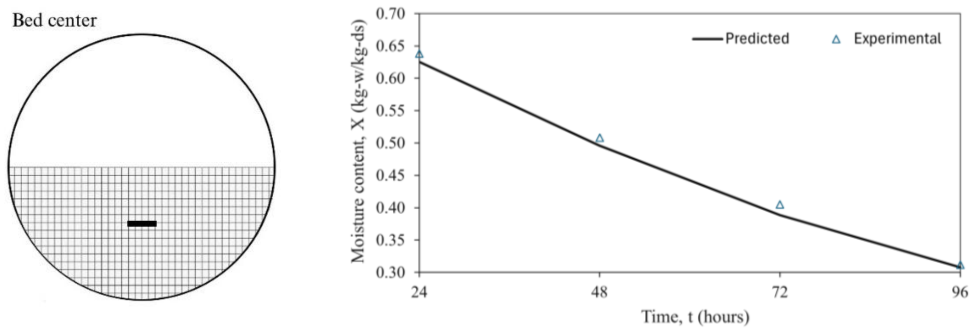

(b) R^2 = 0.998; RMSE = 0.011 kg-w/kg-ds

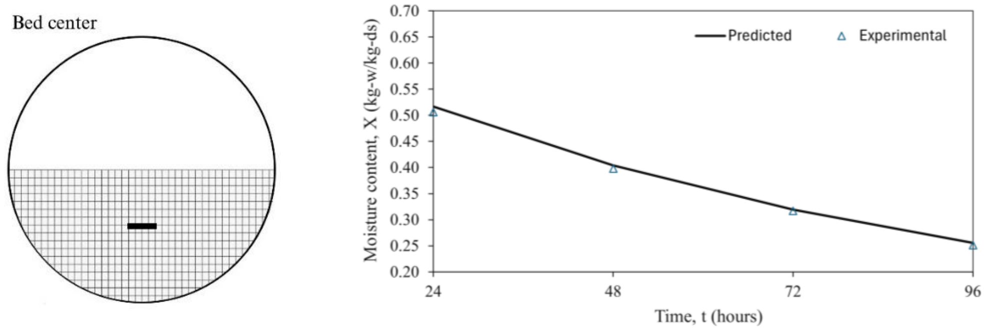

(c) R^2 = 0.999; RMSE = 0.006 kg-w/kg-ds

Figure 4.15. Experimental validation of the moisture contents predicted by the model for drying cooked rice in a partially filled horizontal drum with rotations every 24 hours (CONDITION B) (a - at the surface; b - at the center of the bed; c - at the center of the bed after rotation with homogenized moisture profile).

4.4.CONCLUSION

The drying of rice in a partially filled horizontal drum to produce *Metarhizium anisopliae* spores was simulated and experimentally validated under static and intermittent rotation conditions (every 1 and 24 hours). The drying was isothermal at 30 °C, the drum was filled to 50% of its volume, and dry air flowed at high rates in the headspace. Simulations were also conducted for natural convection drying in plastic packaging, a method commonly used in biomanufacturing. To conduct the simulations, experimental values of effective mass transfer diffusivity (D_{eff}) for wet rice and sorption isotherms were determined. The GAB model was used to describe the sorption isotherms of cooked rice. Drying in plastic packaging required 8 days for all particles to reach the recommended moisture content of 0.250 kg-w/kg-ds, whereas static drying in the drum required 23 days. The extended time required for static drying, as well as the moisture gradient formed between the layers of the bed, make this drum configuration impractical. Intermittent rotation of the drum accelerated the process, requiring 16 and 97 hours for the particles to reach the desired moisture content, with rotation intervals of every 1 and 24 hours, respectively. Experiments in a horizontal drum filled with cooked rice were conducted both statically and with intermittent rotations, and the results showed good agreement between predicted and experimental values. Therefore, the drying process in a horizontal drum with intermittent rotations emerges as a promising alternative for process optimization, allowing for controlled operation with reduced direct labor and scalability.

4.5 REFERENCES

ALVES PEREIRA, J. C. et al. Continuous and Intermittent Drying of Rough Rice: Effects on Process Effective Time and Effective Mass Diffusivity. **Agriculture**, v. 10, n. 7, p. 282, 9 jul. 2020.

ALVES, R. T.; FARIA, M. Pequeno manual sobre fungos entomopatogênicos. **Planaltina (DF), Embrapa Cerrados**, p. 26-31, 2010.

ARPD, Arthropod pesticide resistance database. https://www.pesticideresistance.org/search.php, 2023 (accessed 23 Apryl 2024).

BAKSHI, A. S.; SINGH, R. P. Kinetics of water diffusion and starch gelatinization during rice parboiling. **Journal of Food Science**, v. 45, n. 5, p. 1387–1392, set. 1980.

BATEMAN, R. Production Processes for Anamorphic Fungi IPARC, Silwood Park. **Ascot, Berks. 16pp.** Available online at: http://www. dropdata. net/mycoharvester/Mass_production. PDF, 2007.

BEHERA, G.; SUTAR, P. P. Starch gelatinization and drying of paddy using microwave rotary drum dryer: Optimization, kinetics, and cooking studies. **Drying Technology**, v. 39, n. 7, p. 965–981, 3 maio 2021.

BINGOL, G.; PRAKASH, B.; PAN, Z. Dynamic vapor sorption isotherms of medium grain rice varieties. **LWT - Food Science and Technology**, v. 48, n. 2, p. 156–163, out. 2012.

BRAND, D. et al. Production of fungal biological control agents through solid state fermentation: a case study on Paecilomyces lilacinus against root-knot nematodes. **Micologia Aplicada International**, v. 22, n. 1, p. 31-48, 2010.

BROOKER, D.B. Brooker, BAKKER-ARKEMA, F. W., HALL, C.W. Drying cereal grains, The AVI Publishing Company Inc., Westport, 1974.

BRUNAUER, S.; EMMETT, P. H.; TELLER, E. Adsorption of Gases in Multimolecular Layers. **Journal of the American Chemical Society**, v. 60, n. 2, p. 309–319, fev. 1938.

BUNYAWANICHAKUL, P. et al. Modelling and Simulation of Paddy Grain (Rice) Drying in a Simple Pneumatic Dryer. **Biosystems Engineering**, v. 96, n. 3, p. 335–344, mar. 2007.
CANEDO, M. S.; FIGUEIREDO, M. F. S.; THOMÉO, J. C. Rheological properties of mixtures of sugarcane bagasse and wheat bran during solid-state cultivation. **Brazilian Journal of Chemical Engineering**, v. 39, n. 1, p. 11-22, 2022.
CHAVAN, A. et al. CFD simulation of solar grain dryer. **Drying Technology**, v. 39, n. 8, p. 1101–1113, 14 maio 2021.
CHEN, T. S.; BUCHANAN, W. P.; ARMALY, B. F. Natural convection on vertical and horizontal plates with vectored surface mass transfer. **International Journal of Heat and Mass Transfer**, v. 36, n. 2, p. 479–487, jan. 1993.
CRANK, J. **The mathematics of diffusion**. 2. ed., reprint ed. Oxford: Clarendon Press, 1976.
CUNHA, L. P. et al. Metarhizium anisopliae conidia production in packed-bed bioreactor using rice as substrate in successive cultivations. **Process Biochemistry**, v. 97, p. 104–111, out. 2020.
DA SILVA, M. P. D. et al. Heat analysis of a sugarcane bagasse and wheat bran system in rotating drum bioreactor for cellulase production. In: **Agroenergy**. Woodhead Publishing, p. 351-364, 2024.
DORTA, B.; ARCAS, J. Sporulation of Metarhizium anisopliae in solid-state fermentation with forced aeration. **Enzyme and Microbial Technology**, v. 23, n. 7–8, p. 501–505, nov. 1998.
ELBERT, G. et al. A diffusion model with a moisture dependent diffusion coefficient for parboiled rice. **Drying Technology**, v. 19, n. 1, p. 155–166, 31 jan. 2001.
FARIA, M.; HAJEK, A. E.; WRAIGHT, S. P. Imbibitional damage in conidia of the entomopathogenic fungi Beauveria bassiana, Metarhizium acridum, and Metarhizium anisopliae. **Biological Control**, v. 51, n. 3, p. 346–354, dez. 2009.
FONTES, E. M. G.; VALADARES-INGLIS, M. C. Controle biológico de pragas da agricultura. 2020.
GENCTURK, M. B. et al. Moisture transfer properties of wild rice. **Journal of Food Process Engineering**, v. 8, n. 4, p. 243–261, out. 1986.
GNIELINSKI, V. V. Neue Gleichungen fiir den Wiirme- und den Stoffiibergang in turbulent durchstrSmten Rohren und Kan/ilen. 1975.
GOLDSTEIN, R. J.; SPARROW, E. M.; JONES, D. C. Natural convection mass transfer adjacent to horizontal plates. **International Journal of Heat and Mass Transfer**, v. 16, n. 5, p. 1025-1035, 1973.
GRAJALES, L. M. et al. Mixing and motion of rice particles in a rotating drum. **Powder Technology**, v. 222, p. 167–175, maio 2012.
GUNASEKARAN, S. Grain drying using continuous and pulsed microwave energy. **Drying Technology**, v. 8, n. 5, p. 1039–1047, jan. 1990.
HEDGECOCK, S. et al. Influence of Moisture Content on Temperature Tolerance and Storage of Metarhizium flavoviride Conidia in an Oil Formulation. **Biocontrol Science and Technology**, v. 5, n. 3, p. 371–378, set. 1995.
HONG, T. D.; JENKINS, N. E.; ELLIS, R. H. The effects of duration of development and drying regime on the longevity of conidia of Metarhizium flavoviride. **Mycological Research**, v. 104, n. 6, p. 662–665, jun. 2000.
HORACZEK, A.; VIERNSTEIN, H. Beauveria brongniartii subjected to spray-drying in a composite carrier matrix system. **Journal of Microencapsulation**, v. 21, n. 3, p. 317–330, maio 2004.
IBRAHIM, L. et al. Mass Production, Yield, Quality, Formulation and Efficacy of Entomopathogenic Metarhizium anisopliae Conidia. **British Journal of Applied Science & Technology**, v. 9, n. 5, p. 427–440, 10 jan. 2015.
IGUAZ, A. et al. Modelling effective moisture difusivity of rough rice (Lido cultivar) at low drying temperatures. **Journal of Food Engineering**, v. 59, n. 2–3, p. 253–258, set. 2003.

IGUAZ, A.; VÍRSEDA, P. Moisture desorption isotherms of rough rice at high temperatures. **Journal of Food Engineering**, v. 79, n. 3, p. 794–802, abr. 2007.
ISLAM, MD. R.; THAKER, K. S.; MUJUMDAR, A. S. A Diffusion Model for a Drum Dryer Subjected to Conduction, Convection, and Radiant Heat Input. **Drying Technology**, v. 25, n. 6, p. 1033–1043, 11 jun. 2007.
JARONSKI, S. T. Mass Production of Entomopathogenic Fungi: State of the Art. **Mass Production of Beneficial Organisms**, p. 357–413, 2014.
JARONSKI, S. T.; JACKSON, M. A. Mass production of entomopathogenic Hypocreales. Em: **Manual of Techniques in Invertebrate Pathology**. [s.l.] Elsevier, p. 255–284, 2012.
JENKINS, N. E. et al. Development of mass production technology for aerial conidia for use as mycopesticides. v. 19, n. 1, 1998.
KHATOON, N.; PRAKASH, J. Nutritional Quality of Microwave and Pressure Cooked Rice (Oryza sativa) Varieties. **Food Science and Technology International**, v. 12, n. 4, p. 297–305, ago. 2006.
LE, K. H. et al. Experimental benchmarking of diffusion and reduced models for convective drying of single rice grains. **Drying Technology**, v. 38, n. 1–2, p. 200–210, 2 jan. 2020.
LI, J.; FENG, M.-G. Intraspecific tolerance of Metarhizium anisopliae conidia to the upper thermal limits of summer with a description of a quantitative assay system. **Mycological Research**, v. 113, n. 1, p. 93–99, jan. 2009.
LI, X. et al. Simulation study on coupled heat and moisture transfer in grain drying process based on discrete element and finite element method. **Drying Technology**, v. 41, n. 12, p. 2027–2041, 11 set. 2023.
LIN, Y. et al. Ethanol production by simultaneous saccharification and fermentation in rotary drum reactor using thermotolerant Kluveromyces marxianus. **Applied energy**, v. 105, p. 389-394, 2013.
LIN, S. H. Water uptake and gelatinization of white rice. **LWT-Food Science and Technology**, v. 26, n. 3, p. 276-280, 1993.
LU, R.; SIEBENMORGEN, T. J. Moisture diffusivity of long-grain rice components. **Transactions of the ASAE**, v. 35, n. 6, p. 1955-1961, 1992.
LUANGMALAWAT, P. et al. Effect of temperature on drying characteristics and quality of cooked rice. **LWT - Food Science and Technology**, v. 41, n. 4, p. 716–723, maio 2008.
LUTHRA, K.; SADAKA, S. S. Mathematical modeling of rough rice dehydration with dehumidified air in a fluidized bed drying system. **Applied Engineering in Agriculture**, v. 37, n. 5, p. 783-791, 2021.
MAR, T. T.; LUMYONG, S. Conidial production of entomopathogenic fungi in solid state fermentation. **KKU Research Journal**, v. 17, n. 5, p. 762-768, 2012.
MARKETS AND MARKETS, Bipesticides by type (bioinsecticides, biofungicides, bionematicides), crop type (cereals & grains, oilseeds & pulses), formulation (liquid and dry), source (microbial, biochemical), mode of application, region – Global forecast to 2028. https://www.marketsandmarkets.com/Market-Reports/bi opesticides-267.html?gad_source=1&gclid=Cj0KCQjw_qexBhCoARIsAFgBles 9LWx4LwQWik7SOomvpwyJ5pwIHVqYMu_XqZGEvHe zQY8qyWLyvDoaAvaFEALw_wcB, 2023 (accessed 13 Apryl 2024).
MARRONE, P. G. Status of the biopesticide market and prospects for new bioherbicides. **Pest Management Science**, v. 80, n. 1, p. 81–86, jan. 2024.
MASCARIN, G. M. et al. Current status and perspectives of fungal entomopathogens used for microbial control of arthropod pests in Brazil. **Journal of Invertebrate Pathology**, v. 165, p. 46–53, jul. 2019.
MITCHELL, D. A.; KRIEGER, N. Solid-state cultivation bioreactors. **Essentials in Fermentation Technology**, p. 105-133, 2019.

MOORE, D. et al. Effects of Moisture Content and Temperature on Storage of Metarhizium flavoviride Conidia. **Biocontrol Science and Technology**, v. 6, n. 1, p. 51–62, mar. 1996.

MUKHOPADHYAY, S.; SIEBENMORGEN, T. J.; MAUROMOUSTAKOS, A. Effect of tempering approach following cross-flow drying on rice milling yields. **Drying Technology**, v. 37, n. 16, p. 2137–2151, 10 dez. 2019.

OIKONOMOPOULOU, V. P.; KROKIDA, M. K.; KARATHANOS, V. T. Structural properties of freeze-dried rice. **Journal of Food Engineering**, v. 107, n. 3–4, p. 326–333, dez. 2011.

ORESTE, M. et al. Pathogenicity of Beauveria bassiana (Bals.-Criv.) Vuill. and Metarhizium anisopliae (Metschn.) Sorokin against Galleria mellonella L. and Tenebrio molitor L. in laboratory assays. **Redia**, v. 95, p. 43-48, 2012.

ÖZBEY, M.; SÖYLEMEZ, M. S. Effect of swirling flow on fluidized bed drying of wheat grains. **Energy Conversion and Management**, v. 46, n. 9–10, p. 1495–1512, jun. 2005.

POTRICH, T. D. et al. Metodologia de criação de Tenebrio molitor em laboratório para obtenção de larvas. Passo Fundo: EMBRAPA Trigo, 2007. Disponível em: http://www.cnpt.embrapa.br/biblio/do/p_do82_12.htm. Acesso em: 6 de julho de 2022.

PIYAWANITPONG, C.; THERDTHAI, N.; RATPHITAGSANTI, W. Effect of Precooking and Superheated Steam Treatment on Quality of Black Glutinous Rice. **Journal of Food Quality**, v. 2018, p. 1–9, 6 set. 2018.

RAMESH, M. N. Moisture transfer properties of cooked rice during drying. **LWT - Food Science and Technology**, v. 36, n. 2, p. 245–255, mar. 2003.

REDDY, B. S.; CHAKRAVERTY, A. Equilibrium Moisture Characteristics of Raw and Parboiled Paddy, Brown Rice, and Bran. **Drying Technology**, v. 22, n. 4, p. 837–851, 5 jan. 2004.

RODRÍGUEZ-JASSO, R. M. et al. Fungal fucoidanase production by solid-state fermentation in a rotating drum bioreactor using algal biomass as substrate. **Food and Bioproducts Processing**, v. 91, n. 4, p. 587-594, 2013.

RORDPRAPAT, W. et al. Comparative study of fluidized bed paddy drying using hot air and superheated steam. **Journal of Food Engineering**, v. 71, n. 1, p. 28–36, nov. 2005.

SAHNI, E. K.; CHAUDHURI, B. Contact drying: A review of experimental and mechanistic modeling approaches. **International Journal of Pharmaceutics**, v. 434, n. 1–2, p. 334–348, set. 2012.

SCHMIDT, F. G. V. et al. Metodologia de Aplicação do Fungo Metarhizium anisopliae var. acridum para o Controle do Gafanhoto Rhammatocerus schistocercoides em Campo. 2007.

SCHUTYSER, M. A. I. et al. Heat and water transfer in a rotating drum containing solid substrate particles. **Biotechnology and Bioengineering**, v. 82, n. 5, p. 552–563, 5 jun. 2003.

SHATTUCK, A. et al. Global pesticide use and trade database (GloPUT): New estimates show pesticide use trends in low-income countries substantially underestimated. **Global Environmental Change**, v. 81, p. 102693, jul. 2023.

SILVA, E. G. et al. Heat and Mass Transfer on the Microwave Drying of Rough Rice Grains: An Experimental Analysis. **Agriculture**, v. 11, n. 1, p. 8, 24 dez. 2020.

SIRIPATRAWAN, U.; JANTAWAT, P. Determination of Moisture Sorption Isotherms of Jasmine Rice Crackers Using BET and GAB Models. **Food Science and Technology International**, v. 12, n. 6, p. 459–465, dez. 2006.

SPIESS, W. E. L.; WOLF, W. R. Results of the COST 90 project on water activity. **Physical properties of foods/edited by R. Jowitt... et al**, 1983.

TADA, É. F. R. et al. Mass transport in a partially filled horizontal drum: Modelling and experiments. **Chemical Engineering Science**, v. 214, p. 115448, mar. 2020.

TANG, J.; FENG, H.; SHEN, G. Drum drying. **Encyclopedia of agricultural, food, and biological engineering**, p. 211-214, 2003.

VAN BREUKELEN, F. R. et al. Bioreactor and substrate selection for solid-state cultivation of the malaria mosquito control agent Metarhizium anisopliae. **Process Biochemistry**, v. 46, n. 3, p. 751–757, mar. 2011.
WEBER, F. J. et al. Validation of a model for process development and scale-up of packed-bed solid-state bioreactors. **Biotechnology and bioengineering**, v. 77, n. 4, p. 381-393, 2002.
WOLF, W.; SPIESS, W. E. L.; JUNG, G. Standardization of Isotherm Measurements (Cost-Project 90 and 90 BIS). Em: SIMATOS, D.; MULTON, J. L. (Eds.). **Properties of Water in Foods**. Dordrecht: Springer Netherlands, 1985. p. 661–679.
YADAV, G. P. et al. A comprehensive review on instant rice: Preparation methodology, characterization, and quality attributes. **Food Chemistry Advances**, v. 4, p. 100581, jun. 2024.
ZOMORODIAN, A.; ZARE, D.; GHASEMKHANI, H. Optimization and evaluation of a semi-continuous solar dryer for cereals (Rice, etc). **Desalination**, v. 209, n. 1–3, p. 129–135, abr. 2007.

5. EXPERIMENTAL STUDY AND DISCRETE ELEMENT METHOD (DEM) ANALYSIS OF COOKED RICE SEGREGATION IN A ROTATING DRUM: MOISTURE CONTENT IMPACTS

ABSTRACT

The fungus *Metarhizium anisopliae* is traditionally cultivated on rice, and the pre-drying stage of the substrate still requires optimization. Drying in a horizontal drum with intermittent rotations emerges as a promising alternative. This study investigates the impact of particle moisture content (0.667 and 0.250 kg-w/kg-ds) on mixing efficiency in a rotary drum. The Discrete Element Method (DEM) was employed to simulate the motion regime and particle homogenization, using parameters specifically calibrated for cooked rice, including restitution coefficients, static friction, and rolling friction for both particle-particle and particle-wall contacts. The experiments were conducted in a rotary drum with a diameter of 30 cm and a length of 60 cm, equipped with four blades angled at 45°, operating at 7 rpm with a filling degree of 0.50, to validate the DEM modeling. The results indicated that the model adequately predicted the dynamic repose angle of the cooked rice beds, which was influenced by particle moisture content. Additionally, homogenization was found to be faster for drier particles. Simulations and experiments indicated that complete homogenization was achieved after a minimum of 14 rotations, with mixing indices of 87.56% and 95.94% at 11 rotations for beds with moisture contents of 0.667 and 0.250 kg-w/kg-ds, respectively. Assuming the model accurately represents granular behavior, additional simulations were performed for smaller drums (20 cm in diameter and 33 cm in length). The results showed that reducing the drum diameter, along with the lower number of particles and the use of differently designed blades (two blades angled at 90°), decreased the number of rotations required for homogenization, achieving mixing indices of 96.52% and 98.35% for beds with moisture contents of 0.667 and 0.250 kg-w/kg-ds, respectively. These findings highlight the importance of drum design in optimizing bed mixing and demonstrate its potential to enhance the efficiency of drying processes and large-scale bioinsecticide production.

Keywords: drying; cooked rice; mixing; DEM; moisture content.

5.1 INTRODUCTION

The large-scale production of *Metarhizium anisopliae* spores is carried out through solid-state cultivation (SSC) in plastic bags, using rice as a substrate. Among the process steps, drying stands out as a critical point requiring technological advancements, as it is currently performed by natural convection in climate-controlled rooms under mild temperatures. As an alternative, Ferreira et al. (2025) proposed drying rice in a horizontal drum, through forced convection, with intermittent rotations every hour. These rotations were effective in homogenizing the moisture profile formed during static drying, frequently repositioning the wetter particles to the surface of the bed. This method reduced the operational drying time to 16 hours in a controlled environment, offering a practical and easily applicable solution in biofactories.

Rotary drum drying is widely used in the chemical, pharmaceutical, and food industries (Delele et al., 2015; Trojosky, 2019; Balakrishnan et al., 2022; Nunes et al., 2024) due to the mass transfer provided by the gas-solid contact. However, the processes generally operate with continuous rotations and low filling degrees, conditions opposite to those proposed by Ferreira et al. (2025). Drying with intermittent rotations is more suitable for sensitive materials, such as fungi, as it minimizes mechanical damage and the excessive formation of undesirable fragments, a common effect in processes with continuous rotations. Moreover, the low filling degree compromises productivity, making it essential to develop technologies that enable the efficient scaling of production.

To ensure efficient drying, it is essential to guarantee the homogenization of the bed during rotations. Grajales et al. (2012) determined that 11 rotations at 7 rpm are sufficient for the homogenization of cooked rice beds. However, the impact of particle moisture on movement regime and, consequently, on the mixing was not considered, despite being widely discussed in the literature (Zaalouk; Zabady, 2009; Wandkar et al., 2012; Ponce-García et al., 2013; Brar et al., 2016; Sandra et al., 2020; Moya et al., 2024). For dry particles, primary interactions involve inelastic collisions and friction, while for wet particles, the proximity between them favors the formation of liquid bridges near contact points, resulting in particle binding and altering their mechanical properties (Rong et al., 2020).

However, further investigations are needed to understand the influence of particle moisture on the homogenization process. To this end, in addition to experimental studies, numerical simulations can provide valuable insights to improve our understanding, especially for systems with large numbers of particles. In this regard, the Discrete Element Method (DEM) has been widely used to describe granular behavior, offering a robust alternative to investigate and model these phenomena (Xu et al., 2010; Liu et al., 2017; Brandão et al., 2020; Wu et al., 2022; Sleeuwen et al., 2024). Xu et al. (2010) highlighted in their simulations that particle density and size are predominant factors in the mixing behavior. More specifically, the study revealed that static friction and rolling friction coefficients are the most influential parameters.

The objective of this study was to apply the Discrete Element Method to predict the impact of particle moisture content on the degree of mixing in a horizontal drum during the pre-drying process of cooked rice used in the production of *Metarhizium anisopliae* spores. The ideal number of rotations to ensure bed homogenization during intermittent rotations was determined.

5.1.1 Contact model

The DEM is a computational method through which granular flow at an individual particle level is modeled using Newton's second law. Simultaneously, a displacement-force law is applied to model interactions between particles (particle-particle) and between particles and surfaces (particle-wall), considering the continuous update of contact forces over time. The motion of each particle is described by Eqs. (5.1) and (5.2):

$$m_i \frac{dv_i}{dt} = \sum_j \left(F_n^{ij} + F_t^{ij}\right) + m_i\, g \tag{5.1}$$

$$I_i \frac{d\omega_i}{dt} = \sum_j \left(R_i + F_t^{ij}\right) + \tau_{rij} \tag{5.2}$$

where m_i, v_i, I_i, ω_i, and R_i correspond to the mass, linear velocity, moment of inertia, angular velocity, and radius of particle i, respectively. The normal and tangential forces between particles i and j are represented by F_n^{ij} and F_t^{ij}, while τ_r^{ij} indicates the torque resulting from the interaction.

In this study, the non-linear Hertz-Mindlin contact model was adopted, a classic example of the deformable sphere model, as it is more suitable for dense systems where the interactions between particles are prolonged. To represent the cohesion between particles, the contributions from the Johnson-Kendall-Roberts (JKR) model can be incorporated, which accounts for the influence of cohesive forces, such as van der Waals forces. This model is especially useful for simulating strongly adhesive systems, such as cooked rice beds. However, the application of the JKR model requires additional information, such as the adhesion energy between particles and material-specific parameters, which were not determined or considered in this study.

In the model adopted in this work, the contact force is decomposed into normal and tangential components, both containing damping elements. The tangential component follows Mindlin's theory (Mindlin, 1949), while the normal component is based on Hertz's contact theory (Hertz, 1882). The damping coefficient (β) is directly related to the restitution coefficient, allowing for a more accurate modeling of particle interactions. The restitution coefficient (e_p), which measures the energy dissipation in collisions between solid bodies, can be calculated as the ratio between the velocities before and after the impact, as expressed in Eq. (5.3):

$$e_p = \frac{-v_r}{v_o} \tag{5.3}$$

where v_r (m/s) represents the particle velocity after the collision and v_o (m/s) correspond to the velocity before the impact.

The static friction coefficient (μ_s) quantifies the resistance to relative motion between surfaces and can be determined by Eq. (5.4). This force acts at the contact points between the bodies, in the opposite direction of motion, preventing the initiation of sliding:

$$\mu_s = \tan(\Theta_s) \tag{5.4}$$

where Θ_s is the critical angle of inclination at which the particles begin to slide.

The rolling friction coefficient (μ_r) is calculated by Eq. (5.5) and represents the resistance to the movement of a particle rolling over a surface or other particles:

$$\mu_r = \frac{h_0}{D_r} \tag{5.5}$$

where h_0 is the initial height of particle launch (cm) and D_r corresponds to the distance traveled by the particle from the launch point to rest (cm).

However, these coefficients have not yet been determined for cooked rice particles with varying moisture content. Thus, one of the main objectives of this study is to experimentally determine these coefficients, which are essential parameters for DEM-based simulations.

5.2 MATERIAL AND METHODS

5.2.1 Granular material

The laboratory tests were conducted with raw rice (RR), with moisture contente (MC) of 0.084 kg of water/kg of dry solid (kg-w/kg-ds), and cooked rice (CR) particles, with MC of 0.667 and 0.250 kg-w/kg-ds, corresponding to the initial and final moisture levels of the material during the pre-drying stage after the colonization of cooked rice by *Metarhizium anisopliae*. For the preparation of cooked rice, long grain rice (Oryza sativa) was moistened in a plastic package until it reached 0.667 kg-w/kg-ds, then sterilized in an autoclave at 121ºC for 25 minutes and cooled. The material was kept in a climate chamber for 10 days to standardize moisture content, a period equivalent to that used in biofactories for fungal development. Cooked rice particles, with a moisture content of 0.250 kg-w/kg-ds, were obtained by drying in a BOD incubator at 30°C. Moisture content was monitored using an MB45 infrared moisture analyzer (Ohaus, Parsippany, USA).

To appropriately represent the particles of raw rice and cooked rice in the DEM simulation environment, their dimensions, bulk density (ρ_{bulk}), and sphericity (Φ) were determined. Figure 5.1 illustrates the measurements used to size the particles. The dimensions a and b, as well as the sphericity, were obtained from photographic images of samples containing more than 100 rice grains analyzed using ImageJ software. The bulk density was determined using the volumetric method in a 50 mL measuring cylinder, where the total volume of a given mass of particles was measured directly in the cylinder.

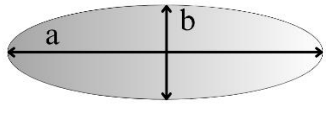

Figure 5.1. Dimensions of rice grains for particle volume determination.

5.2.2 Measurement of DEM input parameters

5.2.2.1 Restitution coefficient

To determine the restitution coefficient (e_p), the experimental setup illustrated in Figure 5.2 was used. The release of the particles occurred via a vacuum gripper (WETEC, Germany), which exerted enough suction force to hold a single particle 70 mm above a flat surface. The suction was then interrupted, allowing the particle to fall freely. For the determination of ep in particle-wall (PW) collisions, a stainless-steel plate 2 mm thick was used. For particle-particle (PP) collisions, this same plate was coated with particles adjusted to the moisture content being analyzed. The instantaneous velocities before and after the impact (Figure 5.2.b) were recorded by a high-speed digital camera (LaVision, GmbH, Göttingen, Germany), equipped with a CMOS sensor (1024 × 1024 pixels) and operating at 5,000 frames per second (FPS). From these velocities, e_p was calculated using Eq. (5.3). Each trial was repeated 10 times to ensure the reliability of the results. The experiments were conducted with CR particles at moisture contents of 0.667 and 0.250 kg-w/kg-ds. Furthermore, the same experimental procedure was applied to raw rice particles for comparative purposes.

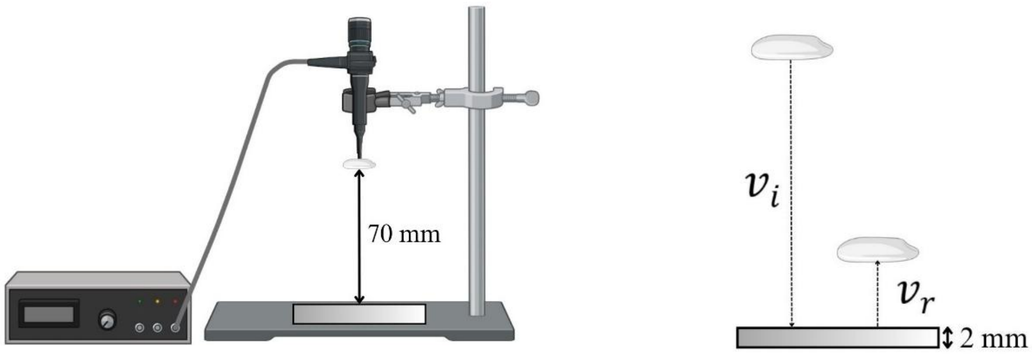

(a) (b)

Figure 5.2. Experimental setup for determining the restitution coefficient (a - vacuum tweezer, fixation support, and flat plate; b – rice particle trajectory before and after the collision).

5.2.2.2 Static friction coefficient

The experimental setup described in Figure 5.3 was used to determine the static friction coefficient (μ_s). The experiment consisted of an inclined plane fixed to a rod that allowed gradual adjustments to the slope. During the tests, the plane was gently tilted until the CR particles started to slide. To prevent rolling instead of sliding, the particles were grouped using adhesive tape. The trials were conducted with CR particles at moisture contents of 0.667 and 0.250 kg-w/kg-ds and with raw rice. The static friction coefficient was determined from the tangent of the critical angle (Θ_s), corresponding to the moment when the motion began, as indicated in Eq. (5.4).

The exact moment of sliding and the determination of the critical angle were captured using a Canon EOS 2000D camera (Canon Inc., Tokyo, Japan), and the angle measurement was made using the ImageJ/Fiji software. The static friction between the particle and the wall was analyzed with a smooth plate (Figure 5.2.b), while particle-particle interactions were evaluated by coating the plate with rice particles (Figure 5.3.b). To ensure the reproducibility of the results, each experiment was repeated 10 times.

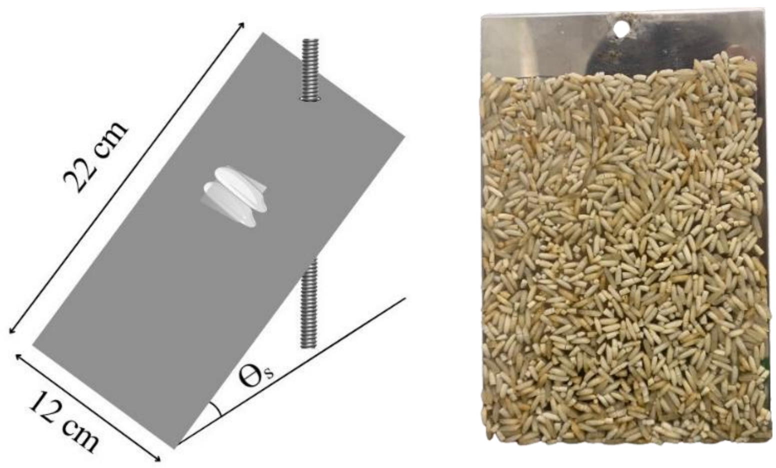

(a) (b)

Figure 5.3. Experimental setup for the determination of the static friction coeficiente (a - flat sloped stainless steel plate; b - surface of the plate covered with rice particles).

5.2.2.3 Rolling friction coefficient

To determine the rolling friction coefficient (μ_r), the experimental setup shown in Figure 5.4 was used. The experiment consisted of two flat stainless steel surfaces, identical to the one illustrated in Figure 5.3.a. One of the surfaces was tilted to allow the release of the particles, while the other remained horizontal. The particles were released from a fixed height of 13 mm (h_0), and the distance traveled until coming to rest in the horizontal plate (D_r) was measured with a vernier caliper. The experiments were conducted with CR particles at moisture contents of 0.667 and 0.250 kg-w/kg-ds, as well as with RR. To determine the particle-particle rolling friction coefficient ($\mu_{r\text{-}PP}$), the horizontal surface was completely covered with the analyzed particles, as represented in Figure 5.3.b.

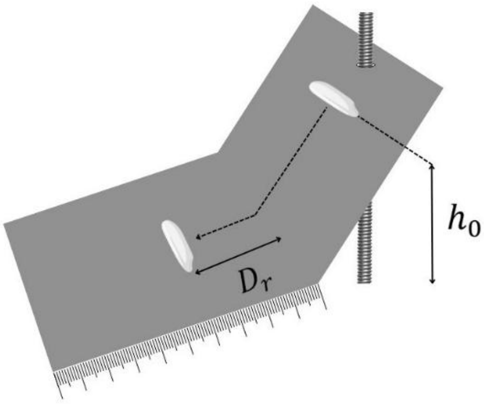

Figure 5.4. Experimental setup for determining the rolling friction coefficient.

5.2.3 Dynamic resting angle

In order to calibrate the parameters and experimentally validate the adopted model, the dynamic resting angle (Θ_d) for raw rice and cooked rice particles, at moisture contents of 0.667 and 0.250 kg-w/kg-ds, were established both experimentally and through simulations.

5.2.3.1 Experimental setup

The rotary drum method (Train, 1958) was adopted to determine the dynamic resting angle of granular materials. For this, the particles were loaded into a drum until a filling degree (*f*) of 0.50 was reached. A drum with a diameter of 20 cm and a length of 45 cm, equipped with four straight blades angled at 45º with the drum wall, was used, as shown in Figure 5.5.a. The lids were made of acrylic to allow visualization of the granular material. The rotation of the drum was carried out by a system of chains and gears connected to an electric motor driven by a frequency converter. The rotation was maintained at a constant speed of 7 rpm for a period of 120 seconds. To identify the angle, a camera (Canon EOS 2000D) was used to record the flow of particles. The dynamic resting angle, shown in Figure 5.5.b, was determined with the help of ImageJ/Fiji software. The tests were repeated three times for each particle set.

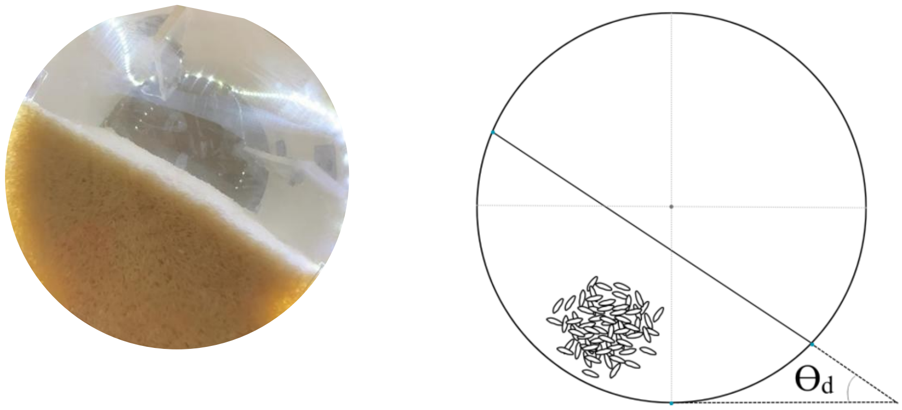

(a) (b)

Figure 5.5. Determination of the dynamic resting angle experimentally (a – drum used for particle movement and b – schematic for determining the dynamic resting angle).

5.2.3.2 DEM simulation

To obtain the dynamic resting angles, simulations were conducted using the open-source software LIGGGHTS. The geometry used in the simulations was built to match the experimental setup drawn using SolidWorks (Dassault Systèmes, Vélizy-Villacoublay, France). To ensure numerical stability during the simulations, a time step of 1×10^{-4} seconds was employed. Table 5.1 details the simulation conditions adopted in this study. The rice particles were modeled as spheres, with the volume adjusted to that of the real particles, established through the dimensions a and b, as shown in Figure 5.1. The simulations were conducted for 120 seconds, rotating the drum at 7 rpm. At the end of this time, images were taken from the simulations to determine the resting angle, as described in Section 5.3.3.1.

Table 5.1. Parameters adopted in the DEM simulations.

Parameter	**Value**	**Reference**
Time step (s)	1×10^{-4}	-
Young modulus (GPa)		
Rice	0.014	Da Costa *et al*. (2014)
Steel	207	Callister; Rethwisch (2012)
Poission ratio (-)		
Rice	0.15	Da Costa *et al*. (2014)
Steel	0.30	Jafari *et al*. (2018)

The other input parameters (restitution coefficient, static friction coefficient, and rolling friction coefficient) were adjusted to calibrate the DEM simulations. Several parameter sets were evaluated to identify the best set representing CR particles at different moisture contents and RR. The selection of the parameters to be tested was based on a fractional factorial design (Jankovic et al., 2021), as shown in Table 5.2. Level 0 represented the interaction coefficients determined experimentally. Level -1 was determined by subtracting half the value of the coefficient obtained experimentally, while level +1 was established by adding half of this value to the experimental coefficient. Thus, the values of the coefficients at levels -1 and +1 were adjusted to represent variations around the average value, corresponding to the minimum and maximum values, respectively.

Table 5.2. Fractional factorial design added for DEM parameter calibration.

Set	$e_{p\text{-}PP}$	$e_{p\text{-}PW}$	$\mu_{s\text{-}PP}$	$\mu_{s\text{-}PW}$	$\mu_{r\text{-}PP}$	$\mu_{r\text{-}PW}$
1	-1	-1	-1	-1	-1	-1
2	1	1	1	1	-1	1
3	1	1	1	1	-1	1
4	-1	-1	-1	-1	-1	-1
5	1	1	1	1	1	1
6	-1	-1	-1	-1	1	-1
7	-1	-1	-1	-1	1	-1
8	1	1	1	1	1	1
9	-1	1	-1	1	-1	1
10	1	-1	1	-1	-1	-1
11	1	-1	1	-1	-1	-1
12	-1	1	-1	1	-1	1
13	1	-1	1	-1	1	-1
14	-1	1	-1	1	1	1
15	-1	1	-1	1	1	1
16	1	-1	1	-1	1	-1
17	0	0	0	0	0	0

5.2.4 Flow regime

The flow regime of particle of cooked rice with moisture contents of 0.667 and 0.250 kg-w/kg-ds in the rotating drum was analyzed visually. For this, the material was loaded into the same horizontal drum used to establish the dynamic resting angle (Figure 5.5.a) until a filling degree of 0.50 was reached. The rotation speed was kept constant at 7 rpm, while the particle flow was captured with a Canon EOS 2000D camera.

5.2.5 Binary mixtures and mixing index

To determine the mixing index of the cooked rice particles at moisture levels of 0.667 and 0.250 kg-w/kg-d, the colored tracer technique was used. For this, a binary mixture was prepared, consisting of non-dyed rice (Figure 5.6.b) and rice dyed with rhodamine (Figure 5.6.c), both with the same moisture content and prepared as described in Section 5.2.1.

A drum with a diameter of 30 cm and a length of 60 cm, equipped with four blades angled at 45º, was used, as shown in Figure 5.7.a. The lids and walls were made of acrylic to allow visualization of the granular material. The dyed rice particles were arranged until reaching a radial height of 7.5 cm, while the non-dyed particles were added until reaching 15 cm, as shown in Figure 5.6.a. The rotation of the drum was carried out by a system of chains and gears connected to an electric motor driven by a frequency converter. The rotation was maintained at a constant speed of 7 rpm for a period of 120 seconds.

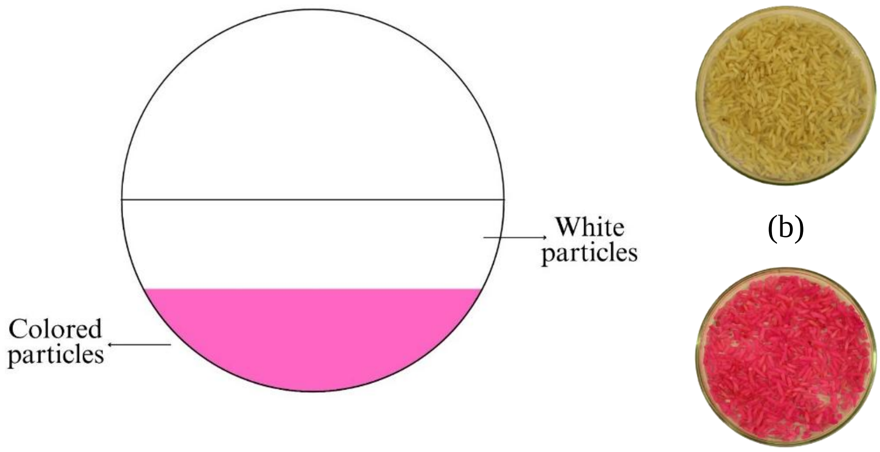

(a) (b) (c)

Figure 5.6. Cooked rice particles (a - position on the drum; b – non-dyed; c – dyed with rhodamine).

The impact of particle moisture on the binary mixture was also investigated through numerical simulations. For this purpose, DEM simulations were conducted using the same conditions described in Table 5.1 and adopting the adjusted parameter set (coefficient of restitution, static friction coefficient, and rolling friction coefficient). The arrangement of particles in the drum followed the scheme illustrated in Figure 5.6. The drum model was drawn in SolidWorks for the simulations (Figure 5.7.b).

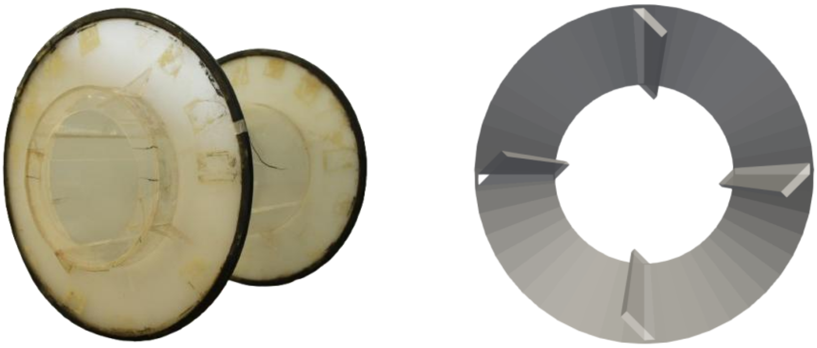

(a) (b)

Figure 5.7. Drum (a) experimental and (b) drawn in SolidWorks adopted for determining the mixing index of cooked rice beds.

The experimental and numerical mixing indexes were determined using an image analysis technique divided into 3 stages, as illustrated in Figure 5.8. In Stage I, images of the granular bed (experimental and numerical) were obtained after each rotation. In Stage II, the resulting frames were exported to ImageJ/Fiji software, where the images were converted to 8-bit grayscale and binarized to produce only black and white pixels. In the final stage (Stage III), the images were divided into 16 cells, and with the help of a Python code, the concentration of black pixels in each cell and the standard deviation (σ) were determined using Eq. (5.6).

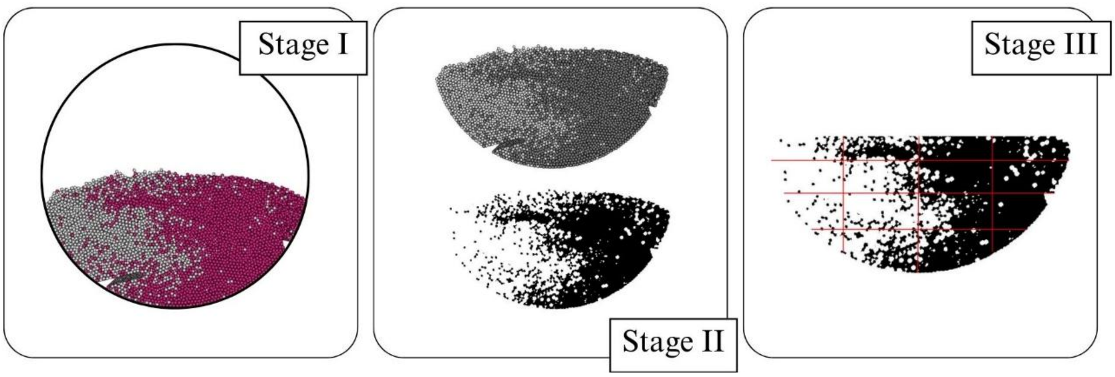

Figure 5.8. Stages of image processing for determining the mixing index.

$$\sigma = \sqrt{\frac{\sum_{i=1}^{N}(C - C_m)^2}{N - 1}} \tag{5.6}$$

where C is the concentration of black pixels in each cell, C_m is the average concentration of black pixels, and N is the number of cells.

The mixing index (M_i), which is a measure of the degree of mixing, was determined using Eq. (5.7). According to Lacey (1997), a mixing index equal to 0 indicates a fully segregated condition, while a value of 1 indicates a completely random state.

$$M_i = \frac{\sigma_0^2 - \sigma_i{}^2}{\sigma_0^2 - \sigma_r^2} \tag{5.7}$$

where σ_0 and σ_r are the sample deviations in the fully segregated state (initial state) and perfectly mixed state, respectively, and σ_i is the sample deviation of a mixture at rotation i.

The mixing process of cooked rice particles at different moisture contents was also simulated using a drum identical to the one experimentally adopted by Ferreira et al. (2025) in intermittent rotation drying. For this, the drum with a diameter of 20 cm and a length of 33 cm, shown in Figure 5.9, was drawn using SolidWorks. Inside the drum, there were two straight longitudinal blades, each 2 cm wide, positioned perpendicular to the drum's wall. The simulation conditions, described in Table 5.1, were kept identical to those outlined in Section 5.2.3.2. These simulations allowed for investigating the impact of the number of blades, angle, and drum diameter on the mixing index.

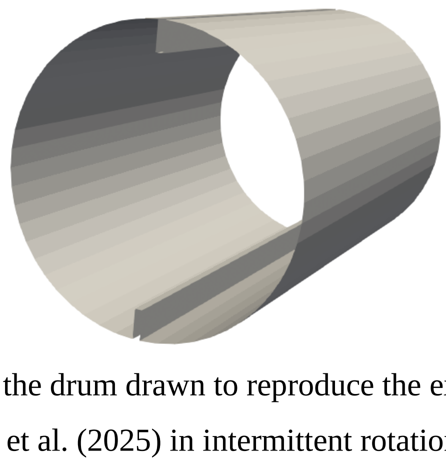

Figure 5.9. Internal view of the drum drawn to reproduce the experimental setup adopted by Ferreira et al. (2025) in intermittent rotation drying.

5.2.6 Statistical analyses

Analyzes of variance (ANOVA) and Tukey tests of comparison of means with a confidence level of 95% were carried out using Microsoft Excel 365 (Microsoft Co., Redmond, USA).

5.3 RESULTS AND DISCUSSION

5.3.1 Particle characterization

Table 5.3 presents the dimensions and sphericity of cooked rice (CR) and raw rice (RR) particles, as well as the bulk density of beds filled with these particles. It was observed that in cooked rice, the reduction in moisture content led to a decrease in particle length (a) and sphericity, although the latter did not show a statistically significant difference. Additionally, particle width (b) was affected by the moisture reduction, as was the bulk density of the bed, both showing statistically significant variations. This behavior is related to particle shrinkage during the drying process, leading to more efficient packing and, consequently, higher bulk density. Compared to raw rice, cooked rice particles exhibit larger dimensions and higher sphericity, regardless of the analyzed moisture content. This increase in dimensions can be explained by the cooking process during sterilization, which causes the grains to swell due to water absorption and structural changes in the starch.

Table 5.3. Granular material properties.

Material	**MC** (kg-w/kg-ds)	**Dimensions** (mm) a	**Dimensions** (mm) b	ρ_{bulk} (kg/m^3)	Φ (-)
RR	0.087	6.62 ± 0.23^{b}	1.40 ± 0.05^{c}	701.52 ± 15.36^{a}	0.49 ± 0.03^{a}
CR	0.250	7.12 ± 0.11^{a}	1.69 ± 0.08^{b}	636.20 ± 13.67^{b}	0.58 ± 0.02^{b}
	0.667	8.35 ± 0.34^{ab}	1.98 ± 0.10^{a}	527.50 ± 22.41^{c}	0.61 ± 0.05^{b}

RR – raw rice; CR – cooked rice; MC – moisture content; ρ_{bulk} – bulk density of the particle beds; Φ – sphericity of the particles. Means followed by the same lowercase letters are not significantly different according to the Tukey test at the 95% confidence level.

5.3.2 Direct measurement of DEM input parameters

The results of the restitution coefficient (e_p), static friction (μ_s), and rolling friction (μ_r) obtained experimentally for cooked and raw rice particles are presented in Figure 5.10. The restitution and static friction coefficients for raw rice are within the ranges reported in the literature (Jia et al., 2021; Wang et al., 2021; Xu et al., 2023). However, it was not possible to verify the adequacy of the rolling friction coefficient, as its experimental determination has not been previously reported in the literature.

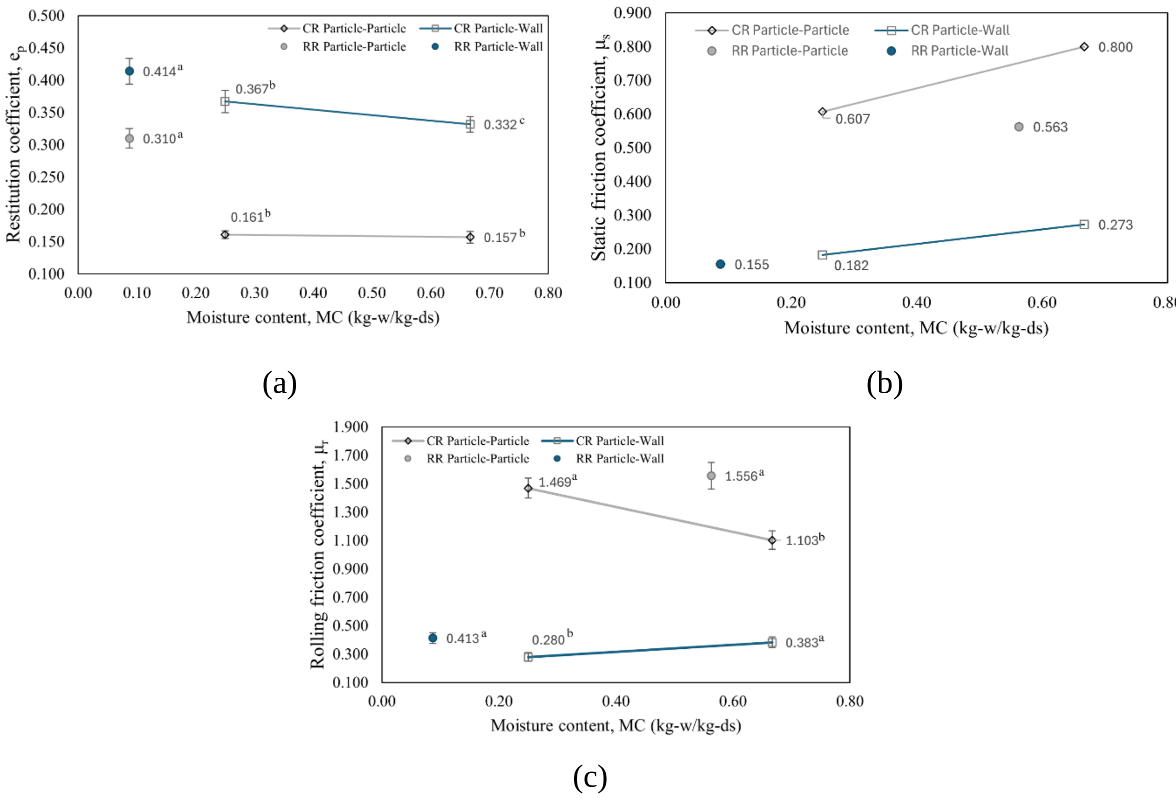

Figure 5.10. DEM input parameters, where (a) coefficient of restitution; (b) static friction coefficient, and (c) rolling friction coefficient for raw rice (RR) and cooked rice (CR). Coefficients describing the same interaction, particle-particle (PP) or particle-wall (PW), followed by the same lowercase letters are significantly different according to the Tukey test at a 95% confidence level.

5.3.2.1 Restitution coefficient

From Figure 5.10.a, it can be observed that the coefficient of restitution decreases with increasing moisture content for both particle-particle and particle-wall (PW) interactions. This behavior suggests that wetter materials dissipate more energy during collisions, possibly due to greater adhesion or increased deformation of moist particles. Cooked rice, at the different moisture levels analyzed, has a moisture content far above equilibrium, forming a significant water film on the particles. This film likely dissipates a large portion of the collision energy between the particles and the surface, reducing the coefficient of restitution. Additionally, the presence of dissolved starch in this water film may contribute to increased particle adhesion to the surface.

However, the reduction in the coefficient of restitution is statistically significant only for PW interactions. Mueller et al. (2011) investigated the impact of different moisture contents on the coefficient of restitution. The authors observed that particle moisture content has minimal influence on the coefficient of restitution (e_p), although it affects the mechanical properties of the particles. Furthermore, raw rice exhibits the highest coefficients of restitution compared to cooked rice, differing significantly in both types of interactions. This suggests that the cooking process, which occurs during the preparation of cooked rice, alters its elastic properties.

5.3.2.2 Static friction coefficient

In Figure 5.10.b, it can be observed that the static friction coefficient of cooked rice increases significantly with higher particle moisture content. This indicates that greater moisture intensifies the resistance to sliding between particles, likely due to the increased thickness of the liquid film, which results in higher cohesion and adhesion between them. In contrast, raw rice exhibits the lowest static friction coefficients, demonstrating that the raw material particles slide with less resistance. Despite the changes induced by the cooking process, particles with lower moisture content (0.250 kg-w/kg-ds) do not show significant differences compared to raw rice.

5.3.2.3 Rolling friction coefficient

Na Figura 5.10.c, uma mudança na tendência do coeficiente de atrito de rolamento é observada ao comparar as interações PP e PW. Para interações PP, o coeficiente aumenta com a redução do teor de umidade, enquanto para interações PW, a tendência oposta é identificada. Em ambos os casos, a redução da umidade das partículas é estatisticamente significativa. Como o coeficiente de atrito de rolamento representa a resistência ao movimento de rolamento de uma partícula (Mohamed; Gutierrez, 2010), valores mais altos indicam menor capacidade de rolamento. Os coeficientes de atrito de rolamento para interações PP são substancialmente maiores do que aqueles para PW, sugerindo que as partículas encontram maior resistência ao rolamento umas sobre as outras do que contra a superfície do aço inoxidável.

Curiosamente, os coeficientes de atrito de rolamento para RR são maiores do que aqueles para CR, o que contradiz as expectativas. Esse comportamento pode ser explicado pela menor esfericidade das partículas RR em comparação com as partículas CR. As partículas de arroz, especialmente no estado bruto, têm formas alongadas e irregulares, tornando a rolagem mais difícil. Em materiais com maior esfericidade ou partículas mais lisas, o atrito de rolamento é geralmente menor, pois essas formas favorecem movimentos de rolagem mais fáceis. Portanto, a maior irregularidade geométrica das partículas RR pode ser responsável pelos maiores coeficientes observados.

5.3.3 Dinamic repose angle and calibration of DEM input parameters

The experimental dynamic repose angles obtained for cooked and raw rice particles are summarized in Table 5.4. A significant reduction in the repose angle is observed as the moisture content of cooked rice particles decreases, a behavior widely documented in the literature (Sadeghi et al., 2010; Bhople et al., 2017; Wu et al., 2022). Compared to cooked rice (CR), the bed formed by raw rice (RR) particles exhibits a lower repose angle. In general, the dynamic repose angle increases significantly with higher particle moisture content. This behavior may be related to the lower cohesion between raw rice particles compared to cooked rice, as the former does not undergo structural changes induced by the cooking process. This structural difference contributes to the formation of beds with lower resistance to movement.

Table 5.4. The experimental angle of repose for raw rice and cooked rice at different moisture contents.

Material	**Moisture content** (kg-w/kg-ds)	**Angle of repose** (°)
Raw rice	0.083	30.62 ± 0.55^{c}
Conidiated rice	0.250	33.83 ± 0.37^{b}
	0.667	44.89 ± 0.34^{a}

Repose angles followed by the same lowercase letters are significantly different according to the Tukey test with a 95% confidence level.

Higher repose angles are associated with lower values of the coefficient of restitution (e_p), as less elastic collisions favor the formation of more stable beds. This happens because lower energy transfer during interactions reduces particle movement (Sunkara, 2013). Additionally, a higher static friction coefficient ($\mu_{s\text{-}PW}$) contributes to greater friction between surfaces, further reducing sliding between particles and the wall (Chung et al., 2022). This combination of factors seems to outweigh the influence of the rolling friction coefficient, highlighting the predominance of less elastic collisions and static friction in granular bed stability.

Figure 5.11 presents a direct comparison between the experimentally obtained dynamic repose angles and the numerical values obtained using the best combination of adjusted coefficients during the simulations (Table 5.5). Additionally, Figure 5.12 summarizes the dynamic repose angles (Θ_d) resulting from each simulation, according to the combinations of the fractional factorial design.

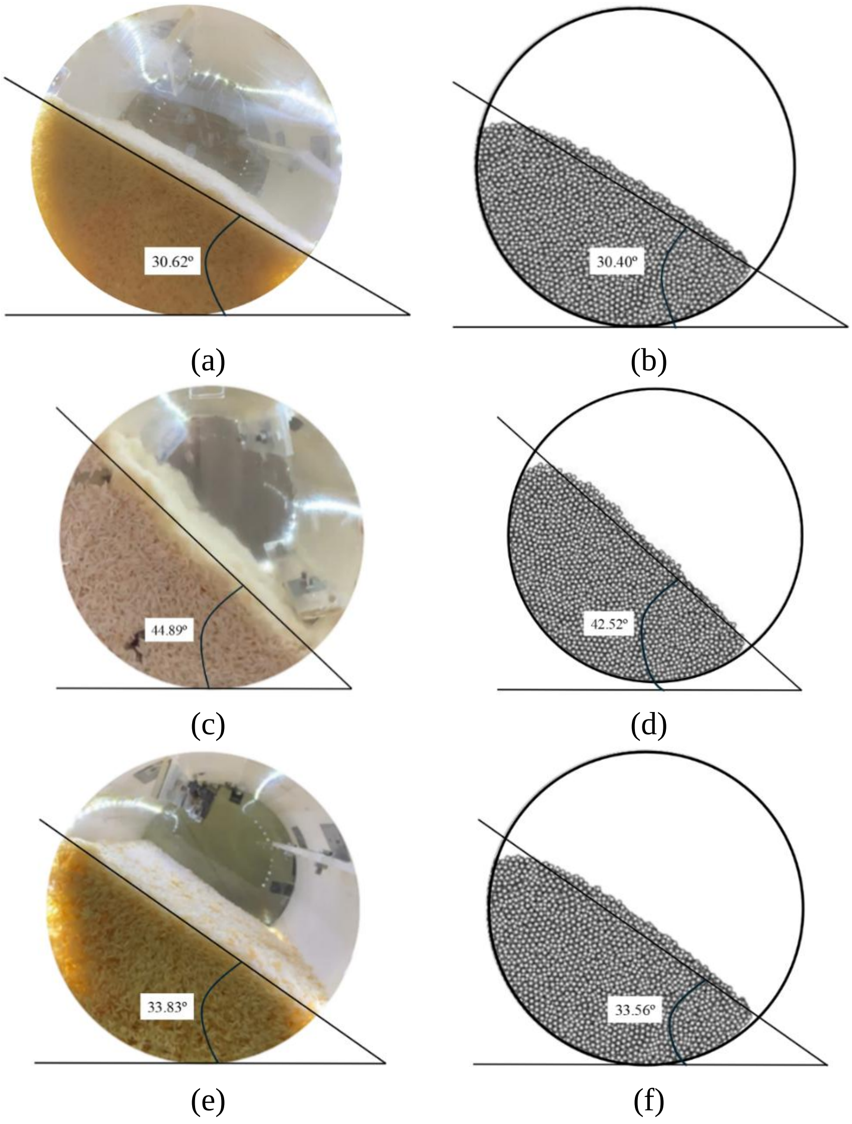

Figure 5.11. Resting angle of raw rice obtained (a) experimentally and (b) through simulations; of cooked rice with a moisture content of 0.667 kg-w/kg-ds obtained (c) experimentally and (d) through simulations; of cooked rice with a moisture content of 0.250 kg-w/kg-ds obtained (e) experimentally and (f) through simulations (Drum with a diameter of 20 cm and a length of 45 cm).

Table 5.5. Restitution, static friction, and rolling friction coefficients that provided the most accurate representation of the dynamic repose angle.

Material	**MC** (kg-w/kg-ds)	**Set**	$e_{p\text{-}PP}$	$e_{p\text{-}PW}$	$\mu_{s\text{-}PP}$	$\mu_{s\text{-}PW}$	$\mu_{r\text{-}PP}$	$\mu_{r\text{-}PW}$
RR	0.084	15	0.155	0.621	0.282	0.233	2.334	0.620
CR	0.250	3	0.242	0.551	0.304	0.273	0.735	0.420
	0.667	3	0.236	0.498	0.400	0.401	0.552	0.575

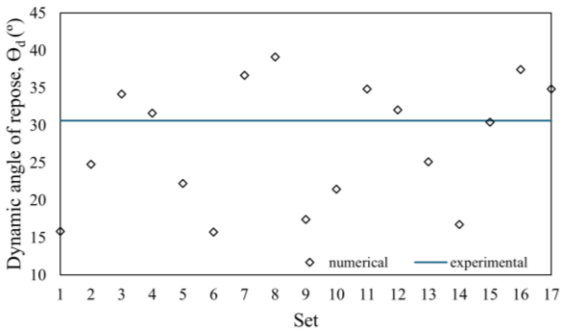

(a)

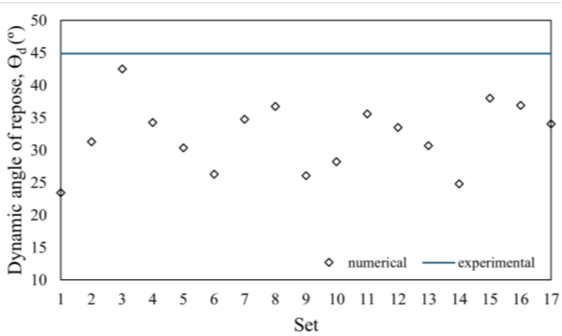

(b)

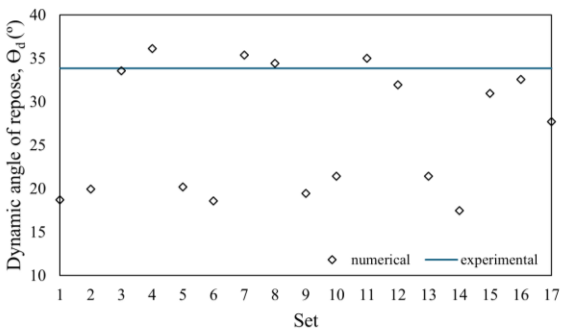

(c)

Figure 5.12. Dynamic repose angles obtained experimentally and numerically from the sets established for the calibration of input parameters for (a) raw rice; (b) cooked rice with moisture content of 0.667 kg-w/kg-ds; and (c) cooked rice with moisture content of 0.250 kg-w/kg-ds.

When observing Sets 17 for both samples, it is noted that they are not capable of accurately representing the static angle of repose. This occurs because the experiments analyze interactions at the level of a single particle, which does not fully reflect the interactions within the bed. It can be observed that Set 3 from the factorial design was effective in reproducing the behavior of cooked rice at both evaluated moisture levels. On the other hand, raw rice exhibited the most accurate numerical repose angle when using parameter Set 15. It is noteworthy that only the levels of coefficients related to particle-particle interactions differ between Set 3 and Set 15, suggesting that repose angles are more strongly associated with particle-particle interactions than with particle-wall interactions. This highlights the predominant influence of the intrinsic properties of granular material on bed behavior. Therefore, incorporating adhesive forces into mathematical models could further enhance the accuracy of granular behavior representation, making it a relevant aspect for future investigations.

5.3.4 Flow regime

The mixing of granular beds is highly sensitive to subtle variations in the size, shape, and density of the constituent particles (Samadani; Kudrolli, 2000). When the moisture content increases, small amounts of interstitial liquid in the system introduce an additional degree of complexity due to the cohesive forces between particles, which add to the frictional forces already present in dry materials. The interstitial liquid also interferes with the particle movement dynamics, promoting the formation of clusters that behave as single units rather than individual grains. This change in the flow regime is clearly observed when comparing the behavior of cooked rice particle beds at different moisture contents, as illustrated in Figure 5.13.

(a) (b)

Figure 5.13. Granular behavior of beds composed of cooked rice particles with moisture content of (a) 0.667 and (b) 0.250 kg-w/kg-ds, using a drum with 20 cm in diameter and 45 cm in length.

According to Mellmann (2001), the Froude number is an effective parameter for predicting the behavior of granular material flow, influenced by the drum dimensions, filling level, rotational speed, and the static friction coefficient of the particles with the wall. The adopted rotational speed, combined with the filling degree and the drum diameter in this study, resulted in a Froude number (Fr) of 8.20×10^{-3}. For Fr numbers ranging from 10^{-2} to 10^{-4} (Figure 3.4), the movement is classified as cascade, within the rolling subtype. However, the more pronounced "S" curvature for the bed composed of cooked rice particles with a moisture content of 0.667 kg-w/kg-ds indicates a transition from the rolling and cascading regimes. For non-spherical particles, the "S" shaped curve occurs at lower rotational speeds than for spherical particles. This indicates that particle shape is likely to influence the transition point between rolling and cascading (Norouzi et al., 2016), and the contributions of adhesion between particles should also not be neglected. For this reason, the movement regime is not faithfully reproduced in the simulation environment, as can be observed in Figure 5.15.

5.3.5 Mixture index

Figure 5.14 presents the mixing index (M) of beds of cooked rice with moisture contents of 0.667 and 0.250 kg-w/kg-ds, obtained experimentally and through DEM simulations, over the drum rotations (N). The drum has a diameter of 30 cm, a length of 60 cm, and four vanes angled at 45°. It can be observed that, even after the first rotation, both beds reach mixing indices above 28%. However, the bed composed of more humid cooked rice particles tends to homogenize more slowly.

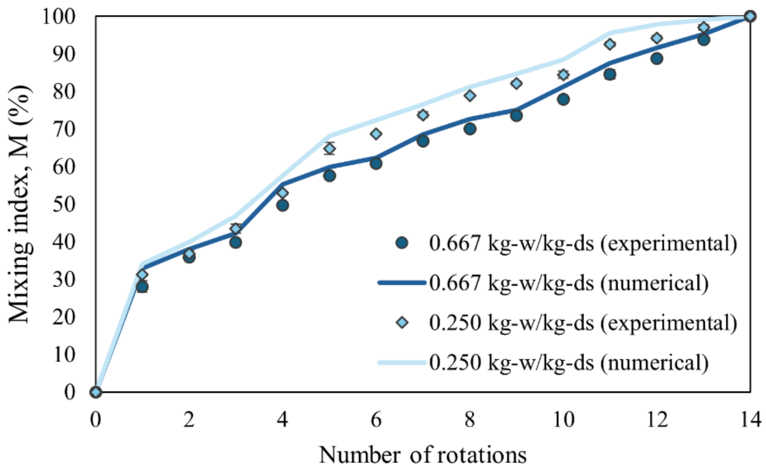

Figure 5.14. Numerical and experimental mixing index for cooked rice particles with moisture content of 0.667 and 0.250 kg-w/kg-ds, using a drum with a diameter of 30 cm and a length of 60 cm.

This behavior can be explained by the lower coefficient of restitution and rolling friction, as well as the higher static friction of the particles with a higher moisture content (0.667 kg-w/kg-ds). These characteristics make the particles more resistant to the initiation of relative movement, hindering sliding between them. Additionally, there is greater energy dissipation during collisions, which reduces particle movement and distribution within the bed. Moreover, the more humid particles are larger and tend to form agglomerates due to capillary forces intensified by the high water content (Louati et al., 2017; Chung et al., 2022), further compromising mixing efficiency. Jarray et al. (2019) explored the effect of cohesive forces on granular mixing by controlling the cohesive force between grains. They reported that non-cohesive particles tend to mix better, leading to more homogeneous mixtures.

Furthermore, a strong agreement between experimental and numerical results is observed, with R^2 values of 0.982 and 0.980 for the cooked rice beds with moisture contents of 0.667 and 0.250 kg-w/kg-ds, respectively. The small differences observed can be attributed to the geometric simplification of rice particles into spherical shapes in the simulations, as well as the absence of parameters accounting for particle cohesion in the model used. These approximations generally affect the accuracy of granular behavior representation, especially in materials with significant cohesive properties (Chung et al., 2022).

Figure 5.15 illustrates the radial binary mixing of cooked rice beds with moisture contents of 0.667 and 0.250 kg-w/kg-ds, obtained experimentally and through simulations. It is observed that, despite corresponding to the same drum rotation, particle positions show considerable differences when comparing experimental and numerical results. This behavior can again be justified by the tendency of particles to approximate a spherical shape, influencing mixing dynamics and mobility within the bed. Spherical particles, due to their rotational symmetry and lower friction during rolling, exhibit greater relative mobility, facilitating mixing in the bed. Even when DEM input parameters were adjusted to represent real particles, the geometric simplification to spheres does not fully capture the effects of interactions generated by irregular shapes. The absence of interlocking and the lower rolling friction observed in spherical particles allow for freer movement, which may result in a greater tendency for mixing in simulations.

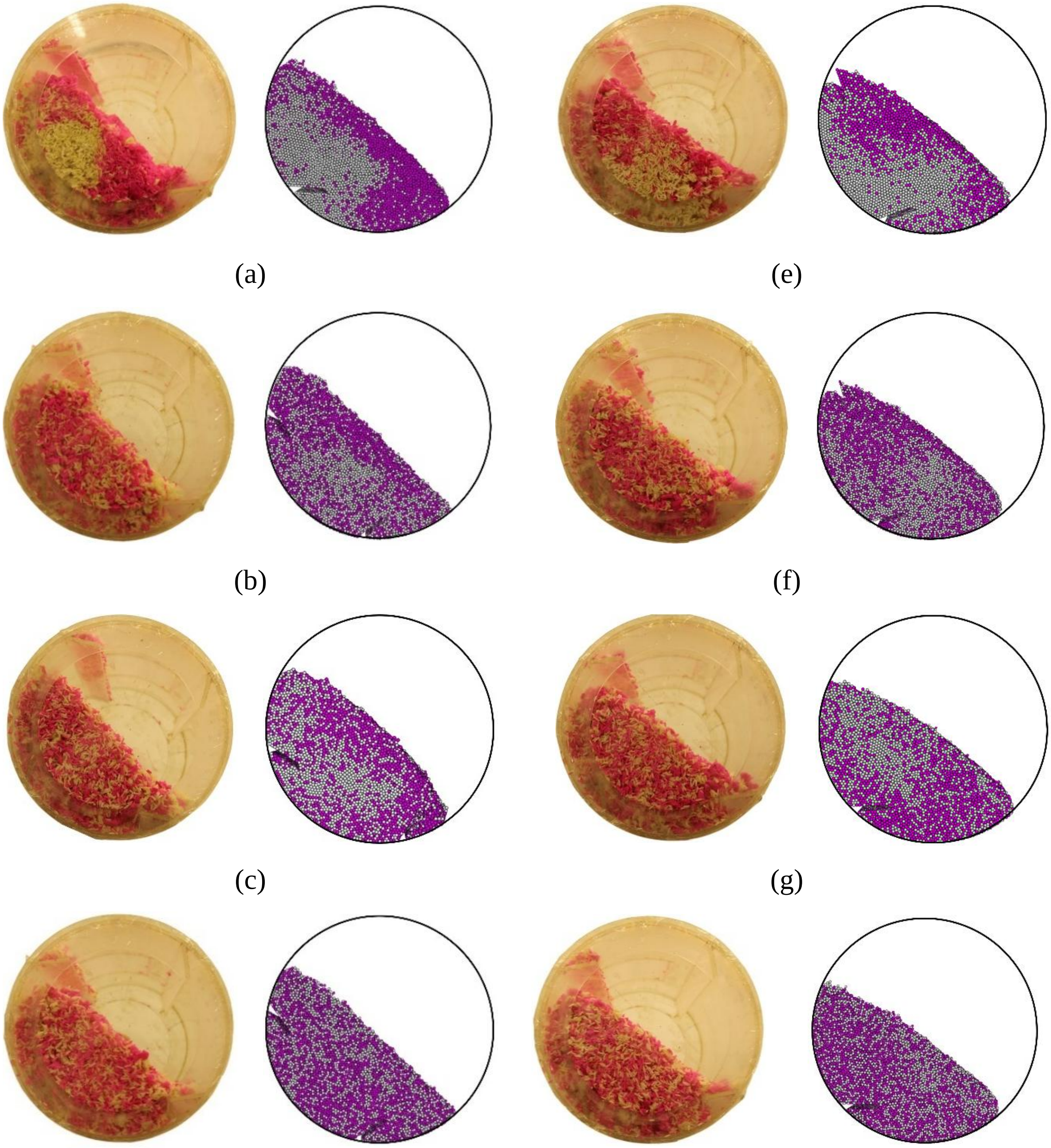

(a) (e) (b) (f) (c) (g) (d) (h)

Figure 5.15. Radial mixture of the experimental and numerical bed of cooked rice particles with moisture content of 0.667 kg-w/kg-ds after (a) 1 rotation, (b) 7 rotations, (c) 11 rotations, (d) 14 rotations, and with moisture content of 0.250 kg-w/kg-ds after (e) 1 rotation, (f) 7 rotations, (g) 11 rotations, and (h) 14 rotations in a drum with a diameter of 30 cm and a length of 60 cm.

Grajales et al. (2012) evaluated the number of rotations required for the complete mixing of cooked rice particles as a function of the drum rotation frequency (1, 4, and 7 rpm) and the particle load (5, 10, and 15 kg). No moisture control was applied to the particles, and the dyed grains represented only 10% of the total weight. The authors found that 11 rotations were sufficient for bed homogenization. However, the results found in this study showed that after 11 rotations, the rice bed with moisture contents of 0.667 and 0.250 kg-w/kg-ds reached experimental mixing indices of 84.59% and 92.59%, respectively, without ensuring complete bed homogenization. The difference in results can be attributed to the different moisture contents adopted in this study but, most importantly, to the amount of dyed particles used, which corresponded to approximately 45% of the total weight.

Figure 5.16 illustrates the variation rate of the mixing index as a function of the number of rotations. According to Seiden and Thomas (2011), the mixing process can present up to three distinct phases: the rapid mixing phase, the slow mixing phase, and the stationary phase. It is observed that, for both beds, the initial variation rate of *M* is relatively high, indicating that in the first few rotations, there is a more significant increase in the mixing index, especially in the fourth rotation. As *N* increases, the variation rate decreases, suggesting that the system is approaching a more homogeneous regime, where the increase in the mixing index is less significant. Thus, in this study, only the rapid and slow mixing phases were identified.

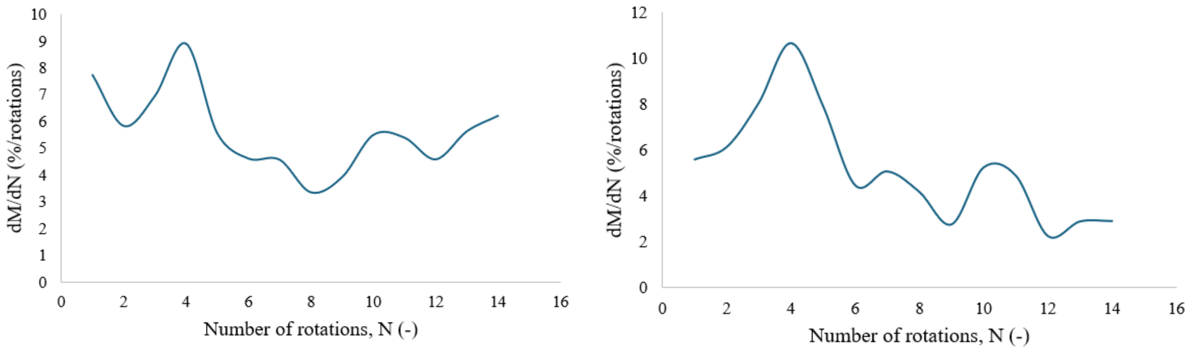

(a) (b)

Figure 5.16. Mixing index variation rate during the rotation of cooked rice beds with moisture content of (a) 0.667 and (b) 0.250 kg-w/kg-ds.

The drum used for the validation of the binary mixing of cooked rice particles does not correspond to the equipment described by Ferreira et al. (2025). While the present study employed a larger drum, the authors used a model with a 20 cm diameter (1.5 times smaller than the one used in the experimental validation) and a length of 33 cm, equipped with two 90° baffles, designed for intermittent rotation drying of rice. Thus, due to the impossibility of conducting experimental validation in the actual drum used for intermittent rotation drying—since it is made of stainless steel and does not allow visualization of the mixing process—the investigation was carried out through DEM simulations. Figure 5.17.a illustrates the simulated mixing index for the cooked rice beds at different moisture contents. It can be observed that the mixing index shows minimal increase after reaching 11 rotations. This trend becomes more evident in Figure 5.17.b, which displays the variation rate of the mixing index over the course of the rotations. In this case, the mixing process exhibits three distinct phases described by Seiden and Thomas (2011).

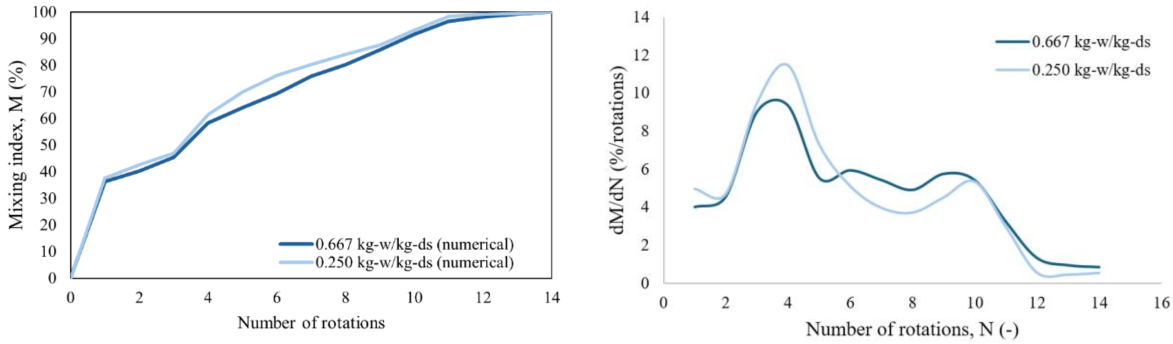

(a) (b)

Figure 5.17. Simulated (a) mixing index for cooked rice particles with moisture content of 0.667 and 0.250 kg-w/kg-ds and (b) mixing index variation rate, using a drum with a diameter of 20 cm and a length of 33 cm.

Assuming that the model is suitable for representing granular material, the simulations confirm that the mixing conditions used by Ferreira et al. (2025) (11 rotations at 7 rpm) are effective in ensuring homogenization throughout the entire intermittent rotation drying process. The faster homogenization observed when using the 20 cm diameter drum, compared to the 30 cm drum, can be attributed to the lower particle concentration due to the smaller diameter and the differences in the design of the employed lifters. Lifters play a fundamental role in promoting the interaction between solid and fluid phases. Additionally, they also influence the residence time of solids in the dryer and the degree of bed mixing (Sunkara, 2013). Straight lifters are recommended for drying highly cohesive and filamentous particles, as they significantly contribute to increasing mixing within the bed (Sunkara, 2013).

Although the angular velocity remains the same, the tangential velocity of the particles is lower in smaller drums. This reduction in tangential velocity decreases the inertial transport of particles along the surface, favoring greater internal agitation, which is essential for mixing. Furthermore, the energy supplied to the drum is distributed more concentrically due to the smaller surface area, resulting in more intense agitation and, consequently, more efficient mixing.

5.4 CONCLUSION

It is concluded that the reduction in moisture content in the particles during the drying process of cooked rice, used in the production of *Metarhizium anisopliae* in a rotating drum, influences the particle movement regime, the dynamic resting angle, and the mixing index. These changes result from alterations in the restitution, static friction, and rolling friction coefficients for particle-particle and particle-wall interactions, except for the ep-PW coefficient. The calibration of input parameters in the DEM simulations enabled the reproduction of resting angles close to experimental values, validating the model to confidently represent the behavior of cooked rice particles at different moisture levels.

Visual comparisons between experimental and numerical mixtures of cooked rice particle beds with different moisture contents show that, although the model does not exactly reproduce the positions of the particles, the mixing indices exhibit good agreement. It was observed that 14 rotations are needed to reach maximum mixing, with the reduction in moisture content accelerating the mixing process. Furthermore, smaller drums demonstrated higher efficiency, achieving stationary mixing after only 11 rotations. These results highlight the potential for bed homogenization in the implementation of more efficient drying systems through horizontal rotating drums with intermittent rotations. This approach has the potential to increase the economic and productive feasibility of large-scale bioinsecticide production, significantly contributing to sustainability in agricultural pest control.

5.5 REFERENCES

ANDRADE-HOYOS, P. et al. Specificity and Biocontrol Potential of Entomopathogenic Fungi. **The Role of Entomopathogenic Fungi in Agriculture**. CRC Press, p. 117-139, 2025.

BALAKRISHNAN, M. et al. Design, development, and evaluation of rotary drum dryer for turmeric rhizomes (*Curcuma longa* L.). **Journal of Food Process Engineering**, v. 45, n. 6, p. e14052, jun. 2022.

BHOPLE, S.; KUMAR, A.; HALDKAR, P. Effect of moisture content on angle of repose for different cereals and pulses. **International Journal of Chemical Studies**, v. 5, n. 5, p. 2283-2286, 2017.

BRANDAO, R. J. et al. Experimental study and DEM analysis of granular segregation in a rotating drum. **Powder Technology**, v. 364, p. 1–12, mar. 2020.

BRAR, H. S.; SIDHU, G. K.; SINGH, A.. Effect of moisture content on engineering properties of oats (Avena sativa L.). **Agricultural Engineering International: CIGR Journal**, v. 18, n. 3, p. 186-193, 2016.
CALLISTER, W. D.; RETHWISCH, D. G. **Materials Science and Engineering**. John wiley & sons, 2020.
CHUNG, Y.-C.; YEH, C.-H.; LIAO, C.-C. Experimental investigation into the wet non-spherical granular segregation and mixing in rotating drums. **Powder Technology**, v. 409, p. 117844, set. 2022.
COSTA, C. A. D. et al. Propriedades mecânicas e de fluxo de produtos agroindustriais. **Revista Brasileira de Engenharia Agrícola e Ambiental**, v. 18, n. 7, p. 774–780, jul. 2014.
DELELE, M. A.; WEIGLER, F.; MELLMANN, J. Advances in the Application of a Rotary Dryer for Drying of Agricultural Products: A Review. **Drying Technology**, v. 33, n. 5, p. 541–558, 4 abr. 2015.
FERREIRA, D. B.; TADA, É. F. R.; THOMÉO, J. C. Simulation of static drying and drying with intermittent rotations in a horizontal drum of rice used in the cultivation of Metarhizium anisopliae. **Chemical Engineering and Processing - Process Intensification**, v. 209, p. 110169, mar. 2025.
GRAJALES, L. M. et al. Mixing and motion of rice particles in a rotating drum. **Powder Technology**, v. 222, p. 167–175, maio 2012.
HERTZ, W. Die sage von Parzival und dem Gral. Schottlaender, 1882.
HONG, T. D.; JENKINS, N. E.; ELLIS, R. H. The effects of duration of development and drying regime on the longevity of conidia of Metarhizium flavoviride. **Mycological Research**, v. 104, n. 6, p. 662–665, jun. 2000.
JAFARI, A.; ABBASI HATTANI, R. Investigation of parameters influencing erosive wear using DEM. **Friction**, v. 8, n. 1, p. 136–150, fev. 2020.
JANKOVIC, A.; CHAUDHARY, G.; GOIA, F. Designing the design of experiments (DOE) – An investigation on the influence of different factorial designs on the characterization of complex systems. **Energy and Buildings**, v. 250, p. 111298, nov. 2021.
JARONSKI, S. T. Mass production of entomopathogenic fungi—state of the art. Mass production of beneficial organisms, p. 317-357, 2023.
JARONSKI, S. T.; JACKSON, M. A. Mass production of entomopathogenic Hypocreales. **Manual of techniques in invertebrate pathology**, v. 2, 2012.
JARRAY, A. et al. Cohesion-driven mixing and segregation of dry granular media. **Scientific Reports**, v. 9, n. 1, p. 13480, 17 set. 2019.
JENKINS, N. E. et al. Development of mass production technology for aerial conidia for use as mycopesticides. v. 19, n. 1, 1998.
JIA, H. et al. Contact parameter analysis and calibration in discrete element simulation of rice straw. **International Journal of Agricultural and Biological Engineering**, v. 14, n. 3, p. 72–81, 2021.
LACEY, P. M. C. The mixing of solid particles. **Chemical Engineering Research and Design**, v. 75, p. S49–S55, dez. 1997.
LIU, X. et al. DEM study on the surface mixing and whole mixing of granular materials in rotary drums. **Powder Technology**, v. 315, p. 438–444, jun. 2017.
LOUATI, H.; OULAHNA, D.; DE RYCK, A. Effect of the particle size and the liquid content on the shear behaviour of wet granular material. **Powder Technology**, v. 315, p. 398–409, jun. 2017.
MAHMOUD, G E.; ABD-EL SALAM, A. B.; AHMED, L. I.. Insecticides: Current status, properties, and the biological degradation strategies. **Development in Waste Water Treatment Research and Processes**, p. 45-70, 2025.

MARRONE, P. G. Status of the biopesticide market and prospects for new bioherbicides. **Pest Management Science**, v. 80, n. 1, p. 81–86, jan. 2024.
MELLMANN, J. The transverse motion of solids in rotating cylinders—forms of motion and transition behavior. **Powder Technology**, v. 118, n. 3, p. 251–270, ago. 2001.
MINDLIN, R. D. Compliance of elastic bodies in contact. 1949.
MOHAMED, A.; GUTIERREZ, M. Comprehensive study of the effects of rolling resistance on the stress–strain and strain localization behavior of granular materials. **Granular Matter**, v. 12, n. 5, p. 527–541, out. 2010.
MOYA, M. et al. Influence of Moisture Content on Some Mechanical Properties of Wheat. **Agronomy**, v. 14, n. 2, p. 347, 8 fev. 2024.
MUELLER, P. et al. The normal and oblique impact of three types of wet granules. **Granular Matter**, v. 13, p. 455-463, 2011.
NOROUZI, H. R.; ZARGHAMI, R.; MOSTOUFI, N. Insights into the granular flow in rotating drums. **Chemical Engineering Research and Design**, v. 102, p. 12–25, out. 2015.
NUNES, G.; DUARTE, C. R.; BARROZO, M. A. S. Experimental and numerical study of an alternative technique for fruit processing: Rotary drum with inert bed for acerola pulp dehydration. **Powder Technology**, v. 433, p. 119284, jan. 2024.
OBA, L. X. D. S. et al. Planting fertilization and Metarhizium anisopliae inoculation in the initial growth of sugarcane. **Revista de agricultura neotropical**, v. 11, n. 1, p. e7712, 9 fev. 2024.
PONCE-GARCÍA, N. et al. Effect of Moisture Content on the Viscoelastic Properties of Individual Wheat Kernels Evaluated by the Uniaxial Compression Test Under Small Strain. **Cereal Chemistry**, v. 90, n. 6, p. 558–563, nov. 2013.
RONG, W. et al. Sensitivity analysis of particle contact parameters for DEM simulation in a rotating drum using response surface methodology. **Powder Technology**, v. 362, p. 604–614, fev. 2020.
SAMADANI, A.; KUDROLLI, A. Segregation Transitions in Wet Granular Matter. **Physical Review Letters**, v. 85, n. 24, p. 5102–5105, 11 dez. 2000.
SANDRA et al. Effect of Moisture Content on Some Physical and Mechanical Properties of 'Genjah Arum' Local Rice (Oryza sativa L) Variety in Banyuwangi. **IOP Conference Series: Earth and Environmental Science**, v. 515, n. 1, p. 012020, 1 jun. 2020.
SADEGHI, M.; ARAGHI, H. A.; HEMMAT, A. Physico-mechanical properties of rough rice (Oryza sativa L.) grain as affected by variety and moisture content. **Agricultural Engineering International: CIGR Journal**, v. 12, n. 3-4, p. 129-136, 2010.

SEIDEN, G.; THOMAS, P. J. Complexity, segregation, and pattern formation in rotating-drum flows. **Reviews of Modern Physics**, v. 83, n. 4, p. 1323-1365, 2011.
SHATTUCK, A. et al. Global pesticide use and trade database (GloPUT): New estimates show pesticide use trends in low-income countries substantially underestimated. **Global Environmental Change**, v. 81, p. 102693, jul. 2023.
SUNKARA, Koteswara Rao. Granular flow and design studies in flighted rotating drums. Tese de Doutorado. Universitätsbibliothek, 2013.
TRAIN, D. Some aspects of the property of angle of repose of powders. **Journal of Pharmacy and Pharmacology**, v. 10, n. Supplement_1, p. 127T-135T, 1958.
TROJOSKY, M. Rotary drums for efficient drying and cooling. **Drying Technology**, v. 37, n. 5, p. 632–651, 4 abr. 2019.
VAN SLEEUWEN, R. et al. Efficient DEM modeling of solid flavor particle mixing in a rotary drum. **Powder Technology**, v. 437, p. 119559, mar. 2024.
WANDKAR, S. V.; UKEY, P. D.; PAWAR, D. A. Determination of physical properties of soybean at different moisture levels. **Agricultural Engineering International: CIGR Journal**, v. 14, n. 2, p. 138-142, 2012.

WANG, J. et al. Influencing Factors Analysis and Simulation Calibration of Restitution Coefficient of Rice Grain. **Applied Sciences**, v. 11, n. 13, p. 5884, 2021.

WU, W.; CHEN, K.; TSOTSAS, E. Prediction of particle mixing time in a rotary drum by 2D DEM simulations and cross-correlation. **Advanced Powder Technology**, v. 33, n. 4, p. 103512, abr. 2022.

XU, C. et al. Determination of Characteristics and Establishment of Discrete Element Model for Whole Rice Plant. **Agronomy**, v. 13, n. 8, p. 2098, 10 ago. 2023.

XU, Y. et al. 2D DEM simulation of particle mixing in rotating drum: A parametric study. **Particuology**, v. 8, n. 2, p. 141–149, abr. 2010.

ZAALOUK, A. K.; ZABADY, F. I. EFFECT OF MOISTURE CONTENT ON ANGLE OF REPOSE AND FRICTION COEFFICIENT OF WHEAT GRAIN. **Misr Journal of Agricultural Engineering**, v. 26, n. 1, p. 418–427, 1 jan. 2009.

ZHOU, Z. et al. Enhancing mixing of cohesive particles by baffles in a rotary drum. **Particuology**, v. 25, p. 104–110, abr. 2016.

6. EXTRACTION OF SPORES OF *METARHIZIUM ANISOPLIAE* IN A ROTARY DRUM

*Chapter accepted for publication in the journal Industrial Crops & Products.

ABSTRACT

The fungus *Metarhizium anisopliae* is widely used as a biological control agent of several agricultural pests. The microbe is produced using rice as substrate and the operation of extraction of spores needs improvement. This study explores an effective method for spore extraction using a rotary drum, with controlled variables including extraction time (4 and 8 hours), fill level (0.25 and 0.50), and drum rotation speed (30 and 60 rpm). The extraction efficiency achieved in this bench-scale setup ranged from 32.93% to 84.24%. Among the key parameters investigated, only the operation time showed a significant influence, with an 8-hour duration yielding the best performance. This improvement was attributed to the reduction in substrate moisture content throughout the process, indicating it as a critical factor affecting extraction performance. Lower moisture content reduced the shear force and impact required for spore detachment, leading to a more efficient extraction. Additionally, the results suggest that spores are detached through particle collisions rather than by the dragging force promoted by the flowing air, which is essential for predicting optimal process configurations. This research, therefore, lays the foundation for the development of more efficient extraction systems, contributing to the cost-effective large-scale production of bioinsecticides.

Keywords: *Metarhizium anisopliae*; extraction; rotary drum; rice; spores; adhesion force.

6.1 INTRODUCTION

Biopesticides have provided more sustainable solutions compared to the indiscriminate use of chemical pesticides, whose continuous application has led to serious environmental consequences, such as the depletion of natural resources, soil and water contamination, and the deterioration of ecosystems. These biological agents not only reduce environmental impacts but also promote plant health and foster a more resilient and ecologically balanced agricultural production (Ferreyra-Suarez et al., 2024). The bioinsecticide market has shown significant growth, with projections to reach $15 billion by 2029, reflecting the increasing demand for sustainable and effective pest control solutions (Marrone, 2024). Currently, it accounts for about 10% of the global pesticide market, driven by various factors such as increased return on investment and growing legal and commercial restrictions on the use of chemical pesticides (Marrone, 2024). Mycoinsecticides accounts for 10% of the global bioinsecticide market, with *Metarhizium anisopliae* representing 16% of this share (Zakia et al., 2020). This fungus has gained prominence due to its effectiveness in controlling over 200 species of agricultural pests (Kruger et al., 2014; Nishi; Sato, 2017; Fontes;Valadares-Inglis, 2020). It is estimated that over 2 million hectares of sugarcane plantations in Brazil are treated with *M. anisopliae* in Brazil (Iwanicki et al., 2019).

The production of conidia of *M. anisopliae* is traditionally carried out through solid-state cultivation (SSC), with rice being widely used as substrate due to its large surface area, low deformation during cultivation, and ability to provide the necessary nutrients for fungal growth (Dorta; Arcas, 1998; Kruger et al., 2014). However, in developing countries, this technique requires intensive manual labor, which can negatively affect both the quantity and quality of the final product (Mendez-Gonzalez et al., 2018). Furthermore, the use of inadequate equipment or adaptations from other processes increases losses during production and can create unhealthy conditions for workers, thereby amplifying the challenges associated with large-scale production. Nevertheless, the rising demand for biopesticides has driven the development of new strategies to expand the production of fungal propagules.

One of the stages that requires greater technological development is the extraction of spores from rice. The traditional extraction method involves the use of shaking sieves (Posada-Flórez, 2008), which is associated with low productivity and potential harm to workers due to spore losses into the environment. A method frequently employed in laboratories is extraction using aqueous solutions of surfactants. However, this method causes imbibition damage to the spores (Faria et al., 2009). Several alternatives have been suggested to improve this stage, including the use of a modified household dryer equipped with fans and cyclones to collect conidia (Jenkins et al., 1998), and a portable concrete mixer combined with a vacuum cleaner for agitation and suction of the spores (Jaronski; Jackson, 2012). However, these artisanal approaches have limitations and are not viable for large-scale production. The same applies to the Mycoharvester spore separator (Liu et al., 2015; Velozo et al., 2023), which, despite having an extraction efficiency of 85%, is not presented as a scalable solution. Liu et al. (2015) compared three spore extraction methods: liquid extraction, vibrating sieves with a 75 μm opening, and double cyclones, achieving extraction efficiencies of approximately 53%, 55%, and 92%, respectively. Thus, extraction using double cyclones stands out in the literature as the most efficient method to date. In this system, the cultivated rice is pneumatically transported, where friction interactions occur. Coarse particles and rice are collected in the cyclone underflow, while the finer particles containing spores are discharged in the overflow and further collected in a cylinder.

In addition to achieving efficiency levels comparable to traditional methods, the proposal for new equipment for spore extraction must offer technological advantages that justify its adoption. To achieve this, it is essential to understand the mechanisms involved in extraction in order to facilitate a successful design and determine the ideal operational conditions (Zastawany et al., 2012). The extraction mechanisms should generate stresses capable of overcoming the adhesive forces that keep the spores attached to the substrate, promoting their release (Gui et al., 2010). Besides the magnitude of the applied forces, the duration of this stress is also critical; the longer the application time, the greater the chance of overcoming adhesion (Levitt, 1980). However, literature still lacks information on the intensity of these forces, and there is a scarcity of studies addressing the variability in adhesion forces observed on different substrates and under varying conditions.

In this context, the rotary drum stands out as a promising alternative for removing spores from substrates due to its high processing capacity and operational flexibility, being one of the most widely used industrial equipment for drying various particulate materials (Tarhan et al., 2010; Govender, 2016; Ferreira et al., 2025). Rotary drums are often used in combination with cyclones to separate fine particles from the downstream gas flow. Cyclones are considered one of the simplest and most economical gas-solid separators due to their high efficiency, adaptability, and relative energy savings (Marinuc; Rus, 2011; Napier-Munn, 2018; El-Emam et al., 2019). Furthermore, this equipment is easy to design and scalable, allowing for quick adaptation to different production needs.

Given this, the aim of this work was to use a rotating drum to extract the spores of M. anisopliae from rice and collect the spores in cyclones. The experiments have been carried out under varying operational conditions to determine the optimal extraction efficiency, and the results were compared with those obtained with the traditional shaking-sieve method. The adhesion force of the spores to the solid substrate was experimentally determined. The study seeks to offer a scalable solution for biofactories, aiming to increase productivity, reduce losses, and improve operational safety.

6.2 MATERIALS AND METHODS

6.2.1 Microorganism

The fungus Metarhizium anisopliae IBCB 425 was kindly provided by the Biological Institute of São Paulo, Brazil. Stock cultures were maintained in test tubes containing potato dextrose agar (PDA) medium and covered by a thin layer of mineral oil at 4°C. The inoculum was prepared by transferring fungal spores to Erlenmeyer flasks containing 50 mL of PDA, which were kept in a climate chamber at 28°C for 15 days. The spores were harvested by adding Tween 80 (0,1% v/v) to the flask and scraping the surface of the culture to suspend them. The spore concentration was adjusted to 107 spores per gram of dry solid substrate (g-ds henceforth) in all experiments.

6.2.2 Spore production of *Metarhizium anisopliae*

Solid-state cultivation was carried out in plastic packaging with a load of 400 g (dry weight) of rice (*Oryza sativa*). The openings of the polypropylene packages were fitted with short PVC tubes 5 cm internal diameter, into which cotton plugs were inserted to allow gas exchange and prevent exogenous contamination. Water was added to the substrate, and it was autoclaved at 121°C for 30 minutes. After cooling, the spore suspension was added to each plastic package, followed by vigorous manual mixing. At the end of the inoculation, the substrate had a moisture content of 0.887 kg of water per kg of dry solid substrate (kg-w/kg-ds henceforth). The fungus was cultivated for 10 days in a climate chamber at 28°C, following the literature (Dorta; Arcas, 1998; Li; Feng, 2009; Cunha et al., 2020).

To facilitate the removal of spores from the substrate, the cultivated rice was pre-dried before the extraction process until reaching a moisture content of 0.250 kg-w/kg-ds. This final moisture content is often used in biofactories prior to the extraction of spores. For this purpose, the packages were opened, and the conidiated rice was placed in trays, which were then kept in a climatic chamber at 30°C. A MB45 infrared balance (OHAUS, Parsippany, USA) was used to determine the moisture content of the substrate. Figure 6.1 illustrates the flowchart of the M. anisopliae spore production process up to the extraction stage, highlighting the moisture levels to be achieved by the rice and spores at each step. In addition to the stages presented, the complete process in biofactories included a final drying stage for the extracted spores and the product formulation. These final steps were not investigated in this study.

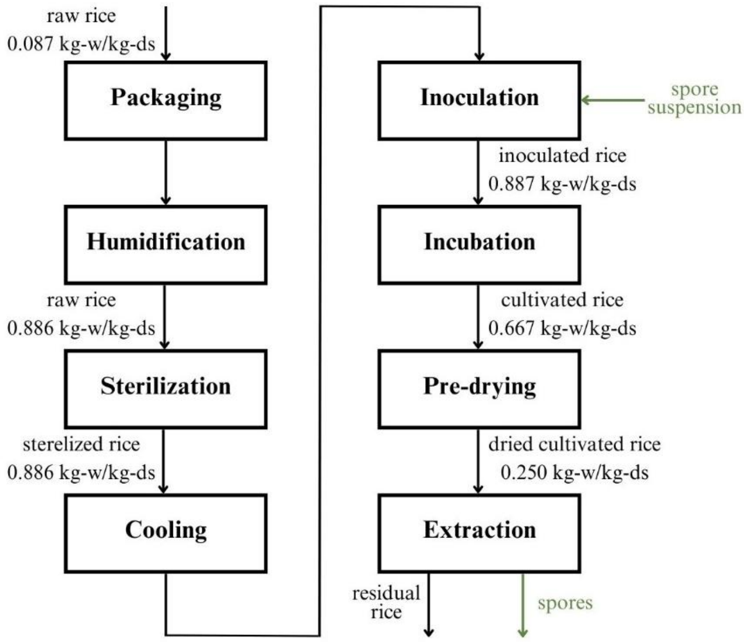

Figure 6.1. Flowchart of the *Metarhizium anisopliae* spore production process.

6.2.3 Spore extraction with vibrating sieves to generate reference data sets

To simulate the extraction of spores often applied in biofactories and to produce reference values for the extraction, experiments of extraction of spores were carried out using an electromagnetic sieve shaker (Bertel, Caieiras, Brazil). The setup included a set of sieves with mesh openings of 0.212, 0.150, 0.106 and 0.037 mm, and the flat-bottom pan. The extraction trials followed a factorial statistical design with randomized blocks, varying the load (L_{rice}) (50, 100, 150, and 200 g) and extraction time (t_s) (10, 15, 20, 25, and 30 minutes). The joints of adjacent sieves were sealed with duct tape to minimize spore loss to the environment. Each treatment was independently repeated three times under the same conditions.

To account for the extracted mass, the sieves were weighed before and after the operation using a semi-analytical balance. The extracted spores were collected using a brush, weighed, and a suspension was prepared by adding 10 mL of 0.1% (v/v) Tween 80 solution per gram of extracted spores. This suspension was homogenized in a reciprocating bath at 120 cycles/min for 20 minutes. The concentration of spores was determined in a hemocytometer using a microscope at 40x magnification. The residual rice retained in the first sieve of the set (0.212 mm opening) was collected, and the remaining spores were removed as described in section 6.2.6. The extraction efficiency was assessed by:

$$\eta_{ext,s}\ (\%) = \frac{(E_{ext,s})}{(E_{ext,s} + E_{unext,s})} \tag{6.1}$$

where $\eta_{ext,s}$ is the spore extraction efficiency using vibrating sieves (%); $E_{ext,s}$ is the extracted spores collected from all the sieves, and $E_{unext,s}$ is the non-extracted spores from the residual rice (conidia) using the shaking sieves.

The model Rosin-Rammler-Bennet (RRB) (Green; Southard, 2018) was applied to the experimental values of the accumulated fraction of spores restrained in the sieves (X_p). The RRB model is represented by the following equation:

$$X_p = 1 - \exp\left({}^{D_p}\!/\!_{D_{63.2}}\right)^{n} \tag{6.2}$$

where D_p is the diameter of particle, $D_{63.2}$ is the diameter of particle corresponding the X = 63.2% and n a constant. The parameters $D_{63.2}$ and n were estimated by fitting the model to the experimental data. The software Origin 9.0 (Origin Lab, Northampton, USA) was used for the fitting procedure of this non-linear model and the algorithm of Levenberg-Marquardt was applied to the optimization of the search of the global minimum.

6.2.4 Cyclone sizing

The design of the two cyclones used to collect the spores after being extracted in the rotary drum was carried out using the correlations described by Massarani (1997). This method requires the particle size distribution of the powder extracted and it was carried out using shaking sieves with a set of sieves with openings of 0.212, 0.180, 0.150, 0.075, and 0.045 mm, and the flat-bottom pan. The experiments were carried out in triplicate, shaking 50 g of spores for 25 minutes. The sieves were weighed before and after the operation to quantify the retained fractions.

The cyclone configuration is characterized by a specific relationship between its dimensions in relation to the diameter of the cylindrical section of the equipment (D_c). Table 6.1 lists the standardized relationships between cyclone dimensions in the Stairmand (Stairmand, 1951) configuration, as represented in Figure 6.2.

Table 6.1. Cyclone dimensions in the Stairmand configuration.

Relationship	Stairmand
B_c/D_c	0.20
D_o/D_c	0.50
H_c/D_c	0.50
L_c/D_c	1.50
S_c/D_c	0.50
Z_c/D_c	2.50
D_u/D_c	0.37

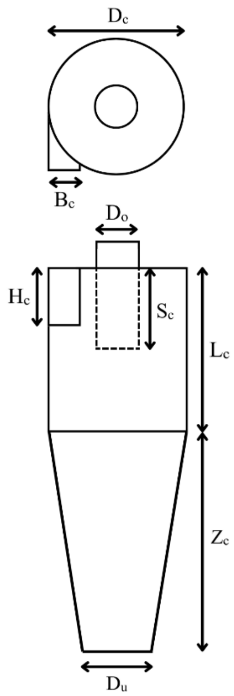

Figure 6.2. Dimensional relationships of the Stairmand configuration for cyclone dimensioning.

The overall efficiency was calculated based on the individual efficiency (η), obtained from Eq. (6.3) for each particle diameter (D_P). The cut diameter (D^*), was determined using Eq. (6.4) (Massarani, 1997):

$$\eta = \frac{\left(\frac{D_P}{D^*}\right)^2}{1 + \left(\frac{D_P}{D^*}\right)^2} \tag{6.3}$$

$$\frac{D^*}{D_c} = K \left[\frac{\mu\, D_c}{Q\ (\rho_s - \rho)}\right]^{1/2} \tag{6.4}$$

where K is a constant that depends on the cyclone configuration, with value of 0.041 for the Stairmand model; μ is the fluid viscosity, Q is the volumetric flow rate of the gas (m^3/s), ρ_s is the specific mass of the spores, with value of 156.67 kg/m^3 and ρ is the specific mass of the fluid. The physical properties of air were obtained from literature at 25ºC (Green; Southard, 2018). The specific mass was determined using the volumetric method, employing a 25 mL measuring cylinder, in which the total volume of a given mass of spores was measured directly.

6.2.5 Spore extraction in rotary drum with two downstream cyclones and filter

Aiming to investigate the proper functioning of the designed cyclone and to outline a more accurate experimental plan, the extraction kinetics in a horizontal rotary drum with spore collection in a cyclone were established. For this, the conditions adopted by Cunha (2020) in preliminary tests were used, which included a filling degree (*f*) of 0.33, a rotation speed (w) of 60 rpm, and an operation time (t_d) of 14 hours. The extraction kinetics were determined using conidiated rice with an initial moisture content of 0.667 kg-w/kg-ds, obtained after the incubation stage, and pre-dried rice with an initial moisture content of 0.250 kg-w/kg-ds. The objective was to investigate the feasibility of eliminating the pre-drying stage in the production process of *M. anisopliae*.

The spore extraction was carried out using the experimental setup represented in Figure 6.3. The system consisted of a horizontal drum 20 cm internal diameter and 33 cm length. Inside the drum, there were two straight longitudinal blades, each 2 cm wide, positioned perpendicularly to the drum wall to improve the movement of the particles. The two designed cyclones were connected in series to collect the spores carried out by the flowing air. To the overflow of the second cyclone was attached a filter to restrain any remaining particles that could be released into the environment. The drum was rotated using a system of rotating rollers (PHD Equipamentos, Piracicaba, Brazil), while dry air was flown throughout the drum to transport the extracted spores to the cyclones. The air was dried in a silica gel column and its flow rate was fixed at 100 L/min, following preliminary experiments. The relative humidity of the air was measured using a digital thermo-hygrometer MTH-1362 (Minipa Inc., Houston, USA). At the end of the extraction period, the airflow rate was increased to 150 L/min for 5 minutes to remove the spores adhered to the drum-wall and transport them to the restraining flask.

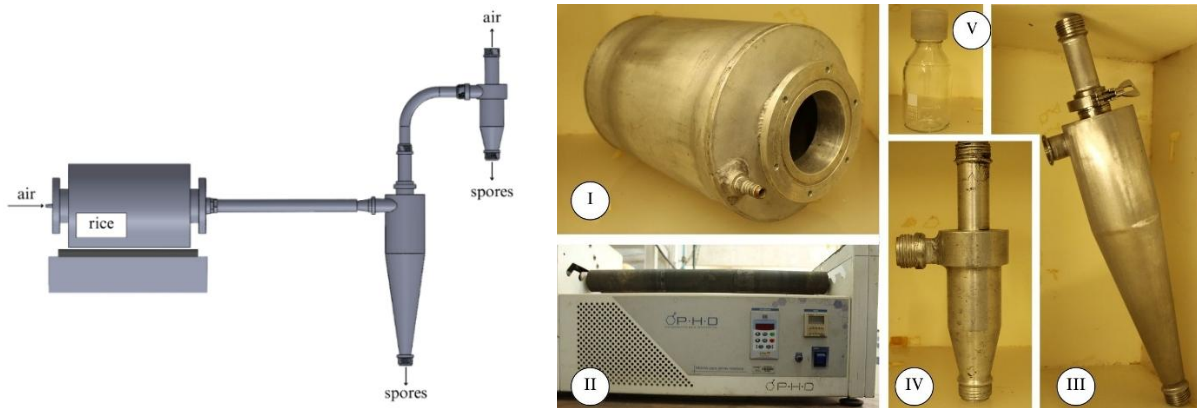

(a) (b)

Figure 6.3. Experimental setup used for spore extraction in a rotary drum: (a) Diagram of the setup; (b) equipment used: I) rotary drum; II) rotator; III) first cyclone; IV) second cyclone; and V) spore restraining flask.

Table 6.2 presents the controlled variables adopted to determine the optimal extraction conditions, which were the drum rotation speed (w), operation time (t), and volumetric filling degree (*f*), as well as other technical details relevant to the process. The filling degree was determined by the ratio between the cross-sectional area of the cylinder occupied by the particles and the total volume of the cylinder, as defined by Mellmann (2001). For the configuration with a filling degree of 0.50, a total of 1.992 kg of dry conidiated rice was used, while for the filling degree of 0.25, the value was 1 kg of dry conidiated rice. The experiments were conducted following a full factorial statistical design at two levels with randomized blocks.

The response variables were the mass of material extracted, which may include mycelium, spores and rice fragments; the total quantity of spores collected in the two cyclones and in the filter; and the quantity of non-extracted spores that remained adhered to the rice after the experiment. The mass of extracted material was determined by weighing the restraining flasks of the two cyclones before and after the operation using an analytical balance. The quantity of restrained spores was determined from the spore suspension described in Section 6.2.3.

Table 6.2. Operational conditions for the extraction experiments in the rotary drum.

Variable		Value
Fixed	Initial moisture content of conidiated rice	0.250 kg-w/kg-ds
	Volumetric air flow rate	100 L/min
	Air velocity in drum cross section	0.053 m/s
	Relative humidity of the air	15%
Controlled	Rotational speed of the drum (w)	30 and 60 rpm
	Drum fill level (f)	0.25 and 0.50
	Extraction time (t)	4 and 8 hours

At the end of the process, the rice retained in the drum was also subjected to liquid extraction, as described in section 6.2.6. The experiment was independently repeated three times for each experimental condition. The extraction and restraining efficiencies were determined according to Eqs. (6.5) and (6.6):

$$\eta_{ext,d}\,(\%) = \frac{(E_{C1} + E_{C2} + E_F)}{(E_{C1} + E_{C2} + E_F + E_{unext})} \tag{6.5}$$

$$\eta_{col}\,(\%) = \frac{(E_{C1} + E_{C2})}{(E_{C1} + E_{C2} + E_F + E_{unext})} \tag{6.6}$$

where $\eta_{ext,d}$ is the spore total extraction efficiency using the rotary drum, E_{C1} is the spores restrained in the underflow of the first cyclone, E_{C2} is the spores restrained in the underflow of the second cyclone, E_F is the spores restrained in the filter, E_{unext} is the non-extracted spores that remained adhered to the rice after the process; and η_{col} is the useful efficiency, which disregards the spores retained in the filter.

6.2.6 Liquid extraction of residual spores on rice and equipment

The spores adhered to the residual rice after the extraction processes were removed through liquid extraction. For this, 5 mL of a 0.1% (v/v) Tween 80 solution was added per gram of dry rice (Cunha et al., 2020). The mixture was agitated in a reciprocating bath at 120 cycles/min for 50 minutes. The spores present in this solution were counted in a Neubauer chamber, using a microscope with 40x magnification. The analysis was performed in triplicate.

6.2.7 Moisture content of spores

Considering that the moisture content of the spores is crucial for ensuring the quality of the final product as well as the process parameters, the moisture content of the spores restrained in each of the cyclones, as well as the moisture content of the material restrained in the filter and in the residual rice, was determined using the infrared balance MB45.

6.2.8 Spore removal by air flow

The minimum air velocities required for spore removal, and the corresponding minimum drag forces, were determined through optical experiments (section 6.2.8.1) and measurements using a magnetic suspension balance (section 6.2.8.2). These techniques act in different velocity ranges as given below. The experiments were conducted using conidiated rice with moisture contents of 0.250, 0.111, and 0.053 kg-w/kg-ds (moisture contents of the conidiated rice at the beginning, after 4 h, and 8 h of extraction in a rotary drum, respectively). To ensure consistency of the results, the experiments were repeated with ten different particles for each moisture content.

The drag force promoted by the flowing air on the spores attached to the rice was determined under conditions similar to those in the rotary drum, to evaluate the role of airflow in the extraction process. The drag force (F_D) was calculated using Eq. (6.7). The drag coefficients (C_D) were determined for particles referred to as “discs” by Zastawny et al. (2012) using the correlations in Eqs. (6.8) to (6.10), which accounted for the particle's angle relative to the airflow. The drag force was calculated for different air velocities, ranging from 0.00021 to 1.25 m/s, corresponding to the minimum and maximum capacities of the experimental setups used in the optical and magnetic suspension balance experiments.

$$F_D = \frac{1}{2}\rho v^2 A_p C_{D(\varphi)} \tag{6.7}$$

$$C_{D(\varphi)} = C_{D(\varphi=0º)} + \left(C_{D(\varphi=90º)} - C_{D(\varphi=0º)}\right) sin^{a0}\varphi \tag{6.8}$$

$$C_{D(\varphi=0º)} = \frac{a1}{Re^{a2}} + \frac{a3}{Re^{a4}} \tag{6.9}$$

$$C_{D(\varphi=90º)} = \frac{a5}{Re^{a6}} + \frac{a7}{Re^{a8}} \tag{6.10}$$

where ν is the air velocity, A_p is the particle reference area, φ is the particle angle, and a0, a1, a2, a3, a4, a5, a6, a7, and a8 are constants, being 1.96, 5.82, 0.44, 15.56, 1.07, 35.41, 0.96, 3.63 and 0.05 respectively, predicted by Zastawny et al. (2012) for disc-shaped particles, and Re is the Reynolds number based on the particle diameter. The dimensions were obtained from photographic images of samples containing more than 100 conidiated rice grains with different moisture contents, analyzed using the ImageJ software.

Based on observations from the optical experiments and measurements taken with the magnetic suspension balance, it was possible to determine the magnitude of the adhesion forces (F_{ad}) between the spores and the substrate at different moisture contents. This was achieved by determining the drag forces associated with air velocities that enable spore detachment, as well as those where removal does not occur, thereby establishing a probable range for the adhesion force.

6.2.8.1 Optical experiments

The optical experiments were conducted in a cuboid glass chamber with dimensions of 20 x 20 x 100 mm, as illustrated in Figure 6.4 (Janocha; Tsotsas, 2021). The air flow varied within the range of 0.0208 to 1.25 m/s, maintaining laminar flow at all velocities. A charge-coupled device (CCD) camera system JAI GO-5000-PMCL, 107 fps (JAI A/S, Copenhagen, Denmark) was used to optically determine the minimum airflow required to remove a visible portion of the spores. The air supplied was dry, and consequently, the moisture content of the particles decreased during the measurement. The air temperature could not be directly controlled, but it was considered constant at 25ºC, reflecting the average temperature of the experimental environment.

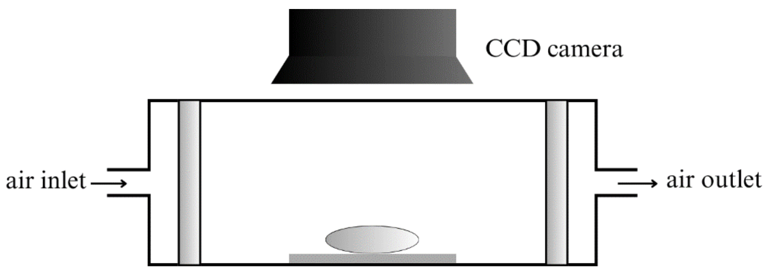

Figure 6.4. Diagram of the experimental setup to determine the minimum airflow required for spore removal.

6.2.8.2 Magnetic suspension balance

The magnetic suspension balance MSB (RUBOTHERM, Bochum, Germany), represented in the schematic in Figure 6.5 (Kwapinski; Tsotsas, 2004; Le et al., 2018), air velocities lower than those employed in the optical experiments. The air flow varied within the range of 0.00021 to 0.0207 m/s, where the upper limit corresponds to the lower limit employed in the optical method and also the maximum achieved by the MSB setup. The air temperature was set at 25ºC, and the air humidity was adjusted to maintain equilibrium with the conidiated rice at different moisture contents (0.250, 0.111, and 0.053 kg-w/kg-ds), based on the sorption and desorption isotherms for rice (Zeymer et al., 2017). The equipment measured the mass variation of a single particle caused by spore removal due to airflow over 20 minutes.

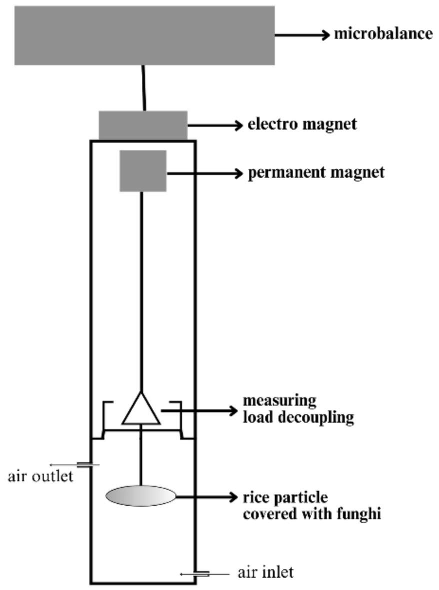

Figure 6.5. Schematic of the magnetic suspension balance experiments.

6.2.9 Statistical analyses

Analyzes of variance (ANOVA) and Tukey tests of comparison of means with a confidence level of 95% were carried out using Microsoft Excel 365 (Microsoft Co., Redmond, USA). ANOVA of the multiple regression analysis was used to determine the influence of each variable on extraction efficiency in sieves and the rotating drum experiments, using Minitab 18 software (Minitab Inc., State College, USA).

6.3 RESULTS AND DISCUSSION

6.3.1 Extraction of spores using vibrating sieves

Little information is available in literature regarding the efficiency of the most commonly used industrial method for extracting spores from cultivated rice. Therefore, the experiments carried out in this work with shaking sieves will serve as a reference for the further experiments in the rotating drum. The extraction efficiency of spores using shaking sieves under different operational conditions is illustrated in the surface response presented in Figure 6.6.

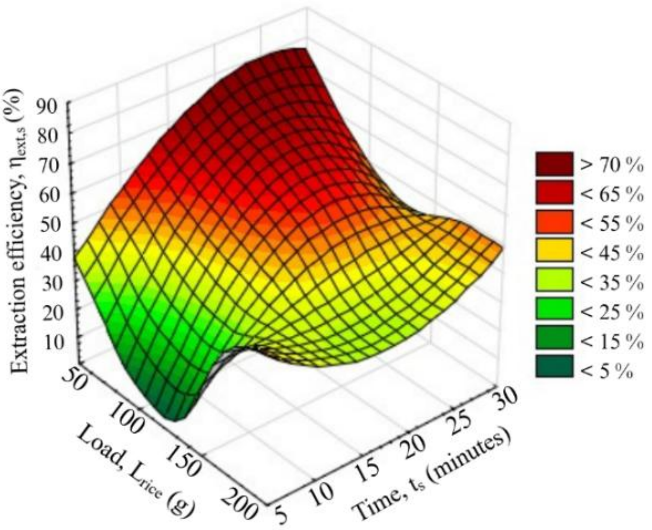

Figure 6.6. Extraction efficiency using vibrating sieves.

ANOVA, presented in Table 6.3, indicated that the statistical model is predictive and that both independent variables, rice load and time, significantly influenced the extraction efficiency. The highest efficiency was achieved with a 50 g load shaken for 25 minutes, reaching 77.45% efficiency, while the lowest extraction occurred with 200 g shaken for 10 minutes, resulting in 12.52%. The highest efficiency observed with the lowest load of conidiated rice (50 g) can be attributed to the high mobility of the particles to collide intensely with each other and with the walls and screens of the sieves, promoting a more effective release of the spores. Jaronski (2014) reports that operations of this type typically achieve extraction efficiencies ranging from 60% to 90%, while Liu et al. (2015) obtained an average extraction efficiency of 55%. Considering that, in industrial conditions, the load of particles in the sieves will be high, it is reasonable to assume that extraction efficiencies will be low.

Table 6.3. Analysis of variance (ANOVA) and multiple regression for the dependence of extraction efficiency on the adopted operational variables.

Variables	**P-value**
Load (L_{rice})	0.0003
Time (t_s)	0.0437
R^2 = 0.714 R^2 (adj) = 0.666 F = 14.977	F-sig = 0.0005

R^2 – coefficient of determination; R^2(adj) – adjusted coefficient of determination; F – F-statistic of the ANOVA test; F-sig: P-value associated with the F-statistic; P-value – Probability associated with the significance test for each coefficient.

6.3.2 Cyclone sizing

To design the cyclones to collect the spores from the outlet air flow leaving the rotary drum, it was necessary to determine the particle size distribution of the extracted material. The accumulated fraction curve is presented in Figure 6.7.a and the fitting of the RRB is presented in Figure 6.7.b. It can be observed that most of the restrained particles (95.79%) have diameter between 0.1 and 0.2 mm and, according to the RRB model, $D_{63.2}$ was estimated as 0.139 mm. The cut diameter (D^*) was estimated at 0.119 mm. The model fitting was good as the determination coefficient (R^2) was of 99%. The first cyclone was designed to collect 88% of particles with diameters ranging from 0.208 mm to 0.074 mm, while the second cyclone was designed to restrain 98% of particles with diameters ranging from 0.074 mm to 0.043 mm. The calculated diameter of the cylindrical section of the cyclone (D_c) and the other dimensions are presented in Table 6.4.

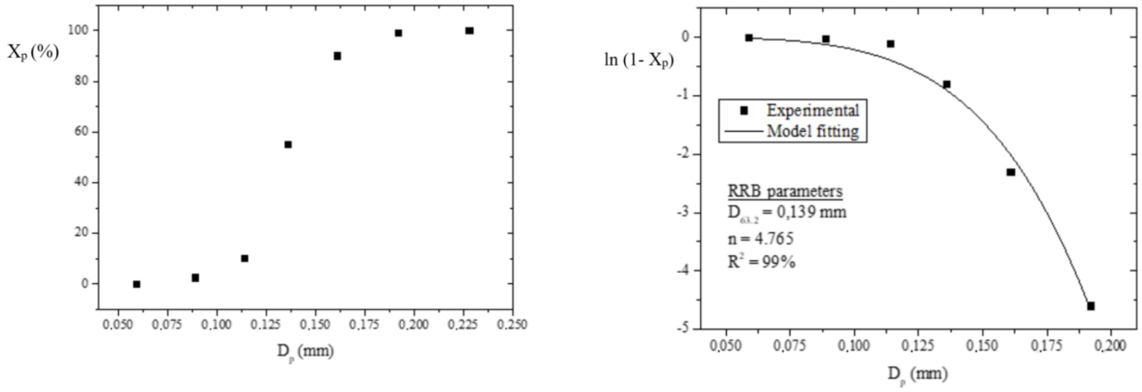

(a) (b)

Figure 6.7. Granulometric distribution of the accumulated mass fraction of spores obtained using shaking sieves (a) and fitting curve and estimated parameters of the RRB model (b).

Table 6.4. Dimensions of cyclones and pressure drop adopting the Stairmand model.

Value	**Cyclone 1**	**Cyclone 2**
D_c (m)	0.148	0.040
B_c (m)	0.030	0.008
D_o (m)	0.074	0.020
H_c (m)	0.074	0.020
L_c (m)	0.222	0.060
S_c (m)	0.074	0.020
Z_c (m)	0.370	0.100
D_u (m)	0.055	0.015
ΔP (Pa)	5.510	1036.810

6.3.3 Kinetic analysis of spore extraction in a horizontal drum

Figure 6.8 presents the extraction kinetics of the collected extract using conidiated rice at moisture contents of 0.667 and 0.250 kg-w/kg-ds. At the end of the 14-hour extraction, both materials reached similar masses of extracted agglomerated material. However, a significant difference in the extraction pattern is observed. With more humid particles, the extraction occurs gradually, whereas for the drier conidiated rice, approximately 45% of the total extracted material (7.07 g) is removed within the first hour of operation. This difference suggests that, under the evaluated conditions, the operation can be interrupted at 8 hours when using drier particles.

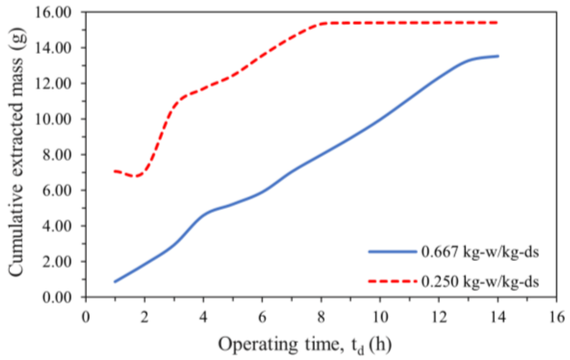

Figure 6.8. Cumulative mass extraction kinetics during rotary drum extraction with moist conidiated rice and pre-dried conidiated rice, rotating at 60 rpm with a filling degree of 0.33 over 14 hours.

Considering that drying is an operation that requires high energy costs, from an economic perspective, it would be advantageous not to perform it beforehand. To achieve this, certain conditions need to be met: i) the energy cost of extraction in the rotary drum should be lower than that of traditional natural convection drying; ii) the extraction efficiency must be maintained; and iii) the spores must reach a low moisture content at the end of the process to avoid high energy consumption during the final drying.

However, one should not overlook the various advantages that slow drying offers for the viability and virulence of the spores (Jaronski, Jackson, 2012; Jaronski, 2014). Therefore, to investigate whether the final moisture content of the spores was adequate, the moisture kinetics of the extracted agglomerated material were determined and are presented in Figure 6.9.

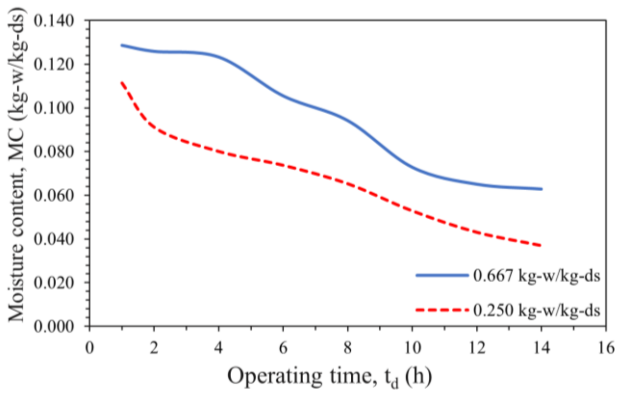

Figure 6.9. Moisture content of extracted spores during rotary drum extraction with moist conidiated rice and pre-dried conidiated rice, rotating at 60 rpm with a filling degree of 0.33 over 14 hours.

It can be observed that both samples follow the same trend in terms of moisture loss during the extraction operations. The agglomerated particles collected in the first hour, from the pre-dried conidiated rice (0.250 kg-w/kg-ds), already have a moisture content of 0.111 kg-w/kg-ds. For the moist conidiated rice, the agglomerate obtained in the first hour has a moisture content of 0.129 kg-w/kg-ds. This suggests that the water present in the conidiated rice is weakly bound to the solid matrix, meaning it is in the intergranular spaces and is therefore easily removed. At the end of the process, the spores have a moisture content of 0.067 and 0.037 kg-w/kg-ds for the moist and dry materials, respectively.

The number of spores extracted throughout the rotary drum extraction process is presented in Figure 6.10. It is observed that most of the spores are extracted in the first hours of the process: 35.22% of the spores are extracted within 2 hours of operation for moist conidiated rice (0.667 kg-w/kg-ds), while for pre-dried conidiated rice, 59.95% of the spores are removed in the same period. This result confirms that prior drying of the material facilitates spore detachment, as previously reported in the literature (Sala et al., 2019). Additionally, it is noted that the operation with conidiated rice at a moisture content of 0.250 kg-w/kg-ds extracts approximately six times more spores. The overall extraction efficiency achieved was 62.36 ± 2.03% and 80.61 ± 4.63% for conidiated rice with moisture contents of 0.667 and 0.250 kg-w/kg-ds, respectively. The extraction efficiencies of both materials were within the expected range for this type of operation, which varies between 60% and 90% (Jaronski, 2014).

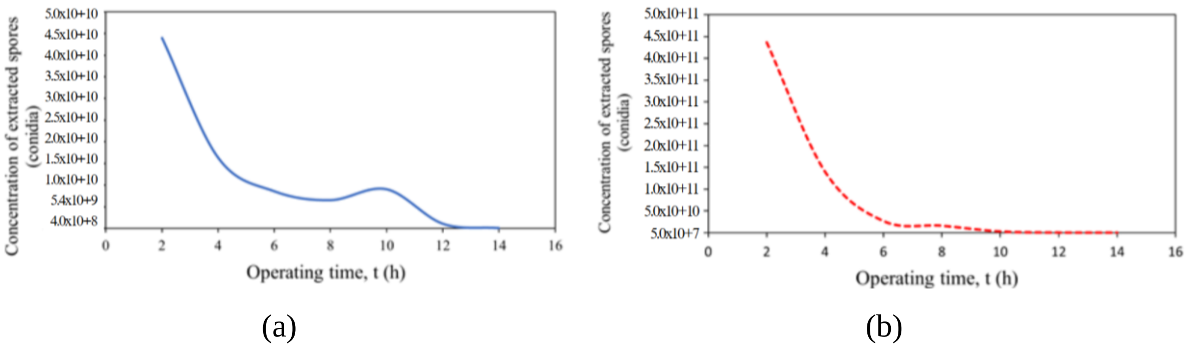

Figure 6.10. Concentration of extracted spores during rotary drum extraction rotating at 60 rpm with a filling degree of 0.33 over 14 hours foi conidiated rice with moisture content of (a) 0.667 and (b) 0.250 kg-w/kg-ds.

6.3.4 Extraction of spores in rotary drum

The experimental results obtained for the experiments of spore extraction are summarized in Table 6.5. Figure 6.11 presents photographs of the cultivated rice prior to the extraction and after 4h and 8h of extraction. Considering that for the analysis of variance only the linear terms have been chosen for the statistical model, this model is predictive at 95% confidence level for the responses $\eta_{ext\text{-}d}$ and η_{col}, and the factor time was the only significant. For the responses E_{ext} and E_{unext} the model is not predictive at the chosen confidence level. The average difference between $\eta_{ext,d}$ and η_{col} is of 3% and indicates that the adopted cyclones can restrain most of the particles.

(a) (b) (c)

Figure 6.11. Rice particles conidized (a) before extraction, (b) after 4 hours of extraction, and (c) after 8 hours of extraction, using a rotation speed of 30 rpm and a filling degree of 0.50.

Analysis of variance (ANOVA) is presented in Table 6.6. The comparison of means using the Tukey test indicates that the trial with the efficiency obtained in Run 7 is significantly higher than the other, except for Run 6. For a new extraction process to be considered industrially viable, it must achieve extraction efficiencies similar to those obtained using shaking sieves. Runs 6 and 7 present extractions efficiencies similar to that achieved with the shaking sieves (section 6.3.1), which are not significantly distinct according to the Tukey test. Considering that Run 6 processes twice the amount of material as Run 7 in the same time, it was assumed that the more suitable condition to adopt is a rotation speed of 30 rpm, a filling degree of 0.50, and an extraction time of 8 hours.

The results of the yield in mass of the extracted material and the concentration of spores are presented in Table 6.7. The comparison of means using Tukey's test revealed that the set of variables significantly influences most of the results related to the extracted mass. On the other hand, there are similarities in the spore concentrations in the extracted material, indicating a relative uniformity in this parameter regardless of the tested conditions, except for the variables adopted in Run 4. It can be observed that a greater extracted mass occurs in trials with a lower filling degree. However, tests conducted with a higher filling degree resulted in a greater concentration of spores per gram of extracted mass. This suggests that experiments with a lower filling degree result in a greater release of fragments of rice and fungal mycelium, driven by increased attrition among particles and between the particles and the drum-wall. The same pattern was observed with prolonged extraction times, possibly due to the gradual exposure of the inner layers of the rice grains, which may influence the release of the components.

Table 6.5. Extraction conditions determined for the set-up with rotary drum, cyclones and filter.

Run	f	t_d (h)	w (rpm)	E_{ext} (C/g-ds)	E_{unext} (C/g-ds)	$\eta_{ext,d}$ (%)	η_{col} (%)
1	0.25	4	30	1.21×10^9	1.64×10^9	38.83 ± 4.39^c	35.78 ± 3.40^d
2	0.50	4	30	9.38×10^8	1.83×10^9	33.93 ± 5.75^c	32.93 ± 5.63^d
3	0.25	4	60	1.85×10^9	2.15×10^9	41.36 ± 2.87^c	36.22 ± 4.28^d
4	0.50	4	60	2.49×10^9	3.41×10^9	40.01 ± 3.89^c	38.25 ± 5.06^d
5	0.25	8	30	1.30×10^9	7.41×10^8	64.09 ± 2.79^b	60.02 ± 0.08^b
6	0.50	8	30	9.24×10^8	1.07×10^9	76.88 ± 3.55^{ab}	73.74 ± 2.18^{ab}
7	0.25	8	60	2.69×10^9	4.22×10^8	86.57 ± 0.62^a	84.24 ± 0.43^a
8	0.50	8	60	1.79×10^9	1.18×10^9	60.92 ± 2.82^b	56.78 ± 2.18^c

Notes: f -volumetric filling degree; t_d – operation time; w - drum rotation speed; E_{ext} - extracted spores; E_{unext} – non-extracted spores; $\eta_{ext,d}$ - spore total extraction efficiency using the rotary drum and η_{col} - useful efficiency; Total extraction efficiency or useful efficiency followed by the same lowercase letters are not significantly different according to Tukey's test at a 95% confidence level.

Table 6.6. Analysis of variance (ANOVA) and multiple regression for the dependence of extraction efficiency on rotation speed, fill level, and operational time.

Variables	P-value
Rotation speed (*w*)	0.612
Filling degree (*f*)	0.526
Time (t_d)	0.008

$R^2 = 0.860$ R^2 (adj) = 0.755 F = 8.206 F-sig = 0.0345

R^2 – coefficient of determination; R^2(adj) – adjusted coefficient of determination; F – F-statistic of the ANOVA test; F-sig: P-value associated with the F-statistic; P-value – Probability associated with the significance test for each coefficient.

In literature, a maximum value of 12.6 mg/g-ds with a concentration of 1.8×10^{10} conidia/g was obtained using two lab-scale cyclones and employing a mass flow rate 150 g of conidiated rice per day (Liu et al., 2015). Although our approach is based on a batch process, which limits comparability with a continuous process, it is observed that the system proposed in this work presents a higher processing capacity than that of Liu and co-workers. From this perspective, the rotary drum approach seems like a promising solution.

By expanding the proposed rotary drum in this study to dimensions of 0.737 m in diameter and 1.216 m in length, it would be capable of meeting the needs of small-scale biofactories, with a daily production capacity of 300 kg, operating in batches, as the one analyzed by Ferreira et al. (2023). This expansion would make the rotary drum viable for industrial-scale operations and provide greater production efficiency to meet daily production demands.

Table 6.7. Mass extracted and spore concentration of the extract. *f* -volumetric filling degree; t_d – operation time; w - drum rotation speed.

Run	***f***	**t** (h)	***w*** (rpm)	**Extracted mass** (mg/g-ds)	**Spore concentration** (conidia/g)
1	0.25	4	30	10.05 ± 0.17^{d}	$1.20 \times 10^{11} \pm 7.00 \times 10^{9}$ bc
2	0.50	4	30	3.83 ± 0.12^{g}	$1.22 \times 10^{11} \pm 9.45 \times 10^{9}$ bc
3	0.25	4	60	12.33 ± 0.23^{c}	$1.50 \times 10^{11} \pm 9.02 \times 10^{9}$ b
4	0.50	4	60	4.41 ± 0.27^{f}	$2.82 \times 10^{11} \pm 1.65 \times 10^{10}$ a
5	0.25	8	30	16.99 ± 0.58^{b}	$7.65 \times 10^{10} \pm 3.29 \times 10^{9}$ de
6	0.50	8	30	9.14 ± 0.15^{e}	$5.08 \times 10^{10} \pm 2.95 \times 10^{9}$ e
7	0.25	8	60	20.09 ± 0.55^{a}	$1.34 \times 10^{11} \pm 2.83 \times 10^{10}$ b
8	0.50	8	60	9.47 ± 0.46^{de}	$9.49 \times 10^{10} \pm 4.46 \times 10^{9}$ cd

Extracted mass or spore concentration followed by the same lowercase letters are not significantly different according to Tukey's test at a 95% confidence level.

Furthermore, the extraction process proposed in this study allows for better control of extraction conditions, requires less labor, and operates in a closed system. Closed extraction systems are of great interest because, although the fungal spores of *M. anisopliae* are non-toxic to humans, prolonged and repeated exposure to high concentrations of powders can induce allergies (Bateman, 2003).

6.3.5 Influence of the moisture content on the extraction process

The moisture content of the materials at the end of each extraction process, restrained in the cyclones, restrained in the filter and of the remaining rice in the drum, is presented in Table 6.8. At the end of the extraction processes, the rice exhibited an average moisture content of 0.111 kg-w/kg-ds and 0.053 kg-w/kg-ds for operations of 4 and 8 hours, respectively. Considering that the initial moisture content of the rice particles was 0.250 kg-w/kg-ds, there is a significant reduction in the moisture content over time, which certainly contributes to the higher efficiencies achieved during longer processes. The comparison of means using the Tukey test indicates that the set of variables significantly influences only the moisture content of the residual rice, showing that an increase in extraction time results in a reduction in the substrate's moisture content.

The airborne conidia of *M. anisopliae* are highly hydrophobic due to the presence of glycoproteins organized into structures known as rodlets (Hegedus, Khachatourians, 1995). Under high moisture content conditions, the water molecules adsorbed on the surface of the substrate form a layer that intensifies capillary interactions and increases the effective contact area, potentially resulting in higher adhesive forces between the spores and the rice (Ankolekar, Labbé, 2010; Mercier-Bonin et al., 2011). Therefore, the drier the solid material, the lower the adhesion forces. Regarding the moisture content of the extracted material, it is observed that the spores restrained in the filter exhibit higher moisture content compared to those restrained in the cyclones. The higher moisture content of the particles retained in the filter suggests that possibly the finer particles are extracted earlier in the process. On the other hand, this could be a result of the longer residence time and contact of the dry air with the particles collected in the cyclones, which ends up drying them. Additionally, the air reaches the filter in a more humid state.

The moisture content of conidia at the end of the industrial process must be below 0.099 kg-w/kg-ds to ensure an adequate shelf life, regardless of whether the product is formulated or not (Jaronski; Jackson, 2012; Jaronski, 2014). Additionally, improperly dried infectious propagules may suffer severe plasma membrane damage when immersed in water for rehydration during the preparation of the spray suspension, which is generally lethal for unicellular organisms (Faria et al., 2009; Faria et al., 2017). Therefore, proper spore drying is essential to prevent mechanical damage caused by the pressure exerted by water as it penetrates the cells (Hoekstra et al., 1999).

Table 6.8. Moisture content of extracted spores and residual rice.

Run	**Moisture content** (kg-w/kg-ds)			
	Cyclone 1	**Cyclone 2**	**Filter**	**Residual rice**
1	0.072 ± 0.004[ab]	0.089 ± 0.019[a]	0.116 ± 0.008[c]	0.100 ± 0.012[b]
2	0.086 ± 0.002[a]	0.089 ± 0.002[a]	0.145 ± 0.010[ab]	0.153 ± 0.026[a]
3	0.067 ± 0.008[ab]	0.073 ± 0.006[a]	0.148 ± 0.019[b]	0.133 ± 0.011[ab]
4	0.071 ± 0.002[ab]	0.080 ± 0.003[a]	0.148 ± 0.010[b]	0.132 ± 0.016[ab]
5	0.066 ± 0.020[ab]	0.071 ± 0.008[a]	0.127 ± 0.007[bc]	0.049 ± 0.009[c]
6	0.062 ± 0.006[ab]	0.080 ± 0.003[a]	0.163 ± 0.001[a]	0.051 ± 0.002[c]
7	0.055 ± 0.002[b]	0.073 ± 0.006[a]	0.126 ± 0.008[bc]	0.046 ± 0.004[c]
8	0.064 ± 0.012[ab]	0.067 ± 0.002[a]	0.110 ± 0.011[c]	0.055 ± 0.006[c]

Moisture content of Residual rice or spores collected in Cyclone 1, Cyclone 2, or Filter followed by the same lowercase letters are not significantly different according to Tukey's test at a 95% confidence level.

6.3.6 Drag forces

The drag forces (F_D) for different air flow velocities, obtained through optical experiments and direct measurement with the magnetic suspension balance, are summarized in Figure 6.12. No spore removal was observed at the air velocities used in the experiments with the MSB equipment, as the particle mass remained constant during the whole measurement, when the air velocity increased from 0.00021 and 0.0207 m/s. In the optical experiments, spore removal was recorded for air flows with velocities exceeding 0.354 m/s for conidiated rice with moisture contents of 0.111 and 0.053 kg-w/kg-ds. For rice particles with a moisture content of 0.250 kg-w/kg-ds, spore release was observed from a minimum velocity of 0.375 m/s. Additionally, it was observed that with air flow velocities greater than 0.833 m/s, the rice particles were carried along by the flow. The calculated air velocity in the drum was 0.053 m/s (Table 6.2) and thus much lower than the minimum velocity documented in Fig. 6.12. It can therefore be concluded that the drag forces induced by the air flow do not have enough intensity for removing dry spores from the substrates.

In general, the drag force required for spore removal is lower for drier particles, due to the lower air velocity needed for spore detachment and smaller dimensions of these particles. However, it is important to highlight some limitations in the experimental procedures adopted. In the optical measures, the lack of control over the air humidity may affect the results.

Additionally, the determination of the minimum air velocity for spore removal was performed visually, which could introduce errors due to the perception of the observer.

The apparent small variation of F_D with moisture content of the samples is explained with the uncontrolled air humidity and temperature in the optical measurement. It must be assumed that the particles dried during the measurement and that this affected the monitored spore removal. Most seemingly, all samples are suspected to achieve low moisture contents during the experiment. The presented curves can thus be taken as an orientation for the minimum force required to remove dry spores.

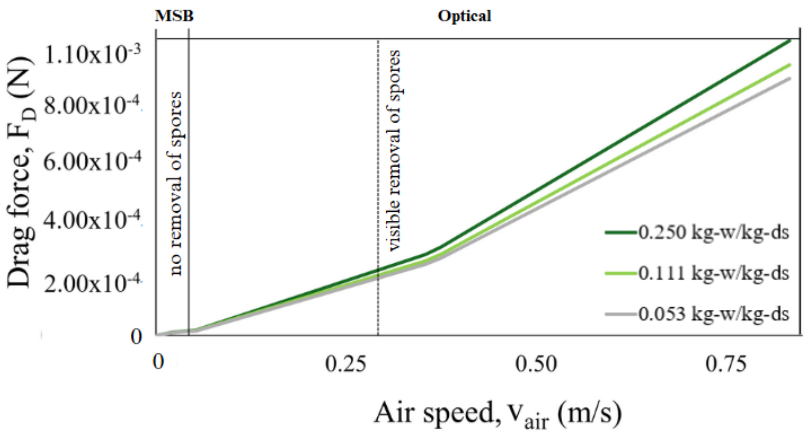

Figure 6.12. Drag forces correlated to minimum air velocities according to Eq. 6.7 yielding spore removal. Data in the range between 0.00021 and 0.0207 m/s was obtained by MSB measurements, whereas data above 0.0208 m/s were obtained by the optical method.

As the adhesion forces increase with moisture content (Figure 6.13), the removal of wet spores by the flowing air can be excluded. Although the values obtained are estimates, they provide a broader and more detailed view of the interaction between spores and the substrate, contributing to a better understanding of the adhesion process and, consequently, the extraction mechanism. What can be inferred from Figure 6.13 is that the release of spores must be a result of mechanical stress between particles and particles and drum wall, characterized by both its intensity and duration (Levitt, 1981). However, further studies with more precise measurements are needed to validate these findings and refine the understanding of the forces involved.

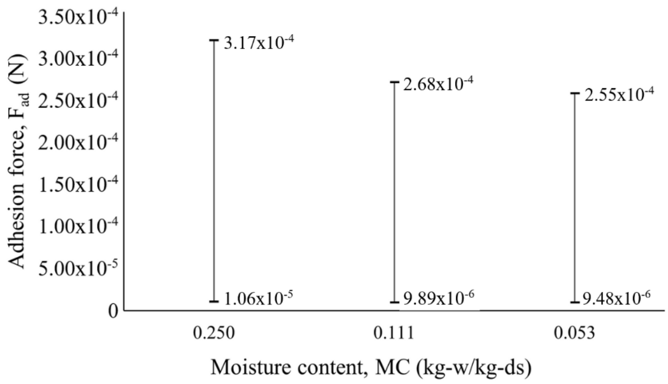

Figure 6.13. Adhesion force ranges between spores and rice particles with different moisture contents.

The atomic force microscope (AFM) was used by Greenfield et al. (2014) to measure the adhesion force of fungal spores of *M. anisopliae* to various insect surfaces, revealing adhesion forces in the range of 10^{-9} N for the different surfaces analyzed. However, the mentioned study investigates the adhesion of free spores sprayed on the carcasses of insects. Moreover, the adhesion and detachment operations in AFM are extremely challenging to determine, as they cannot be directly visualized, generating significant uncertainty regarding the force measurement. As far as is known, there is no literature describing the adhesion force of spores that are directly linked to the mycelial network and the substrate. However, it is known that the incubation time significantly influences the detachment of the spores (Teertstra et al., 2017). In general, older spores exhibit lower binding forces and are more easily detached (Li et al., 2018). Additionally, spores located farther away from the substrate surface tend to display a lower adhesion force compared to those situated internally (Krijgsheld et al., 2013).

6.4 CONCLUSION

It is concluded that the method for extracting and collecting *Metarhizium anisopliae* spores using a rotary drum coupled with a cyclone system proved to be effective. The extraction efficiency using sieves was determined, reaching 77.45% under optimal rice load and time conditions, serving as a reference for the drum trials. The cyclones were designed based on the experimentally obtained particle size distribution of the extracted material. Extraction in the drum was conducted by varying the filling degree, time, and rotational speed. Efficiencies above 76% were achieved, with a high concentration of collected spores (73.74%). The best experimental conditions were observed with a 0.50 filling degree, 30 rpm rotation, and 8-hour operation time. It was highlighted that the moisture content of the substrate is a critical factor for extraction efficiency, directly influencing the required operation time. The drag force needed for spore removal decreases as particle moisture is reduced, which also lowers the adhesion forces between the spores and the substrate, estimated between 1.06×10^{-5} and 3.17×10^{-4} N. The experimental results indicate that while air plays a fundamental role in modifying adhesion forces by reducing particle moisture, the airflow used during extraction does not generate drag forces strong enough to detach the spores. These findings contribute to the development of more efficient extraction systems, positively impacting the economic and productive viability of large-scale bioinsecticide manufacturing. Future studies may further explore this dynamic through Discrete Element Method (DEM) simulations, allowing for a more precise understanding of particle interactions and spore behavior during extraction.

6.5 REFERENCES

ANKOLEKAR, C.; LABBÉ, R. G. Physical Characteristics of Spores of Food-Associated Isolates of the *Bacillus cereus* Group. **Applied and Environmental Microbiology**, v. 76, n. 3, p. 982–984, fev. 2010.

BECHARA, I. J. et al. Histopathological events and detection of Metarhizium anisopliae using specific primers in infected immature stages of the fruit fly Anastrepha fraterculus (Wiedemann, 1830)(Diptera: Tephritidae). **Brazilian Journal of Biology**, v. 71, p. 91-98, 2011.

CUNHA, L. P. et al. Metarhizium anisopliae conidia production in a packed-bed bioreactor using rice as substrate in successive cultivations. **Process Biochemistry**, v. 97, p. 104–111, out. 2020.

CUNHA, L. P. da. **Produção de esporos do fungo Metarhizium anisopliae IBCB 425 utilizando biorreator de leito empacotado**. 2020. Dissertation (Ph.D. in Food Engineering and Science) – Institute of Biosciences, Letters, and Exact Sciences, São Paulo State University, São Paulo, 2009.

DORTA, B.; ARCAS, J. Sporulation of Metarhizium anisopliae in solid-state fermentation with forced aeration. **Enzyme and Microbial Technology**, v. 23, n. 7–8, p. 501–505, nov. 1998.

EL-EMAM, M. A.; SHI, W.; ZHOU, L. CFD-DEM simulation and optimization of gas-cyclone performance with realistic macroscopic particulate matter. **Advanced Powder Technology**, v. 30, n. 11, p. 2686-2702, 2019.

FARIA, M.; HAJEK, A. E.; WRAIGHT, S. P. Imbibitional damage in conidia of the entomopathogenic fungi Beauveria bassiana, Metarhizium acridum, and Metarhizium anisopliae. **Biological Control**, v. 51, n. 3, p. 346–354, dez. 2009.

FARIA, M. et al. Susceptibility of the biocontrol fungi Metarhizium anisopliae and Trichoderma asperellum (Ascomycota: Hypocreales) to imbibitional damage is driven by conidial vigor. **Biological Control**, v. 107, p. 87-94, 2017.

FERREIRA, D. B.; MENDES, F. B.; THOMÉO, J. C. Assessment of the Techno-Economic Feasibility of Semicontinuous Production of Metarhizium anisopliae Spores. **Industrial & Engineering Chemistry Research**, v. 62, n. 43, p. 17385-17393, 2023.

FERREIRA, D. B.; THOMÉO, J. C. Simulation of static drying and drying with intermittent rotations in a horizontal drum of rice after *Metarhizium anisopliae* cultivation. Chemical Engineering and Processing, 2025.

FERREYRA-SUAREZ, D.; GARCÍA-DEPRAECT, O.; CASTRO-MUÑOZ, R. A review on fungal-based biopesticides and biofertilizers production. **Ecotoxicology and Environmental Safety**, v. 283, p. 116945, set. 2024.

FONTES, E. M. G.; VALADARES-INGLIS, M. C. **Controle biológico de pragas da agricultura**. 2020.

GREEN, D. W.; SOUTHARD, M. Z. **Perry´s Chemical Engineers' Handbook**, 9th Ed. McGraw-Hill Co., 2018.

GREENFIELD, B. P. J. et al. Conidia of the insect pathogenic fungus, *Metarhizium anisopliae*, fail to adhere to mosquito larval cuticle. **Royal Society Open Science**, v. 1, n. 2, p. 140193, out. 2014.

GOVENDER, I. Granular flows in rotating drums: A rheological perspective. **Minerals Engineering**, v. 92, p. 168-175, 2016.

GUI, N.; FAN, J. R.; CHEN, S. Numerical study of particle–particle collision in swirling jets: A DEM–DNS coupling simulation. **Chemical Engineering Science**, v. 65, n. 10, p. 3268–3278, maio 2010.

HOEKSTRA, F. A. et al. Imbibitional leakage from anhydrobiotes revisited. **Plant, Cell & Environment**, v. 22, n. 9, p. 1121-1131, 1999.

HEGEDUS, D. D.; KHACHATOURIANS, G. G. The impact of biotechnology on hyphomycetous fungal insect biocontrol agents. **Biotechnology Advances**, v. 13, n. 3, p. 455–490, jan. 1995.

IWANICKI, N. S. et al. Monitoring of the field application of Metarhizium anisopliae in Brazil revealed high molecular diversity of Metarhizium spp in insects, soil and sugarcane roots. **Scientific reports**, v. 9, n. 1, p. 4443, 2019.

JANOCHA, M.; TSOTSAS, E. In‐depth investigation of incremental layer build‐up from dried deposited droplets. **AIChE Journal**, v. 68, n. 2, p. e17445, 2022.

JARONSKI, S. T.; JACKSON, M. A. Mass production of entomopathogenic Hypocreales. Em: **Manual of Techniques in Invertebrate Pathology**, p. 255–284, 2012.

JARONSKI, S. T. Mass Production of Entomopathogenic Fungi: State of the Art. Em: **Mass Production of Beneficial Organisms**, p. 357–413, 2014.

JENKINS, N. E. et al. Development of mass production technology for aerial conidia for use as mycopesticides. v. 19, n. 1, 1998.

KRIJGSHELD, P. et al. Development in Aspergillus. **Studies in Mycology**, v. 74, p. 1–29, mar. 2013.

KRUGER, R. D. et al. Solid Substrate Production and Formulation of an Isolate of Metarhizium anisopliae for Biological Control of Stem Bug Tibraca limbativentris. 2014.

KWAPINSKI, W.; TSOTSAS, E. Determination of kinetics and equilibria for adsorption of water vapor on single zeolite particles by a magnetic suspension balance. **Chemical Engineering & Technology: Industrial Chemistry‐Plant Equipment‐Process Engineering‐Biotechnology**, v. 27, n. 6, p. 681-686, 2004.

LE, K. H.; TSOTSAS, E.; KHARAGHANI, A. Continuum-scale modeling of superheated steam drying of cellular plant porous media. **International journal of heat and mass transfer**, v. 124, p. 1033-1044, 2018.

LEVITT, J. Responses of plants to environmental stresses. **Water, radiation, salt, and other stresses**, v. 2, 1981.

LI, J.; FENG, M.-G. Intraspecific tolerance of Metarhizium anisopliae conidia to the upper thermal limits of summer with a description of a quantitative assay system. **Mycological Research**, v. 113, n. 1, p. 93–99, jan. 2009.

LI, X.; ZHANG, T.; WANG, S. Measuring detachment of *Aspergillus niger* spores from colonies with an atomic force microscope. **Indoor Air**, v. 28, n. 5, p. 744–753, set. 2018.
LIU, H. et al. Optimised fermentation conditions and improved collection efficiency using dual cyclone equipment to enhance fungal conidia production. **Biocontrol Science and Technology**, v. 25, n. 9, p. 1011–1023, 2 set. 2015.
MARINUC, M.; RUS, F. Effect of particle size and input velocity on cyclone separation process. **Bulletin of the Transilvania University of Brasov. Series II: Forestry• Wood Industry• Agricultural Food Engineering**, p. 117-122, 2011.
MARRONE, P. G. Status of the biopesticide market and prospects for new bioherbicides. **Pest Management Science**, v. 80, n. 1, p. 81–86, jan. 2024.
MASSARANI, G. **Fluidodinâmica em sistemas particulados**. Editora E-papers, 1997.
MELLMANN, J. The transverse motion of solids in rotating cylinders—forms of motion and transition behavior. **Powder technology**, v. 118, n. 3, p. 251-270, 2001.
MENDEZ-GONZALEZ, F.; LOERA, O.; FAVELA-TORRES, E. Conidia production of Metarhizium anisopliae in bags and packed column bioreactors. **Current Biotechnology**, v. 7, n. 1, p. 65–69, 1 mar. 2018.
MERCIER-BONIN, M. et al. Orientation and detachment dynamics of Bacillus spores from stainless steel under controlled shear flow: Modelling of the adhesion force. **International Journal of Food Microbiology**, v. 146, n. 2, p. 182–191, mar. 2011.
NAPIER-MUNN, Tim. The dense medium cyclone–past, present and future. **Minerals Engineering**, v. 116, p. 107-113, 2018.
NISHI, O.; SATO, H. Species diversity of the entomopathogenic fungi Metarhizium anisopliae and M. flavoviride species complexes isolated from insects in Japan. **Mycoscience**, v. 58, n. 6, p. 472–479, nov. 2017.
POSADA-FLÓREZ, F. J. Production of *Beauveria bassiana* Fungal Spores on Rice to Control the Coffee Berry Borer, *Hypothenemus hampei* , in Colombia. **Journal of Insect Science**, v. 8, n. 41, p. 1–13, mar. 2008.
SALA, A. et al. Current developments in the production of fungal biological control agents by solid-state fermentation using organic solid waste. **Critical Reviews in Environmental Science and Technology**, v. 49, n. 8, p. 655-694, 2019.
STAIRMAND, C. J. The design and performance of cyclone separators. **Trans. Inst. Chem. Engrs.**, *29*, 356-362, 1951.
TARHAN, S.et al. Product quality and energy consumption when drying peppermint by rotary drum dryer. **Industrial Crops and Products**, v. 32, n. 3, p. 420-427, 2010.
TEERTSTRA, W. R. et al. Maturation of conidia on conidiophores of Aspergillus niger. **Fungal Genetics and Biology**, v. 98, p. 61–70, jan. 2017.
VELOZO, S. G. M. et al. From the dual cyclone harvest performance of single conidium powder to the effect of Metarhizium anisopliae on the management of Thaumastocoris peregrinus (Hemiptera: Thaumastocoridae). **PLOS ONE**, v. 18, n. 3, p. e0283543, 27 mar. 2023.
ZAKI, O. et al. Limiting factors of mycopesticide development. **Biological Control**, v. 144, p. 104220, 2020.
ZASTAWNY, M. et al. Derivation of drag and lift force and torque coefficients for non-spherical particles in flows. **International Journal of Multiphase Flow**, v. 39, p. 227–239, mar. 2012.
ZEYMER, J. S. Equilíbrio higroscópico e análise termodinâmica da sorção de água em grãos de arroz em casca. 2017.

7. CHARACTERIZATION OF *Metarhizium anisopliae* SPORE EXTRACTION IN A ROTARY DRUM USING DISCRETE ELEMENT METHOD (DEM)

ABSTRACT

The fungus *Metarhizium anisopliae* is typically cultivated on rice, and the process of extracting its spores from the substrate requires optimization. In biofactories, this operation is often performed using shaking sieves; however, rotating drums presents a promising alternative. This study investigates the impact of drum rotation speeds (30 and 60 rpm) and particle moisture content levels (0.250, 0.111, and 0.053 kg-w/kg-ds) on the spore extraction efficiency. The discrete element method (DEM) was used to simulate the movement regime and particle collisions during extraction. The tested drum was 20 cm diameter and 40 cm length and conidiated rice was used. The input parameters for the DEM (coefficient of restitution, static friction, and rolling friction for particle-particle and particle-wall contacts) were directly determined for conidiated rice. Experiments have been carried out to validate the model. The results showed that although higher rotation speeds (60 rpm) increased the frequency and intensity of particle collisions, this did not correspond to a significant improvement in extraction efficiency compared to 30 rpm, as already observed in experiments. The analysis suggests that excessive particle fragmentation and energy dissipation may limit the benefits of higher rotation speeds. Additionally, DEM allowed the study of particle motion in different regimes, which was also not possible in experiments because of the limited optical access. It revealed that the transition from cascading to cataracts flow regimes from 30 rpm to 60 rpm may introduce less efficient particle movements, reducing the effectiveness of spore detachment. These findings highlight the importance of balancing rotation speed, moisture content, and collision dynamics to optimize spore extraction processes.

Keywords: DEM; rice; spores; extraction; moisture content; collisions.

7.1 INTRODUCTION

The growing awareness of the adverse effects of excessive agrochemical use (Bagheri et al., 2025) has driven the search for more sustainable agricultural practices and, consequently, the use of bioinsecticides (Shattuk et al., 2023; Ferreyra-Suarez et al., 2024). Entomopathogenic fungi play a crucial role in pest biocontrol due to their ability to infect insects through the cuticle, unlike bacteria and viruses that require ingestion to act (Alves; Lopes, 2008; Saminathan et al., 2025). Among these fungi, *Metarhizium* and *Beauveria* stand out in integrated pest management programs (Panwar & Szczepaniec, 2024), particularly *Metarhizium anisopliae*.

Effective against more than 200 insect species, *M. anisopliae* is widely used for pest control in sugarcane fields, as well as other crops and pastures (Kruger et al., 2014; Nishi; Sato, 2017; Fontes; Valadares-Inglis, 2020). Its production traditionally occurs through solid-state cultivation (SSC), using rice as a substrate in plastic packaging. This process involves multiple steps, including humidification, sterilization, inoculation, incubation, pre-drying, spore extraction, and drying. However, the production processes, largely unchanged since the 1970s (Jenkins et al., 1998), still rely on labor-intensive manual steps, hindering industrial-scale expansion (Mendez-Gonzalez et al., 2018). Among the critical and limiting steps is spore extraction, traditionally performed using vibrating screens, which have low capacity and result in significant losses to the environment (Posada-Flórez, 2008; Liu et al., 2015).

To optimize the extraction of *Metarhizium anisopliae* spores, Ferreira et al. (accepted at Industrial Crops & Products) proposed an innovative system based on a rotating drum with a diameter of 20 cm and a length of 40 cm, coupled with cyclones for spore collection. In this process, the drum's rotation promotes spore detachment, which is then captured by the airflow and directed to the cyclones. The study evaluated the impact of fill level, rotation speed, and operational time on extraction efficiency. The results indicated that higher rotation speeds and fill levels could improve extraction; however, only operational time had a statistically significant impact, with efficiencies ranging from 60.92% to 86.57%.

Although this approach represents an advancement over traditional methods, the study by Ferreira et al. (accepted at Industrial Crops & Products) suggested that particle collisions play a crucial role in controlling extraction efficiency. It was anticipated that this effect would be driven by a higher number of collisions, as well as an expected increase in collision forces under such conditions. Additionally, it was hypothesized that higher particle moisture content requires more energy for spore-substrate separation due to potentially greater adhesion forces between them. The authors observed that the moisture content of the rice particles decreases during the extraction process, and it was assumed that this reduces adhesion forces between the spores and the substrate surface, thus requiring lower collision forces for detachment. However, the number and intensity of collisions, as well as the influence of substrate moisture on these parameters, cannot be directly determined through experimental methods, limiting the system's optimization. Moreover, the feasibility of scaling up this process to meet the demands of biomanufacturing facilities remains unknown.

To overcome this barrier, numerical simulations, especially those based on the Discrete Element Method (DEM), emerge as a valuable tool. DEM is widely used to simulate the behavior of particulate materials in various industrial processes, providing a detailed and quantitative understanding of phenomena that are difficult to observe experimentally and has proven to be a tool capable of predicting the dynamics of large particle assemblies (Cundall; Strack, 1979; Rong et al., 2020; Zheng et al., 2024). However, most of the studies found in the literature that use rotating drums are limited to investigating the movement regimes, mixing, and heat transfer of granular materials (Komossa et al., 2014; Yazdani; Hashemabadi, 2019; Ji et al., 2020; Lin et al., 2024; Chou et al., 2025), with few studies focusing on collisions. The applicability of DEM simulations, however, depends on the precise definition of input parameters, which are related to the physical properties of the particles and their contact interactions, including the coefficient of restitution, static friction, and rolling friction (Barrios et al., 2013).

This study aimed to apply the Discrete Element Method to predict the movement regime and collisions of conidial rice particles during the spore extraction process of *M. anisopliae* in a rotating drum, correlating the results with the experimental extraction efficiency obtained. The method predicts the impact of drum rotation speed and particle moisture content on the velocities and forces reached by the rice grains during the extraction process, as well as estimates the collision frequency. This study, therefore, serves as a foundation for designing rotating drums, including the flight arrangement and geometry, to achieve the necessary collision forces for spore detachment, in addition to enabling the scaling of the process. Since the experimental study revealed that airflow plays a secondary role in the removal of already detached spores, the research focuses solely on collisions, without considering the effect of airflow.

7.1.1 Discrete element method model

The Discrete Element Method (DEM) uses Newton's second law to calculate the motion of individual particles and a displacement-force law to describe the contacts between particles (particle-particle) and between particles and walls (particle-wall), updating the contact forces over time. The motion of each particle is determined by Eqs. (7.1) and (7.2):

$$m_i \frac{dv_i}{dt} = \sum_j \left(F_n^{ij} + F_t^{ij}\right) + m_i\, g \tag{7.1}$$

$$I_i \frac{d\omega_i}{dt} = \sum_j \left(R_i + F_t^{ij}\right) + \tau_{rij} \tag{7.2}$$

where m_i, v_i, I_i, ω_i and R_i represent the mass, linear velocity, moment of inertia, angular velocity, and radius of particle i, respectively. F_n^{ij}, F_t^{ij} and τ_{rij} represent the normal and tangential force components, and the torque between particles i and j, respectively.

DEM models can be divided into two main types: rigid sphere and soft sphere. In the rigid sphere model, collisions are treated as binary and instantaneous, which is suitable only for systems with a low concentration of particles. In contrast, the soft sphere model is more appropriate for systems with a high concentration of particles, where the contacts between them are more prolonged. In this work, the nonlinear Hertz–Mindlin contact model was adopted, a classic example of the soft sphere. The contact force is divided into normal and tangential components, both with damping elements, as represented in Eq. (7.3) and reported in the literature (Mindlin, 1949; Mindlin; Feresiewicz, 1990; Brandão et al., 2024). In this model, the tangential component of the contact forces is described by Mindlin's theory (Mindlin, 1949), while the normal component is based on Hertz's contact theory (Hertz, 1882).

$$F_c^{ij} = F_n^{ij} + F_{nd}^{ij} + F_t^{ij} + F_{td}^{ij} \tag{7.3}$$

where F_c^{ij} is the contact force between particles i and j, F_{nd}^{ij} and F_{td}^{ij} are the normal and tangential damping forces, respectively.

The parameters used in DEM simulations can be classified into two main groups (Coetzee, 2017): physical property parameters, which include particle density, size, shape, Poisson's ratio, and Young's modulus; and contact parameters, which encompass the coefficient of static friction (μ_s), the coefficient of rolling friction (μ_r), and the coefficient of restitution (e_p).

The e_p, which quantifies energy dissipation during collisions between solid bodies, can be calculated from the ratio of the velocities before and after the collision, as shown in Eq. (7.4):

$$e_p = \frac{-v_r}{v_o} \tag{7.4}$$

where v_r in m/s is the velocity of the particle after the collision and v_o in m/s is the velocity of the particle before the collision.

The μ_s determines the resistance force to relative motion between bodies or between bodies and surfaces and can be estimated through Eq. (7.5). This force acts at the contact points between the surfaces, in the opposite direction of the motion, preventing the initiation of sliding.

$$\mu_s = \tan(\Theta_s) \tag{7.5}$$

where Θ_s is the angle of inclination at which the particles begin to slide.

Rolling friction coefficient is established through Eq. (7.6) and describes the force that resists the movement of a particle rolling on a surface or over other particles.

$$\mu_r = \frac{h_0}{D_r} \tag{7.6}$$

where h_0 is the launch height of the particles (cm) and D_r is the distance traveled by the particle after leaving the launch device until it reaches its resting point (cm).

The application of appropriate parameter values is essential to ensure that the simulation results align with experimental data. However, these coefficients have never been determined for rice particles with spore loads and different moisture contents. Even when parameters are measured accurately, simulations may exhibit discrepancies at the macroscopic level, making it necessary to adopt a calibration method to align the model’s response with experimental observations (Wei et al., 2020). Still, simulation results may differ at the macroscopic level due to factors such as particle shape. Non-spherical particles are often approximated as a single sphere in dense systems to simplify contact detection, thereby reducing computation time (Li et al., 2025).

7.2 MATERIALS AND METHODS

7.2.1 Metarhizium anisopliae

The fungus *Metarhizium anisopliae* IBCB 425 was kindly provided by the Biological Institute of São Paulo, Brazil. The stock cultures were maintained in test tubes with potato-dextrose-agar (PDA) medium, covered with a thin layer of mineral oil, and stored at 4°C. To prepare the inoculum, fungal spores were transferred to Erlenmeyer flasks containing 50 mL of PDA, which were incubated in a climate chamber at 28°C for 15 days. The spore harvest was performed by adding Tween 80 (0.1% v/v) to the flask and scraping the surface of the culture to suspend the spores. The spore concentration was adjusted to 10^7 spores per gram of dry solid substrate (g-ds).

7.2.2 Solid state cultivation in plastic packaging

Solid state cultivation was performed in polypropylene plastic containers with a load of 400 g-ds of long rice (*Oryza sativa*), which will be identified in this work as raw rice (RR), purchased from local retailers. The openings of the containers were connected to PVC tubes 5 cm ID, where cotton plugs were inserted to allow gas exchange and prevent contamination. The substrate was moistened and sterilized in an autoclave at 121°C for 30 minutes. After cooling, in a laminar flow chamber, the spore suspension was incorporated into each plastic container, followed by vigorous manual mixing. At the end of the inoculation, the substrate had a moisture content of 0.923 kg of water per kg of dry substrate (kg-w/kg-ds). The fungus was incubated for 10 days in a climate chamber at 28°C, as described in the literature (Dorta; Arcas, 1998; Li; Feng, 2009; Cunha et al., 2020). After the incubation period, the containers were opened, and the conidiated rice (CDR) was placed in trays, which were maintained in a climate chamber at 30°C until reaching three distinct moisture contents: 0.250, 0.111, and 0.053 kg-w/kg-ds. These moisture levels correspond to the initial moisture, as well as the moisture after 4 and 8 hours of extraction of the conidiated rice, respectively. An MB45 infrared balance (OHAUS, Parsippany, USA) was used to check the moisture content of the substrate.

7.2.3 Particle characterization

In order to adequately represent the conidiated rice particles in the DEM simulation environment, their dimensions, sphericity (Φ), bulk density (ρ_{bulk}) and porosity (ε) were determined. Figure 7.1 illustrates the measurements used for particle sizing, considering that the width (b) is equivalent to the thickness, while "a" represents the particle length. The dimensions a, b and the sphericity were obtained from photographic images of samples containing more than 100 conidiated rice grains with different moisture contents, analyzed using the ImageJ software.

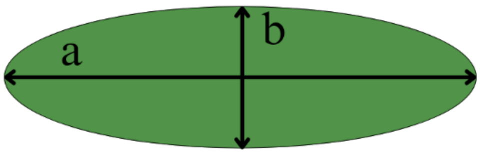

(a) (b)

Figure 7.1. (a - Measurements for characterizing particle size, where "a" represents the length and "b" the width of the conidiated rice particles and b – conidiated rice particles).

The bed porosity (ε) was determined using the volumetric method in a 50 mL measuring cylinder. The total volume of a given mass of particles was directly measured in the cylinder (bulk density – ρ_{bulk}), and the particle volume was determined by adding toluene to fill the void spaces between the particles in the cylinder (particle density – ρ_p) (Casciatori et al., 2014). The bed porosity was calculated using its classical definition [Eq. (7.7)]. The same experiments were conducted to characterize the raw rice particles.

$$\varepsilon = 1 - \frac{\rho_p}{\rho_{bulk}} \tag{7.7}$$

where ε is the bed porosity; ρ_{bulk} is the bulk density (kg/m³), and ρ_p is the particle density (kg/m³).

7.2.4 DEM input parameters

7.2.4.1 Restitution coefficient

The experiment was conducted to determine the e_p of conidiated rice particles with different moisture contents (0.250, 0.111, and 0.053 kg-w/kg-ds) using the experimental setup illustrated in Figure 7.2. The particles were released using a vacuum tweezer (Rewatronick, Germany), which applied sufficient suction force to hold a particle at a height of 70 mm above a flat surface. The suction was then interrupted, allowing the particle to fall freely.

To measure e_p in particle-wall (PW) collisions, a 2 mm thick stainless steel plate was used. For particle-particle (PP) collision measurements, the same plate was coated with particles at the investigated moisture content (Figure 7.2.c). Instantaneous velocities before and after the collision were measured using a high-speed digital camera (LaVision, GmbH, Göttingen, Germany) with a CMOS sensor (1024 × 1024 pixels), operating at 5,000 frames per second (FPS). Each experiment was repeated 10 times to ensure result accuracy. The same experiment was also performed using raw rice particles for comparison purposes.

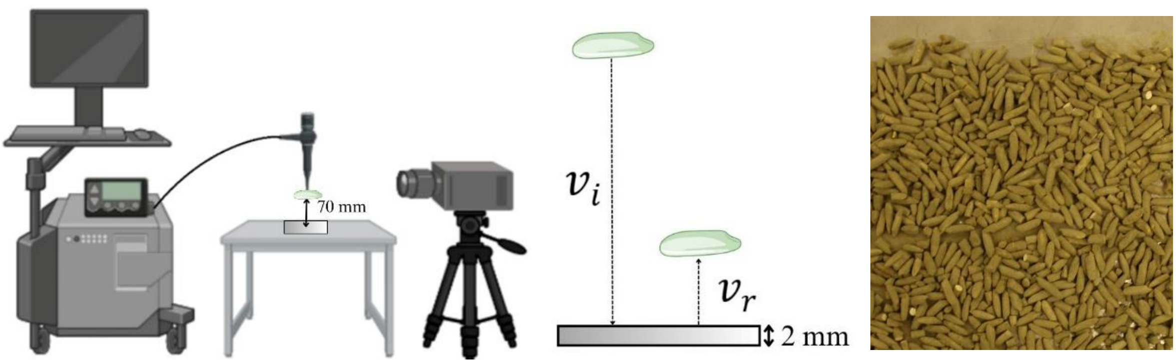

(a) (b) (c)

Figure 7.2. Coefficient of restitution (a - experimental setup for determining the coefficient of restitution; b – representation of the trajectory of rice particles before and after collision and c - plate covered with conidiated rice particles to assess the particle-particle contact).

7.2.4.2 Static friction coefficient

To determine the static friction coefficient (μ_s), the experimental setup described in Figure 7.3 was used, consisting of an inclined plane attached to a rod that allowed for angle adjustments. During the experiments, the plane was gradually tilted until the conidiated rice (CDR) particles began to slide. To ensure that the particles slid instead of rolling, they were grouped using adhesive tape. The experiments were conducted with CDR particles at moisture contents of 0.250, 0.111, and 0.053 kg-w/kg-ds. The static friction coefficient was calculated as the tangent of the critical angle (Θ_s) at which movement initiated, as indicated in Eq. (7.5).

To capture the exact moment of sliding and determine the critical angle, a camera Canon EOS 2000D (CANIN INC., Tóquio, Japão) was used, and the angle measurement was performed using the ImageJ/Fiji software. The static friction between the particle and the wall (PW) was evaluated using a smooth plate (Figure 7.3.b), while particle-particle (PP) interactions were analyzed by coating the plate with rice particles. Each experiment was repeated 10 times to ensure result reproducibility. Additionally, the same procedure was conducted using raw rice (RR) particles for comparison purposes.

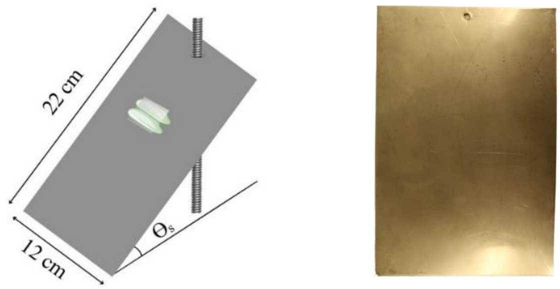

(a) (b)

Figure 7.3. Experimental setup for determining the static friction coefficient.

7.2.4.3 Rolling friction coefficient

To determine the rolling friction coefficient (μ_r), the experimental setup shown in Figure 7.4 was used. The experiment consisted of two flat stainless steel surfaces, identical to those shown in Figure 7.3.b. One of the surfaces was inclined to allow the release of the particles, while the other remained horizontal. The particles were released from a fixed height of 13 mm (h_0), and the distance traveled until resting (D_r) was measured with the help of a ruler. The experiments were conducted with conidiated rice particles (CDR) at moisture contents of 0.250, 0.111, and 0.053 kg-w/kg-ds, as well as with raw rice (RR). To determine the particle-particle (PP) rolling friction coefficient, the horizontal surface was completely covered with the analyzed particles.

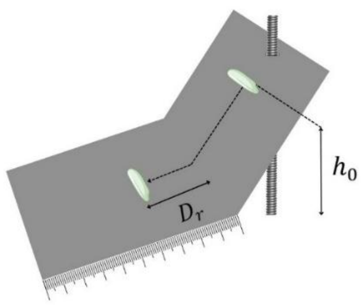

Figure 7.4. Experimental setup for determining the rolling friction coefficient.

7.2.5 Static resting angle

To calibrate the input parameters for the DEM simulation and experimentally validate the adopted model, the static angle of repose (ϴ) for conidiated rice particles with moisture contents of 0.250, 0.111, and 0.053 kg-w/kg-ds, as well as for raw rice, was determined both experimentally and through simulations.

7.2.5.1 Experimental setup

The fixed funnel method (Beakawi; Baghabra, 2018) was used to determine the static resting angle (ϴ), according to the setup described in Figure 7.5. In this procedure, the particles were loaded into a funnel at a height of 5 cm above a 9 cm diameter Petri dish. The funnel had a containment at its outlet, allowing the particles to be released after the complete loading. The flow of particles, as well as the pile formed, was recorded using a Canon EOS 2000D camera (CANON INC., Tokyo, Japan). The angle was then determined with the help of the ImageJ/Fiji software, as shown in the Figure 7.5.b. Each experiment was repeated three times for each type of particle.

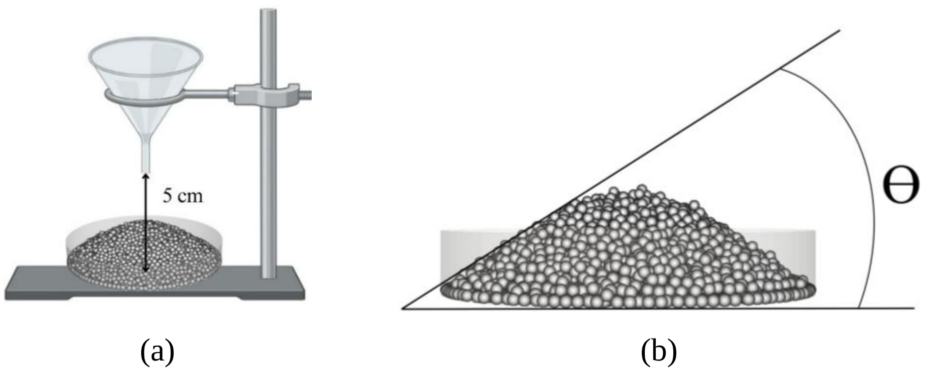

Figure 7.5. Determination of the angle of repose using the fixed funnel method (a – experimental setup and b – particle pile and static angle of repose).

7.2.5.2 DEM simulations

To obtain the numerical angles of repose, simulations were conducted using the open-source software LIGGGHTS. The geometry used in the simulations was drawn to match the experimental setup. To ensure numerical stability during the simulations, a time step of $1x10^{-4}$ seconds was employed. Table 7.1 details the simulation conditions adopted in this study. The rice particles were modeled as spheres, with their volume adjusted to match that of the real particles, as determined by dimensions *a* and *b*, as shown in Figure 7.1.

Table 7.1. Parameters adopted in the DEM simulations.

Parameter	Value	Reference
Time step (s)	$1x10^{-4}$	-
Young modulus (GPa)		
Rice	0.014	Da Costa *et al*. (2014)
Steel	207	Callister; Rethwisch (2012)
Poisson ratio (-)		
Rice	0.15	Da Costa *et al*. (2014)
Steel	0.30	Jafari *et al*. (2018)

Considering that the main objective of this study is to establish the collision forces and frequencies of rice particles during the extraction process, and that these are determined by the fraction of initial kinetic energy dissipated, the values of the restitution coefficient used in the simulations directly corresponded to those experimentally obtained. The other input parameters (μ_s and μ_r) were adjusted to calibrate the DEM simulations. Several sets of parameters were evaluated to identify the best set representing the conidiated rice particles at different moisture contents and raw rice. The selection of parameters to be tested was based on a fractional factorial design (Jankovic et al., 2021), as summarized in Table 7.2.

Table 7.2. Fractional factorial design added for DEM parameter calibration.

Set	$\mu_{s\text{-}PP}$	$\mu_{s\text{-}PW}$	$\mu_{r\text{-}PP}$	$\mu_{r\text{-}PW}$
1	-1	-1	-1	-1
2	-1	-1	1	1
3	1	-1	-1	1
4	1	-1	1	-1
5	-1	1	1	-1
6	-1	1	-1	1
7	1	1	1	1
8	1	1	-1	-1
9	0	0	0	0

The level 0 represented the interaction coefficients determined experimentally. The level -1 was determined by subtracting half of the value of the experimentally obtained coefficient, while the level +1 was established by adding half of this value to the experimental coefficient. Thus, the coefficient values at levels -1 and +1 were adjusted to represent variations around the average value, corresponding to the minimum and maximum values, respectively. While the level 0 represented the experimentally determined interaction coefficients. The dependent variable used was the static angle of repose. The simulated responses for each parameter set were compared with the experimental data.

7.2.6 Movement regime

Given the challenge of measuring internal flows in extraction processes due to the opaque nature of the flow environment, the movement regime of raw rice particles was assessed. To do this, the particles were loaded into a drum to reach a fill degree (*f*) of 0.50. A 20 cm diameter and 45 cm length drum, equipped with four angled blades at 45º, as shown in Figure 7.6, was used. The drum covers were made of acrylic to allow visualization of the granular material. To facilitate the visualization of the particles, LED lights were installed inside the drum. The drum was rotated by a chain and gear system connected to an electric motor controlled by a frequency converter. The rotation was maintained at a constant 30 rpm, and the particle flow was recorded by a Canon EOS 2000D camera.

The experimental movement regime was visually compared with the results obtained in the simulations conducted using the LIGGGHTS software. The geometry used in the simulations was modeled to match the experimental configuration, drawn in SolidWorks (Dassault Systèmes, Vélizy-Villacoublay, France). The raw rice particles were modeled as spheres, with the volume adjusted to match the real particles. The experimental conditions described in Table 7.1 were maintained in the simulations, including the experimentally obtained coefficient of restitution. The additional input parameters (static friction coefficient and rolling friction coefficient) were adjusted according to the best set of parameters that adequately represented the particles.

Figure 7.6. Rotating drum used to establish the movement regime of raw rice particles.

7.2.7 Particle collisions

Considering that the release of spores occurs exclusively due to the collision of particles during the spore extraction process proposed by Ferreira et al. (accepted at Industrial Crops & Products), the characterization of these collisions is of great interest to understand their relationship with extraction efficiency. To this end, simulations were conducted using the LIGGGHTS software, adopting the same conditions described in Table 1. The drum with a diameter of 20 cm and a length of 33 cm, shown in Figure 7.7, was drawn using SolidWorks (Dassault Systèmes, Vélizy-Villacoublay, France) to accurately represent the experimental setup used by Ferreira et al. (accepted at Industrial Crops & Products). Inside the drum, there were two straight longitudinal blades, each 2 cm wide, positioned perpendicular to the drum wall.

The reduction of the moisture content of conidiated rice particles during the extraction process, as identified by the authors, was also considered, as this factor can impact the extraction efficiency. To represent this effect in the simulation environment, the number of particles was kept constant in all experiments, while the diameter of the particles was adjusted according to the moisture content. Knowing that 2 kg of conidiated rice (dry basis) (Ferreira et al., accepted at Industrial Crops & Products) with a moisture content of 0.250 kg-w/kg-ds are loaded into the drum to begin the extraction process, and based on bulk density, bed porosity, and the volume of a single particle, a total of 315,000 particles was fixed in the simulations. The simulations were conducted with a bed filling degree of 0.50 and drum rotation speeds (V_{drum}) of 30 and 60 rpm. The number of collisions, as well as the collision forces and velocities reached by the particles, were quantified using Python code. In addition to the collisions, the movement regime of the bed during the extraction process was evaluated, an analysis that could not be performed experimentally due to the release of spores, which prevents any visualization.

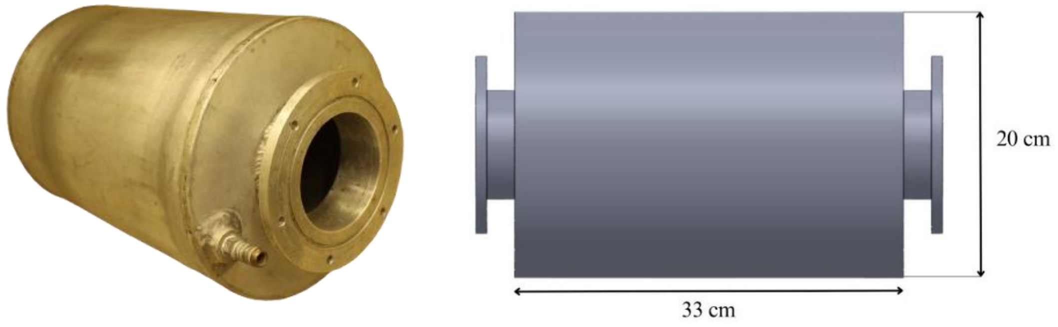

(a) (b)

Figure 7.7. Rotary drum used in spore extraction (a – experimental and b – drawn in SolidWorks).

7.2.8 Statistical analysis

Analyzes of variance (ANOVA) and Tukey tests of comparison of means with a confidence level of 95% were carried out using Microsoft Excel 365 (Microsoft Co., Redmond, USA).

7.3 RESULTS AND DISCUSSION

7.3.1 Particle characterization

Table 7.3 presents the dimensions and sphericity of conidiated rice and raw rice particles used to approximate them as spheres in the DEM simulations, as well as the bulk density and porosity of the beds filled with these particles. It is observed that moisture reduction leads to a decrease in particle size and a consequent increase in bulk density. The same trend is observed for porosity and particle sphericity. Compared to raw rice, conidiated rice exhibits larger dimensions, except for particles with a moisture content of 0.053 kg-w/kg-ds. This effect arises from physical structure changes in the grains caused by sterilization, where cooking induces swelling (Ferreira et al., 2025), while subsequent moisture removal during drying causes shrinkage. Additionally, drying makes the particles more brittle, reducing the average size of the ensemble. On the other hand, the formation of the spore layer on the grain surface also affects their size. Based on microscopy data presented by Ferreira et al. (2025), this layer is estimated to have an average thickness of 0.110 ± 0.024 mm. However, it is important to note that the thickness of the spore layer on the rice particles was not directly measured or controlled in this study.

Table 7.3. Granular material properties.

Material	MC (kg-w/kg-ds)	**Particles dimensions** (mm) a	b	Φ	ρ_{bulk} (kg/m³)	ε
RR	0.087	5.89 ± 0.11[a]	1.21 ± 0.05[ac]	0.49 ± 0.03[a]	736.52 ± 15.36[a]	0.53 ± 0.07[a]
CDR	0.250	6.91 ± 0.15[b]	1.52 ± 0.06[b]	0.60 ± 0.05[b]	682.50 ± 12.52[b]	0.49 ± 0.08[a]
	0.111	6.03 ± 0.21[a]	1.27 ± 0.08[a]	0.51 ± 0.04[a]	731.50 ± 18.27[a]	0.42 ± 0.05[a]
	0.053	5.76 ± 0.16[a]	1.12 ± 0.03[c]	0.47 ± 0.02[a]	742.60 ± 19.31[a]	0.40 ± 0.06[a]

RR – raw rice; CDR – conidiated rice; MC – moisture content; Φ – esfericidade; ρ_{bulk} – densidade bulk; ε – porosity. Means followed by the same lowercase letters are not significantly different according to the Tukey test at the 95% confidence level.

7.3.2 Experimental determination of DEM input parameters

To accurately represent the movement of rice in DEM simulations, the coefficients of restitution (e_p), static friction (μ_s), and rolling friction (μ_r) were experimentally measured for particle-particle (PP) and particle-wall (PW) interactions, both for raw rice and conidiated rice. Figure 7.8 presents the obtained values and the results of the Tukey test for comparing the means among different conidiated rice samples. The coefficients of restitution and static friction for raw rice fall within the ranges reported in the literature (Jia et al., 2021; Wang et al., 2021; Xu et al., 2023). However, it was not possible to verify the suitability of the rolling friction coefficient since its experimental determination has not been previously reported in the literature.

7.3.2.1 Restitution coefficient

In Figure 7.8.a, it can be observed that the coefficient of restitution decreases with increasing moisture content, both for PP interactions and PW interactions. This behavior is widely reported in the literature (Mueller et al., 2011; Dong et al., 2018; Li et al., 2019). This reduction indicates that wetter materials are less elastic, dissipating more energy during collisions due to increased adhesion forces, deformation, and friction (Boettcher et al., 2017; Yardeny et al., 2020). Although there was a decrease in the coefficients, statistical analysis indicates that moisture did not significantly affect PP interactions. Mueller et al. (2011) investigated the impact of different moisture levels on spherical plastic particles' coefficients of restitution. The authors observed that particle moisture content minimally influences the coefficient of restitution, although it affects the particles' mechanical properties. For particle-wall interactions, only conidiated rice particles with higher moisture content (0.250 kg-w/kg-ds) exhibited statistically significant differences.

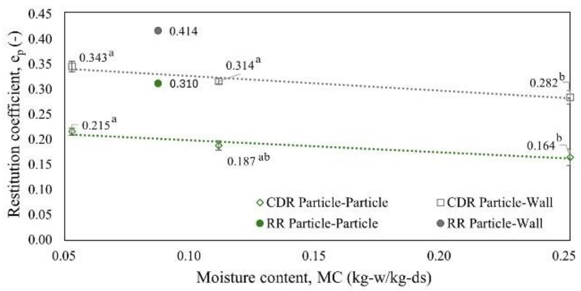

(a)

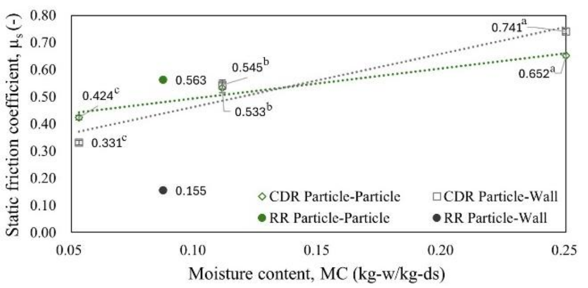

(b)

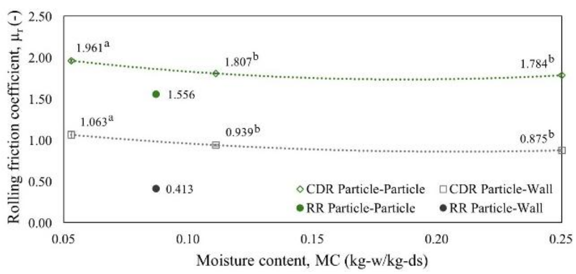

(c)

Figure 7.8. DEM input parameters, where (a) coefficient of restitution; (b) static friction coefficient, and (c) rolling friction coefficient for raw rice (RR) and conidiated rice (CDR). Coefficients describing the same interaction, particle-particle (PP) or particle-wall (PW), followed by the same lowercase letters are significantly different according to the Tukey test at a 95% confidence level.

Overall, comparing conidiated rice with raw rice shows that the coefficients for raw rice are higher. This suggests that the grain's increased softness, caused by cooking, and its consequent higher deformation significantly influence the coefficient of restitution. The coefficient of restitution is affected by a combination of factors related to both material properties and process conditions, extending beyond the influence of moisture. Additionally, inherent experimental uncertainties, such as the variable thickness of the spore layer and potential drying of particles during measurement, especially if the experiment is not conducted quickly, can impact the results obtained.

7.3.2.2 Sliding friction coefficient

In Figure 7.8.b, it can be observed that the static friction coefficient decreases with the reduction in moisture content of the conidiated rice particles, both for PP and PW interactions. Statistical analysis indicates that moisture affects the coefficients. It is known that as moisture content decreases, the grains become less sticky, resulting in a reduction of cohesive forces between the grains and the contact surface. This, in turn, reduces the angle required for the particle to slide, thus lowering the static friction coefficients. The impact of moisture on the magnitude of frictional force in granular plant materials has been investigated by several researchers (Adebowale et al., 2012; Kara et al., 2012; Shafaei; Kamgar, 2017; Kopeć-Jarosz; Wójcik, 2021), showing increases in static friction with rising moisture content.

Additionally, it is believed that the mycelium and spore coating promote resistance to sliding, possibly due to its irregularity and increased surface roughness. Furthermore, the presence of loose material in the coating may intensify this resistance, impacting the system's dynamics. Additionally, adhesion forces play a relevant role in this process, being attributed to hydrophobins and the MAD1 and MAD2 proteins (Wösten, 2001; Wang; St Leger, 2007), secreted by the fungus *M. anisopliae*. This fungus stands out as an organism capable of utilizing these protein adhesives to anchor its spores to hosts, plants, and surfaces (Vasselli; Shaw, 2022).

7.3.2.3 Rolling friction coefficient

Figure 7.8.c presents the rolling friction coefficients for conidiated rice particles, considering both PP and PW interactions. An increase in the coefficients is observed as the moisture content of the particles decreases. However, statistically significant differences were identified only for the drier conidiated rice particles (0.053 kg-w/kg-ds).

Rolling resistance typically exhibits extremely low magnitudes for spherical particles (Zhou et al., 1999), usually ranging between 0.010 and 0.020 (Jia et al., 2021; Xu et al., 2023). When analyzing the sphericity of the conidiated rice samples, it is observed that more spherical particles tend to have lower rolling friction coefficients. Since this coefficient represents the resistance to the movement of a rolling particle (Mohamed; Gutierrez, 2010), higher values indicate a lower rolling capacity. Therefore, the high coefficients found in this study may be attributed both to the irregular shape of the rice particles (Figure 7.1.b) and to increased surface roughness, particle deformation, and adhesive forces.

7.3.3 Static resting angle and calibration of DEM input parameters

The experimental resting angles obtained for cultivated rice particles and raw rice are summarized in Table 7.4. A slight reduction in the resting angle is observed with the decrease in moisture content of the particles, a behavior widely documented in the literature (Sadeghi et al., 2010; Bhople et al., 2017; Wu et al., 2022). However, this variation did not result in statistically significant differences. Instead, a significant difference is observed only between the resting angles of raw rice particles and conidiated rice particles.

Table 7.4. The experimental angle of repose for raw rice and conidiated rice at different moisture contents.

Material	**Moisture content** (kg-w/kg-ds)	**Angle of repose** (°)
Raw rice	0.083	24.31 ± 0.87[b]
Conidiated rice	0.250	33.92 ± 1.70[a]
	0.111	33.31 ± 1.81[a]
	0.053	33.55 ± 1.01[a]

Means followed by the same lowercase letters are not significantly different according to the Tukey test at the 95% confidence level.

This behavior can be attributed to the greater cohesive forces between conidiated rice particles, intensified by the cooking process, as well as intermolecular interactions such as van der Waals forces, electrostatic forces, and hydrophobic forces resulting from fungal activity (Krull et al., 2010). These forces have a significant impact on the properties of granular materials and can cause substantial deviations from the typical behavior of particulate systems (Li, 2005). Moreover, the lower rolling resistance of raw rice particles, reflected in their lower μr, may contribute to the reduction of the particle pile formed (Figure 7.9.a) and consequently to the resting angle. It is also observed that, although the increase in μ_s (the only coefficient significantly affected by particle moisture) has a positive effect on the resting angle, this effect is neutralized by the combined contributions of the coefficient of restitution and the rolling friction coefficient.

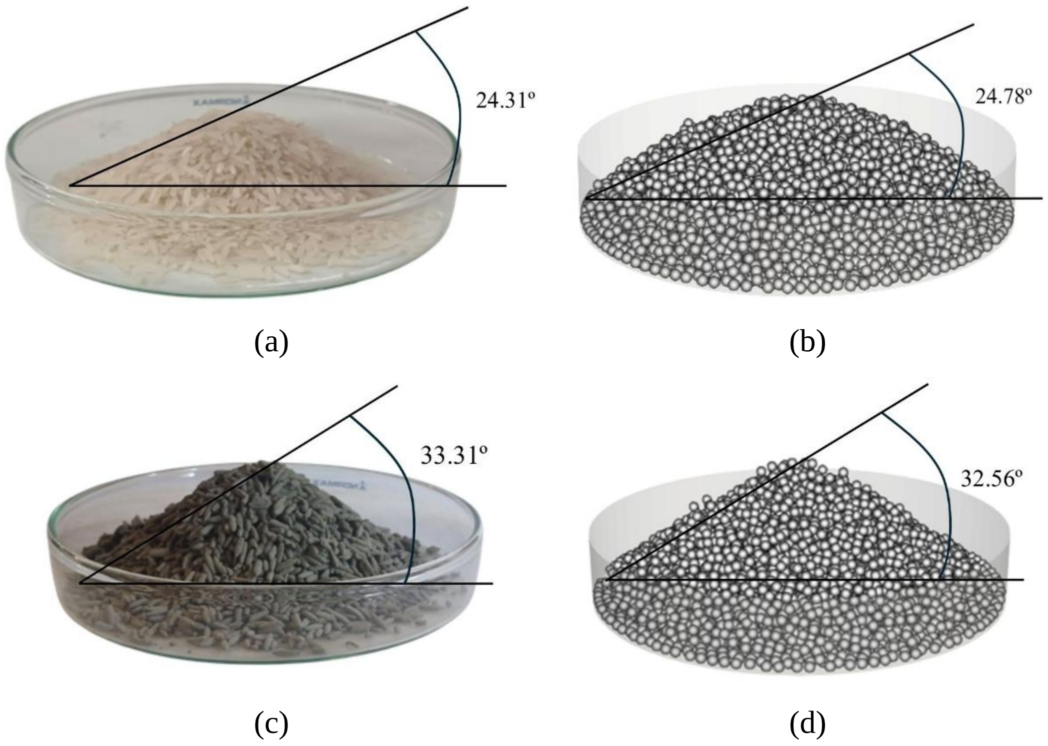

Figure 7.9. Resting angle (a) of raw rice obtained experimentally and (b) through simulations adopting static friction and rolling friction coefficients of 0.845 and 0.778 for particle-particle interactions and 0.233 and 0.207 for particle-wall interactions, respectively; (c) of conidiated rice with a moisture content of 0.111 kg-w/kg-ds obtained experimentally and (d) through simulations adopting static friction and rolling friction coefficients of 0.267 and 2.711 for particle-particle interactions and 0.818 and 0.470 for particle-wall interactions, respectively.

Considering that the resting angle does not vary significantly with moisture content, the calibration plan for the input parameters for DEM simulations, as represented in Table 7.5, was established using the experimental coefficients obtained for conidiated rice with an average moisture content (0.111 kg-w/kg-ds). Table 7.5 also presents the calibration plan for input parameters to describe raw rice and the numerical resting angles obtained by adopting each parameter set. It can be observed that Set 5 is the one that most closely matches the experimental resting angle, with an absolute error of 1.03º (Figure 7.9.c). In contrast, Set 9, which uses the coefficients directly measured for the particles, does not ideally represent the behavior of the granular material. The analysis of the best parameter set indicates that the particle-particle static friction coefficient ($\mu_{S\text{-}PP}$) should be as low as possible, while the particle-particle rolling friction coefficient ($\mu_{r\text{-}PP}$) should be as high as possible. This combination reduces both the sliding and rolling of the particles in contact, allowing the numerical resting angle to approach the experimental value. In contrast, the set that best matches the resting angle of raw rice particles (Set 8) he highest $\mu_{s\text{-}PP}$ and the lowest $\mu_{r\text{-}PP}$ possible.

Table 7.5. Static resting angles and absolute errors were obtained with the sets established for the calibration of DEM input parameters.

Set	Raw rice						Conidiated rice					
	$\mu_{s\text{-}PP}$	**$\mu_{s\text{-}PW}$**	**$\mu_{r\text{-}PP}$**	**$\mu_{r\text{-}PP}$**	**Θ_{num} (°)**	**E_{abs} (°)**	**$\mu_{s\text{-}PP}$**	**$\mu_{s\text{-}PW}$**	**$\mu_{r\text{-}PP}$**	**$\mu_{r\text{-}PP}$**	**Θ_{num} (°)**	**E_{abs} (°)**
1	0.282	0.078	0.778	0.207	25.85	1.54	0.267	0.273	0.904	0.470	30.62	2.97
2	0.282	0.078	2.334	0.602	30.65	6.34	0.267	0.273	2.711	1.409	31.23	2.36
3	0.845	0.078	0.778	0.602	21.47	2.84	0.800	0.273	0.904	1.409	31.19	2.40
4	0.845	0.078	2.334	0.207	26.14	1.83	0.800	0.273	2.711	0.470	30.45	3.14
5	0.282	0.233	2.334	0.207	30.40	6.09	0.267	0.818	2.711	0.470	32.56	1.03
6	0.282	0.233	0.778	0.602	27.42	3.11	0.267	0.818	0.904	1.409	31.52	2.07
7	0.845	0.233	2.334	0.602	31.13	6.82	0.800	0.818	2.711	1.409	31.98	1.61
8	0.845	0.233	0.778	0.207	24.78	0.47	0.800	0.818	0.904	0.470	30.45	3.14
9	0.563	0.155	1.556	0.413	27.86	3.55	0.533	0.545	1.807	0.939	31.64	1.95

μ_s – sliding friction coefficient; μ_r – rolling friction coefficient; PP – particle-particle interaction; PW – particle-wall interaction; Θ_{num} – numerically obtained static resting angle; E_{abs} – absolute error between the experimental and numerical resting angles.

The small difference between the simulated responses and experimental results can be attributed to the geometric simplification adopted in the simulations, where rice particles were approximated as spheres. Several authors have identified the simplification of particle shape as one of the main challenges of DEM simulations due to its significant influence on the mechanical behavior of granular materials (Cleary, 2010; Markauskas et al., 2010; Höhner et al., 2014). As the non-circularity of particles increases, the shear resistance of the granular material also increases. Comparisons between particle shape approximation schemes show that particles with sharp edges lead to a greater increase in the microstructural resistance of the particle assembly, intensifying the impact of angularity on the material's behavior (Cleary, 2008). However, the results of this study support this simplification, which, in simulations of dense systems, facilitates contact detection and reduces computation time without significantly compromising the representativeness of granular behavior.

7.3.4 Movement regime

The extraction process in a rotating drum with spore collection in cyclones proposed by Ferreira et al. (accepted at Industrial Crops & Products) still requires some essential characterizations, such as the ideal rotational speed and its impacts on collision frequency, to ensure its efficient application in an industrial environment. The authors evaluated the impact of drum rotational speed (30 and 60 rpm), extraction time (4 and 8 hours), and drum fill level (0.25 and 0.50) on spore extraction efficiency. They observed that extraction time was the only factor that significantly impacted extraction efficiency. Regarding the other process variables evaluated by the authors, it was found that there is an economic advantage to using a higher fill level of 0.50, while uncertainties remain about the ideal rotational speed to be adopted in the process.

The rotational speed of the drum directly influences the particle movement regimes within the bed. Basically, the movement of particles inside the drums can be divided into three distinct regions: the active layer, where most of the movement and particle interactions occur; the passive layer, characterized by a more stable and cohesive flow; and the interface region, which separates these two layers and influences the material's transition within the system (Mellmann, 2001). When regimes are reached where particles predominantly remain in the active layer, the interaction between them increases, intensifying friction. This phenomenon favors the removal of the superficial spore layer, thereby improving extraction efficiency. According to Mellmann (2001), the Froude number is an effective parameter to predict the movement behavior of granular materials, influenced by drum dimensions, fill level, and rotational speed. The 30 and 60 rpm speeds used in the extraction process result in Froude numbers of 0.101 and 0.402, respectively, classifying both cases as cascade-type regimes, and cascade subtype (Mellmann, 2011). The cascade regime is characterized by the projection of particles into the free gas space. With the increase in rotational speed, there is an increase in the number of particles launched and the extent of their trajectories until a uniform veil is formed along the drum's diameter.

However, measuring the internal flow in extraction processes is challenging due to the opaque flow environment. This issue does not arise for raw rice particles. Figure 7.10 visually compares the experimental and simulated movement regimes, both characterized by the cascade-type movement regime and rolling subtype. Additionally, the three distinct movement regions can be identified.

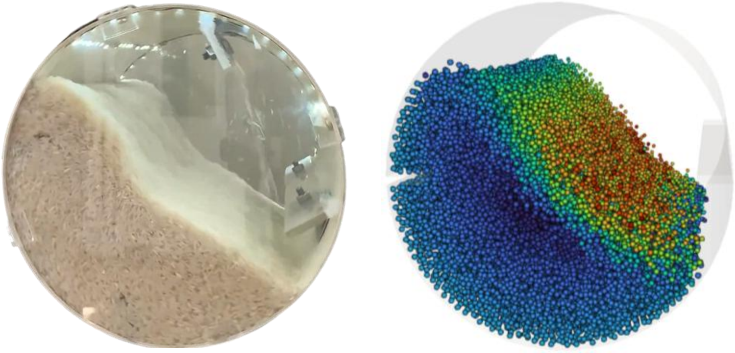

(a) (b)

Figure 7.10. Movement regime of raw rice particles: (a) experimental and (b) numerical.

Due to the good agreement between the static angles of repose and the proper characterization of the particle movement regime for raw rice, it is assumed that the movement regime simulated by the DEM approach for conidial rice particles faithfully represents the experimental behavior, even though a direct validation cannot be provided. The movement regimes obtained in the simulations using DEM, with drum rotations of 30 and 60 rpm, are presented in Figure 7.11. During the simulations, the number of particles was kept constant, while their dimensions were adjusted to represent the reduction caused by drying throughout the process (Ferreira et al., accepted at Industrial Crops & Products). Thus, the CDR spheres with moisture contents of 0.250, 0.111, and 0.053 kg-w/kg-ds were modeled with radii of 1.26 mm, 1.07 mm, and 0.97 mm, respectively.

As a result, a significant decrease in the drum filling degree was observed. For both drum rotation speeds, it was noted that reducing the filling degree decreased the extent of the interface region. The decrease in the filling degree also increases the frequency with which particles enter the active region of the bed, where more intense collisions occur, especially when a drum speed of 60 rpm is used. These more vigorous impacts favor the detachment of the spores, reinforcing the influence of particle moisture reduction on the extraction efficiency, as experimentally verified by Ferreira et al. (accepted at Industrial Crops & Products).

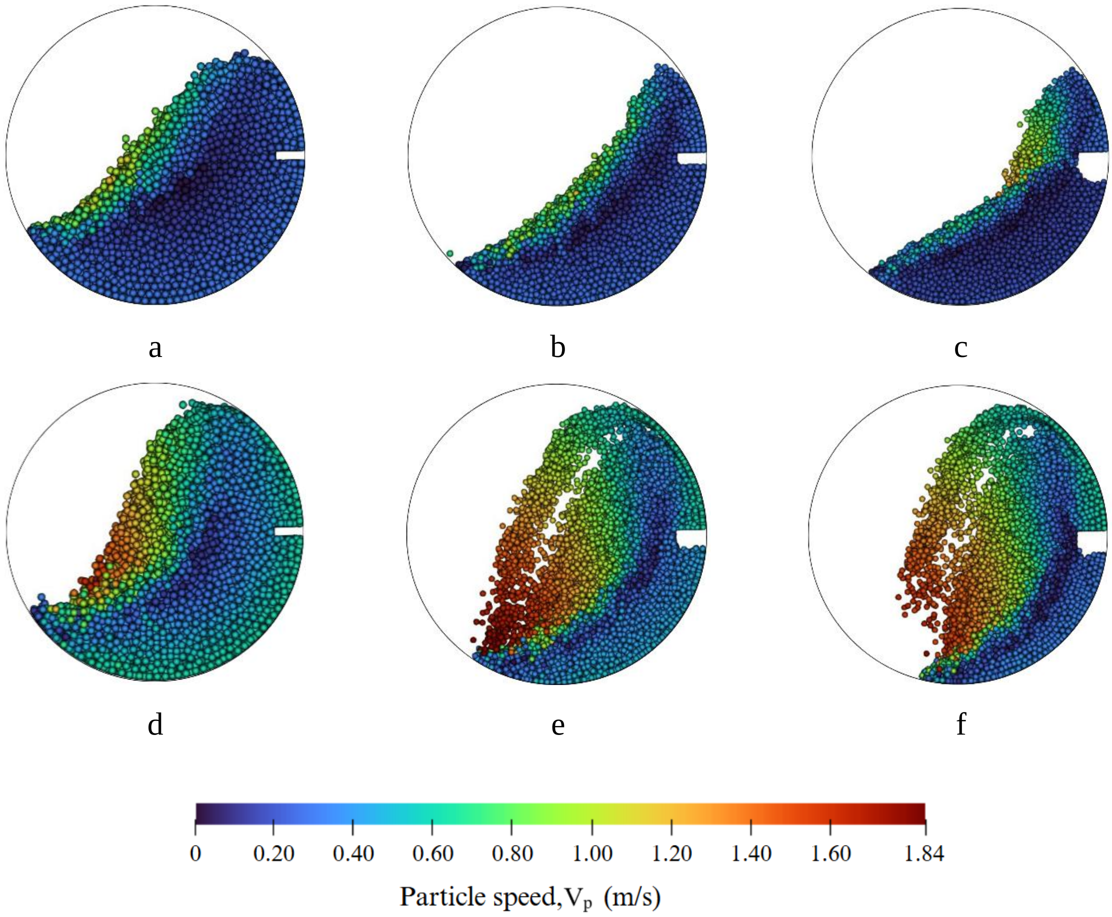

Figure 7.11. Movement of conidial rice in the extraction drum rotating at 30 rpm for particles with moisture of (a) 0.250 ($e_{p\text{-}PP}$ = 0.164; $e_{p\text{-}PW}$ = 0.297), (b) 0.111 ($e_{p\text{-}PP}$ = 0.187; $e_{p\text{-}PW}$ = 0.314), and (c) 0.053 kg-w/kg-ds ($e_{p\text{-}PP}$ = 0.215; $e_{p\text{-}PW}$ = 0.343), and at 60 rpm for particles with moisture of (d) 0.250 ($e_{p\text{-}PP}$ = 0.215; $e_{p\text{-}PW}$ = 0.343), (e) 0.111 ($e_{p\text{-}PP}$ = 0.187; $e_{p\text{-}PW}$ = 0.314), and (f) 0.053 kg-w/kg-ds ($e_{p\text{-}PP}$ = 0.215; $e_{p\text{-}PW}$ = 0.343). The coefficients $\mu_{s\text{-}PP}$ = 0.267; $\mu_{s\text{-}PW}$ = 0.818; $\mu_{r\text{-}PP}$ = 2.711; $\mu_{r\text{-}PW}$ = 0.470 were kept constant across all experiments.

7.3.5 Frequency of collisions

Considering that in the rotary drum extraction process, the release of spores intensifies due to the higher frequency of collisions between particles and between them and the drum wall, it is essential to quantify the forces and the number of collisions that enable the extraction efficiencies observed experimentally by Ferreira et al. (accepted at Industrial Crops & Products). Additionally, this understanding is crucial for the proper scaling of the process. The collision frequencies obtained from the simulations are presented in Figure 7.12.

In general, collisions between particles occur more frequently than those between particles and the drum wall. It is noted that at a drum rotation speed of 30 rpm, the collision frequency does not show significant variation with the reduction in particle moisture. However, at 60 rpm, the variation is more intense, justified by the expansion of the active layer as particle moisture decreases. This can be explained by the fact that the increase in speed promotes the ejection of particles into the headspace, instead of keeping them on the surface of the active layer as happens at 30 rpm, reducing the number of collisions. Furthermore, the higher number of collisions at 30 rpm can be explained by the slower movement of the particles. At this speed, the centrifugal force is lower, reducing particle dispersion.

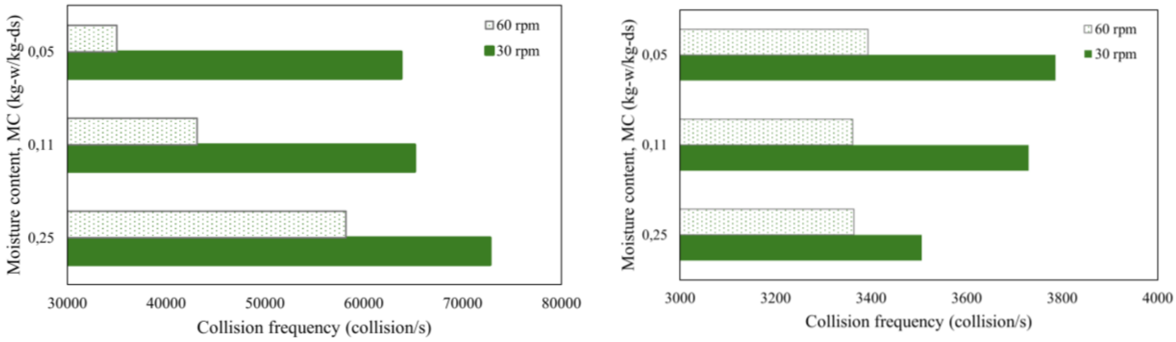

a b

Figure 7.12. Collision frequency (a) between particles and (b) between particles and the wall for conidial rice at different moisture contents.

The particle velocities and collision forces are summarized in Table 7.6. This includes the minimum and maximum velocities reached by the particles, V_{min} and V_{max}, respectively, as well as the average particle velocities ($\bar{V}$). It also includes the minimum and maximum forces observed during collisions between particles and between particles and the wall of the drum, F_{min}, and F_{max}, respectively, along with the average collision force ($\bar{F}$). In general, it is observed that both the velocities and the collision forces increase as the moisture content decreases. This behavior can be partly explained by the higher restitution coefficients observed in the particles with lower moisture content, although this difference is not statistically significant. This results in less energy dissipation during collisions, as suggested by Xie et al. (2022). Consequently, the particles rebound with relatively higher velocities, leading to more intense collisions. Moreover, the average collision forces are higher when the drum is rotated at 60 rpm, justified by the higher average velocities reached by the particles.

Given that spore release occurs frequently through collisions, higher forces are desirable. However, these forces must exceed the adhesive forces for effective spore removal. These forces were experimentally determined by Ferreira et al. (accepted at Industrial Crops &

Products), that is, indirectly, based on the derivation of drag forces between the air and the spores, as well as the determination of the minimum air velocity required for spore removal. According to the authors, the adhesive forces between the spores and rice are in the range of 1.06×10^{-5} to 3.17×10^{-4} N, 9.89×10^{-6} to 2.68×10^{-4} N, and 9.48×10^{-6} to 2.55×10^{-4} N, for particles with moisture contents of 0.250, 0.111, and 0.053 kg-w/kg-ds, respectively. The forces achieved by collisions between particles, as well as between the particles and the wall of the drum, are shown in Figure 7.13.

Table 7.6. Velocities and collision forces are achieved during spore extraction by conidial rice particles of different moisture contents.

w (rpm)	**MC** (kg-w/kg-ds)	$\mathbf{v_{min}}$ (m/s)	$\mathbf{v_{max}}$ (m/s)	$\bar{\mathbf{v}}$ (m/s)	$\mathbf{F_{min}}$ (N)	$\mathbf{F_{max}}$ (N)	$\bar{\mathbf{F}}$ (N)
30	0.250	0.001	1.303	0.159	1.93×10^{-8}	0.323	0.015
	0.111	0.002	1.319	0.239	6.51×10^{-8}	0.477	0.019
	0.053	0.003	1.329	0.268	9.26×10^{-8}	0.571	0.033
60	0.250	0.003	1.652	0.489	1.74×10^{-8}	0.524	0.018
	0.111	0.004	1.771	0.491	3.86×10^{-8}	0.716	0.026
	0.053	0.008	1.836	0.500	1.61×10^{-7}	0.804	0.035

w – drum rotation speed; MC – moisture content; v_{min} – minimum velocity reached; v_{max} – maximum velocity reached; $\bar{v}$ – average particle velocity; F_{min} – minimum collision force reached; F_{max} – maximum collision force reached; $\bar{F}$ – average collision force of the particles.

It can be observed that the collision forces exceeding the adhesive forces are more frequent at 60 rpm. However, at 30 rpm, more than 97% of the collision forces also exceed the adhesive forces, indicating that in both movement regimes analyzed, the spore detachment occurs in almost all interactions, considering the adhesive force as the control parameter. These results reinforce that the rotation speed has little impact on extraction efficiency, as experimentally indicated by Ferreira et al. (accepted at Industrial Crops & Products). The high speed of 60 rpm maybe generating excessively intense collisions, dissipating a significant amount of energy in the form of heat, deformation, or particle fragmentation. This suggests that although the forces involved exceed the necessary limits to dislodge the spores, the extraction efficiency does not increase proportionally, as part of this energy is lost or not effectively used for spore detachment.

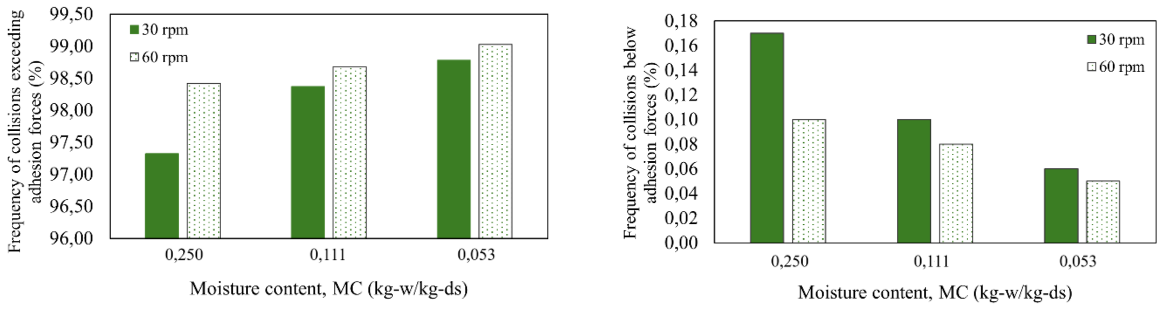

a b

Figure 7.13. Collision frequency with forces (a) exceeding and (b) below the adhesion range established by Ferreira et al. (accepted at Industrial Crops & Products).

In general, although beds composed of drier particles exhibit a lower total number of collisions, they show a higher frequency of collisions that exceed adhesive forces. However, during the extraction process, fragmentation of the rice particles occurs, which was not considered in this study. This fragmentation results in a greater number of particles and, consequently, a higher number of collisions than those simulated in this study, potentially even surpassing the collision frequencies observed for more humid particles. Furthermore, it is known that there is a physical limit where the remaining spores are so strongly attached to the rice, as demonstrated by Ferreira et al. (accepted at Industrial Crops & Products), that significantly greater (and perhaps impractical) forces would be required to remove them through collisions.

Finally, considering the higher collision frequency when adopting a drum rotation speed of 30 rpm, as well as the lower energy consumption of the equipment at lower speeds, this appears to be the most favorable condition for the extraction process. In future studies, different geometries, such as adding more blades to the drum, can be evaluated, provided they meet the requirement of exceeding adhesive forces while maintaining the frequencies observed within the magnitudes achieved in this study.

7.4 CONCLUSION

It is concluded that the reduction of moisture content in particles during the extraction process of *Metarhizium anisopliae* spores in a rotary drum positively affects the movement regime of the particles, as well as their velocities, collision frequencies, and forces. Despite these impacts, the reduction in moisture content does not significantly alter the coefficients of restitution or rolling friction, nor the static angles of repose. The calibration of input parameters for DEM simulations enabled the reproduction of repose angles close to experimental values, validating the adopted approach.

The movement regime of raw rice was simulated and experimentally validated, providing a reliable model for the behavior of conidiated rice particles at different moisture levels. The simulations revealed that, during the extraction process at both evaluated rotation speeds (30 and 60 rpm), over 97% of collision forces exceed the adhesion forces of the spores to the rice, ensuring effective removal. Among these conditions, the rotation speed of 30 rpm was considered ideal, as it promotes more frequent collisions during the extraction process. These results open new possibilities for implementing more efficient extraction systems, with the potential to enhance the economic and productive viability of large-scale bioinsecticide production, contributing to sustainability in agricultural pest control.

7.5 REFERENCES

ADEBOWALE, A. A. et al. Effect of Variety and Initial Moisture Content on Physical Properties of Improved Millet Grains. **Nigerian Food Journal**, v. 30, n. 1, p. 5–10, 2012.

ALVES, S.B.; LOPES, R.B. (Ed.). Controle microbiano de pragas na América Latina: avanços e desafios. Piracicaba: FEALQ. p.69-110, 2008.

BAGHERI, A. et al. Occupational Exposure to Pesticides, Personal Protection, and Willingness to Reduce Chemical Sprayings Among Iranian Greenhouse Farmers. **Journal of Agromedicine**, v. 30, n. 1, p. 14–26, 2 jan. 2025.

BARRIOS, G. K. P. et al. Contact parameter estimation for DEM simulation of iron ore pellet handling. **Powder Technology**, v. 248, p. 84–93, nov. 2013.

BEAKAWI AL-HASHEMI, H. M.; BAGHABRA AL-AMOUDI, O. S. A review on the angle of repose of granular materials. **Powder Technology**, v. 330, p. 397–417, maio 2018.

BHOPLE, S.; KUMAR, A.; HALDKAR, P. Effect of moisture content on angle of repose for different cereals and pulses. **International Journal of Chemical Studies**, v. 5, n. 5, p. 2283-2286, 2017.

BOETTCHER, R.; EICHMANN, S.; MUELLER, P. Influence of viscous damping and elastic waves on energy dissipation during impacts. **Chemical Engineering Science**, v. 199, p. 571–587, maio 2019.

BRANDÃO, R. J. et al. A systematic evaluation of DEM input parameters measurement and calibration. **Powder Technology**, v. 448, p. 120157, 2024.

CASCIATORI, F. P. et al. Flow configuration and Packing Density of Sugarcane Bagasse and Wheat Bran Affecting Enzymes Production by Solid-State Fermentation. **BioEnergy Research**, v. 17, n. 1, p. 187–197, 26 set. 2023.

CHOU, S.; HSIAU, S.; LIU, S. Experimental study of heat transfer and transport properties of granular material in indirectly heated rotary drums. **International Journal of Heat and Mass Transfer**, v. 238, p. 126485, 2025.

CLEARY, P. W. The effect of particle shape on simple shear flows. **Powder Technology**, v. 179, n. 3, p. 144–163, jan. 2008.

CLEARY, P. W. DEM prediction of industrial and geophysical particle flows. **Particuology**, v. 8, n. 2, p. 106–118, abr. 2010.
COETZEE, C. J. Review: Calibration of the discrete element method. **Powder Technology**, v. 310, p. 104–142, abr. 2017.
CUNDALL, P. A.; STRACK, O. D. L. A discrete numerical model for granular assemblies. **Géotechnique**, v. 29, n. 1, p. 47–65, mar. 1979.
CUNHA, L. P. et al. Metarhizium anisopliae conidia production in packed-bed bioreactor using rice as substrate in successive cultivations. **Process Biochemistry**, v. 97, p. 104–111, out. 2020.
DONG, M. et al. Experimental measurement of the normal coefficient of restitution of micro-particles impacting on plate surface in different humidity. **Powder Technology**, v. 335, p. 250–257, jul. 2018.
DORTA, B.; ARCAS, J. Sporulation of Metarhizium anisopliae in solid-state fermentation with forced aeration. **Enzyme and Microbial Technology**, v. 23, n. 7–8, p. 501–505, nov. 1998.
FERREIRA, D. B. et al. Extraction of spores of Metarhizium anisopliae in a rotary drum coupled with cyclones. Accepted at Industrial Crops & Products. 2025.
FERREIRA, D. B.; TADA, É. F. R.; THOMÉO, J. C. Simulation of static drying and drying with intermittent rotations in a horizontal drum of rice used in the cultivation of Metarhizium anisopliae. **Chemical Engineering and Processing - Process Intensification**, v. 209, p. 110169, mar. 2025.
FERREYRA-SUAREZ, D.; GARCÍA-DEPRAECT, O.; CASTRO-MUÑOZ, R. A review on fungal-based biopesticides and biofertilizers production. **Ecotoxicology and Environmental Safety**, v. 283, p. 116945, set. 2024.
FONTES, E. M. G.; VALADARES-INGLIS, M. C. Controle biológico de pragas da agricultura. 2020.
HERTZ, W. **Die sage von Parzival und dem Gral**. Schottlaender, 1882.
HÖHNER, D.; WIRTZ, S.; SCHERER, V. A study on the influence of particle shape and shape approximation on particle mechanics in a rotating drum using the discrete element method. **Powder Technology**, v. 253, p. 256–265, fev. 2014.
JANKOVIC, A.; CHAUDHARY, G.; GOIA, F. Designing the design of experiments (DOE) – An investigation on the influence of different factorial designs on the characterization of complex systems. **Energy and Buildings**, v. 250, p. 111298, nov. 2021.
JENKINS, N. E. et al. Development of mass production technology for aerial conidia for use as mycopesticides. v. 19, n. 1, 1998.
JI, S.; WANG, S.; ZHOU, Z. Influence of particle shape on mixing rate in rotating drums based on super-quadric DEM simulations. **Advanced Powder Technology**, v. 31, n. 8, p. 3540–3550, ago. 2020.
JIA, H. et al. Contact parameter analysis and calibration in discrete element simulation of rice straw. **International Journal of Agricultural and Biological Engineering**, v. 14, n. 3, p. 72–81, 2021.
KARA et al. The Effect of Moisture Content on the Thermal Properties of Red Lentil Seeds. **Transactions of the ASABE**, v. 55, n. 6, p. 2301–2306, 2012.
KOMOSSA, H. et al. Transversal bed motion in rotating drums using spherical particles: Comparison of experiments with DEM simulations. **Powder Technology**, v. 264, p. 96–104, set. 2014.
KOPEĆ-JAROSZ, A.; WÓJCIK, A. The Impact of Moisture and Number of Contact Points on the Process of Friction in Plant Granular Materials. **Processes**, v. 9, n. 2, p. 215, 25 jan. 2021.
KRUGER, R. D. et al. Solid Substrate Production and Formulation of an Isolate of Metarhizium anisopliae for Biological Control of Stem Bug Tibraca limbativentris. 2014.

KRULL, R. et al. Morphology of filamentous fungi: linking cellular biology to process engineering using Aspergillus niger. **Biosystems Engineering II: Linking Cellular Networks and Bioprocesses**, p. 1-21, 2010.

LI, H. **Impact of cohesion forces on particle mixing and segregation**. Ph.D. Dissertation. University of Pittsburgh. 2005.

LI, J.; FENG, M.-G. Intraspecific tolerance of Metarhizium anisopliae conidia to the upper thermal limits of summer with a description of a quantitative assay system. **Mycological Research**, v. 113, n. 1, p. 93–99, jan. 2009.

LI, M.; YU, Y.; SAXÉN, H. Numerical and experimental study of particle shape effect on pile properties based on a 3D sinter model. **Powder Technology**, v. 452, p. 120496, fev. 2025.

LI, X. et al. Experimental and theoretical studies of the relationship between dry and humid normal restitution coefficients. **Journal of Aerosol Science**, v. 129, p. 16–27, mar. 2019.

LIN, L. et al. Optimized structure design for binary particle mixing in rotating drums using a combined DEM and gaussian process-based model. **Digital Chemical Engineering**, v. 12, p. 100175, set. 2024.

LIU, H. et al. Optimised fermentation conditions and improved collection efficiency using dual cyclone equipment to enhance fungal conidia production. **Biocontrol Science and Technology**, v. 25, n. 9, p. 1011–1023, 2 set. 2015.

MARKAUSKAS, D. et al. Investigation of adequacy of multi-sphere approximation of elliptical particles for DEM simulations. **Granular Matter**, v. 12, n. 1, p. 107–123, fev. 2010.

MELLMANN, J. The transverse motion of solids in rotating cylinders—forms of motion and transition behavior. **Powder Technology**, v. 118, n. 3, p. 251–270, ago. 2001.

MENDEZ-GONZALEZ, F.; LOERA, O.; FAVELA-TORRES, E. Conidia production of Metarhizium anisopliae in bags and packed column bioreactors. **Current Biotechnology**, v. 7, n. 1, p. 65–69, 1 mar. 2018.

MINDLIN, R. D. **Compliance of elastic bodies in contact.** 1949.

MINDLIN, R. D.; DERESIEWICZ, H. Elastic spheres in contact under varying oblique forces. 1953.

MOHAMED, A.; GUTIERREZ, M. Comprehensive study of the effects of rolling resistance on the stress–strain and strain localization behavior of granular materials. **Granular Matter**, v. 12, n. 5, p. 527–541, out. 2010.

MUELLER, P. et al. The normal and oblique impact of three types of wet granules. **Granular Matter**, v. 13, n. 4, p. 455–463, ago. 2011.

NISHI, O.; SATO, H. Species diversity of the entomopathogenic fungi Metarhizium anisopliae and M. flavoviride species complexes isolated from insects in Japan. **Mycoscience**, v. 58, n. 6, p. 472–479, nov. 2017.

POSADA-FLÓREZ, F. J. Production of *Beauveria bassiana* Fungal Spores on Rice to Control the Coffee Berry Borer, *Hypothenemus hampei* , in Colombia. **Journal of Insect Science**, v. 8, n. 41, p. 1–13, mar. 2008.

RONG, W. et al. Sensitivity analysis of particle contact parameters for DEM simulation in a rotating drum using response surface methodology. **Powder Technology**, v. 362, p. 604-614, 2020.

SADEGHI, M.; ARAGHI, H. A.; HEMMAT, A. Physico-mechanical properties of rough rice (Oryza sativa L.) grain as affected by variety and moisture content. **Agricultural Engineering International: CIGR Journal**, v. 12, n. 3-4, p. 129-136, 2010.

SAMINATHAN, N. et al. Entomopathogenic fungi: translating research into field applications for crop protection. **Arthropod-Plant Interactions**, v. 19, n. 1, p. 8, fev. 2025.

SHAFAEI, S. M.; KAMGAR, S. A comprehensive investigation on static and dynamic friction coefficients of wheat grain with the adoption of statistical analysis. **Journal of Advanced Research**, v. 8, n. 4, p. 351–361, jul. 2017.

SHATTUCK, A. et al. Global pesticide use and trade database (GloPUT): New estimates show pesticide use trends in low-income countries substantially underestimated. **Global Environmental Change**, v. 81, p. 102693, jul. 2023.

VASSELLI, J. G.; SHAW, B. D. Fungal spore attachment to substrata. **Fungal Biology Reviews**, v. 41, p. 2–9, set. 2022.

WANG, C.; ST LEGER, R. J. The MAD1 Adhesin of *Metarhizium anisopliae* Links Adhesion with Blastospore Production and Virulence to Insects, and the MAD2 Adhesin Enables Attachment to Plants. **Eukaryotic Cell**, v. 6, n. 5, p. 808–816, maio 2007.

WANG, J. et al. Influencing Factors Analysis and Simulation Calibration of Restitution Coefficient of Rice Grain. **Applied Sciences**, v. 11, n. 13, p. 5884, 24 jun. 2021.

WEI, H. et al. Measurement and simulation validation of DEM parameters of pellet, sinter and coke particles. **Powder Technology**, v. 364, p. 593–603, mar. 2020.

WÖSTEN, H. A. B. Hydrophobins: Multipurpose Proteins. **Annual Review of Microbiology**, v. 55, n. 1, p. 625–646, out. 2001.

WU, Y. et al. Three-Dimensional physical similarity simulation experiments for a transparent shaft coal pocket wall in coal mines. **ACS omega**, v. 7, n. 19, p. 16442-16453, 2022.

XIE, C. et al. Investigation of the effect of filling level on the wear and vibration of a SAG mill by DEM. **Particuology**, v. 63, p. 24–34, abr. 2022.

XU, C. et al. Determination of Characteristics and Establishment of Discrete Element Model for Whole Rice Plant. **Agronomy**, v. 13, n. 8, p. 2098, 10 ago. 2023.

YARDENY, I.; PORTNIKOV, D.; KALMAN, H. Experimental investigation of the coefficient of restitution of particles colliding with surfaces in air and water. **Advanced Powder Technology**, v. 31, n. 9, p. 3747–3759, set. 2020.

YAZDANI, E.; HASHEMABADI, S. H. The influence of cohesiveness on particulate bed segregation and mixing in rotating drum using DEM. **Physica A: Statistical Mechanics and its Applications**, v. 525, p. 788–797, jul. 2019.

ZHENG, Q. J. et al. Interparticle forces and their effects in particulate systems. **Powder Technology**, v. 436, p. 119445, mar. 2024.

ZHOU, Y. C. et al. Rolling friction in the dynamic simulation of sandpile formation. **Physica A: Statistical Mechanics and its Applications**, v. 269, n. 2–4, p. 536–553, jul. 1999.

8. GENERAL CONCLUSIONS AND FUTURE WORK

8.1 GENERAL CONCLUSION

The research on the extraction and drying of *Metarhizium anisopliae* spores in rotary drum systems has brought significant advances in understanding and optimizing the process. The reduction in particle moisture during drying directly affects the movement and mixing dynamics, while, during extraction, it impacts their velocities, collision forces, and the efficiency in removing the spores. The use of a rotary drum configured for spore extraction proved to be efficient, with high purity and yield, standing out as a scalable solution for large-scale bioinsecticide production. Furthermore, the implementation of intermittent rotations in the drying of grains proved to be a promising strategy to optimize drying time and improve mixing homogeneity, positively impacting the economic viability of the process. These advances have the potential to contribute to the sustainability of agricultural production, enabling the efficient production of bioinsecticides from *Metarhizium anisopliae* and opening new possibilities for the design of extraction and drying systems.

8.2 FUTURE WORK

Although the results obtained are promising, there are several areas that can be explored in future work to further optimize the process:

- Considering the need to replace rice as a substrate, an important research line would be to evaluate different agro-industrial residues for spore production, investigating the impact of their physical and thermal properties on extraction and drying rates.
- Scaling up the process: Expanding the scale of spore drying and extraction in rotary drums, with the adaptation of processes for large volumes and optimization of operational parameters.
- Spore Viability and Virulence: Assess the impact of adopting spore extraction systems (sieves with a mechanical shaker and horizontal rotating drums) and drying with intermittent rotations on the virulence and viability of the extracted spores.
- Study of air flow in cyclones: Investigate the behavior of air flow with spores inside cyclones using computational fluid dynamics (CFD) simulation, to optimize the efficiency in spore separation and transport.

- Full integration in the rotary drum: Conduct all stages of M. anisopliae production inside a rotary drum, including inoculation, cultivation, drying, and extraction, in order to optimize the entire process in an integrated and efficient manner.

APPENDIX A - LIGGGHTS CODE ADOPTED IN DEM SIMULATIONS

```
###Header for General commands###

atom_style      granular
boundary        f f f
units           si
communicate     single vel yes
newton          off

###System variables###

#Definition of boundaries
variable xmin equal 0.3
variable xmax equal 0.3

variable ymin equal 0.6
variable ymax equal 0.6

variable zmin equal 0.6
variable zmax equal 0.6

#Definition of the timestep

variable dt equal 1e-4

###Specific variables for current simulation###
variable natoms equal 2        #1 -> particle #2->drum parts

####variable for material properties####

####Young Modulus####
variable        youngmodulus1       equal   1
variable        youngmodulus2       equal   1

####Poission ratio####
variable        poission1       equal   1
variable        poission2       equal   1

####variable for contact properties####

####coefficient of restitution####
variable        CoR11 equal   1
variable        CoR12 equal   1
variable        CoR21 equal   1
variable        CoR22 equal   1
```

```
####sliding friction coefficient####
variable	sf11	equal	1
variable	sf12	equal	1
variable	sf21	equal	1
variable	sf22	equal	1

####rolling friction coefficient####
variable	rf11	equal	1
variable	rf12	equal	1
variable	rf21	equal	1
variable	rf22	equal	1

####variable for particle####

#Number of particle radius
variable	nradii	equal	1
variable	radius1equal	1
variable	frac1	equal	1
variable	densityequal	1

####filling parameters####

variable	filltime equal	1
variable	fillmass equal	1
variable	fillmassrate equal	${fillmass}/${filltime}
variable	fillsteps	equal	${filltime}/${dt}
variable	rotatime	equal	1
variable	rotasteps	equal	${rotatime}/${dt}

####screw velocities####

variable	drumPeriod	equal	1

###Definition of simulationbox###

region	reg block ${xmin} ${xmax} ${ymin} ${ymax} ${zmin} ${zmax} units box
create_box	2 reg
neighbor	0.004 bin
neigh_modify delay 0

###Definition of the contact models###

pair_style gran model hertz tangential history rolling_friction epsd2
```

```
pair_coeff      * *
timestep ${dt}
fix             integrator all nve/sphere
fix             gravi all gravity 9.81 vector 0.0 0.0 -1.0

###Definition of Material properties###

fix             m1 all property/global youngsModulus peratomtype ${youngmodulus1}
${youngmodulus2}
fix             m2 all property/global poissonsRatio peratomtype ${poission1} ${poission2}
fix             m3 all property/global coefficientRestitution peratomtypepair ${natoms}
${CoR11} ${CoR12} ${CoR21} ${CoR22}
fix             m4 all property/global coefficientFriction peratomtypepair ${natoms} ${sf11}
${sf12} ${sf21} ${sf22}
fix             m5 all property/global coefficientRollingFriction peratomtypepair ${natoms}
${rf11} ${rf12} ${rf21} ${rf22}

###Generation and Loading of the Geometry.stl###

fix             Drum   all mesh/surface file Drum.stl type 2
fix             Front  all mesh/surface file Front.stl type 2
fix             Back   all mesh/surface file Back.stl type 2
fix             walls  all wall/gran model hertz tangential history rolling_friction epsd2 mesh
n_meshes 3 meshes Drum Front Back

###Generation and Insertion of the particles###

fix     pts1 all particletemplate/sphere 10487 atom_type 1 density constant ${density} radius
constant ${radius1}
fix     pdd1 all particledistribution/discrete 32452867 ${nradii} pts1 ${frac1}
fix     ins_mesh all mesh/surface/planar file Insertionsface.stl type 1 scale 1
fix     ins all insert/stream seed 86028157 distributiontemplate pdd1 mass ${fillmass}
massrate ${fillmassrate} overlapcheck yes all_in yes vel constant 0 0 -0.10 insertion_face
ins_mesh extrude_length 0.1

compute colForcePP all pair/gran/local
compute colForcePW all wall/gran/local

###Dumping of the data for post-processing to visualize###

shell   mkdir post

###Definition of the dumptime###
```

```
variable dumptime equal 1     # Every 0.05 s 1 image
variable dumpstep equal ${dumptime}/${dt}          #Transform to iteration steps

dump   dmpvtk all custom/vtk ${dumpstep} post/particles_*.vtk id type x y z vx vy vz fx fy fz radius mass
dump   dmpDrum  all mesh/stl ${dumpstep} post/Drum*.stl Drum
dump   dmpFront all mesh/stl ${dumpstep} post/Front*.stl Front
dump   dmpBack         all mesh/stl ${dumpstep} post/Back*.stl  Back
dump    colInfoForcePP all local/gran/vtk ${dumpstep} colForcePP/ForcePP*.vtk colForcePP
dump          colInfoForcePW   all   local/gran/vtk   ${dumpstep}   colForcePW/ForcePW*.vtk colForcePW

####Run the simulation filling and rotation###

run       ${fillsteps}
unfix ins
run       ${fillsteps}
fix       MoveDrum    all  move/mesh  mesh  Drum   rotate  origin  0  0  0  axis  1.  0.  0.  period ${drumPeriod}
fix       MoveFront    all  move/mesh  mesh  Front  rotate  origin  0  0  0  axis  1.  0.  0.  period ${drumPeriod}
fix       MoveBack    all  move/mesh  mesh  Back   rotate  origin  0  0  0  axis  1.  0.  0.  period ${drumPeriod}
run       ${rotasteps}
```

APPENDIX B - ADDITIONAL ANALYSIS

B.1 X-RAY IMAGES

The particle beds of cooked rice, rice fermented at different moisture contents, and fermented rice after 4 and 8 hours of extraction were investigated using µ-CT (XCT-1600 HR System from Nordson Matrix Technologies GmbH, Feldkirchen, Germany), as shown in Figure B.1 with the parameters provided in Table B.1. A cylindrical holder made of PEEK with an internal diameter of 20 mm and height of 120 mm was adopted to accommodate the particles. The image resolution was defined by varying the distance between the sample holder and the X-ray source. The analyses were conducted in triplicate for the same set of particles. The radiography results obtained were then reconstructed into a stack of grayscale images using the Volex software developed by the Fraunhofer Institute for Integrated Circuits, IIS, Erlangen, Germany.

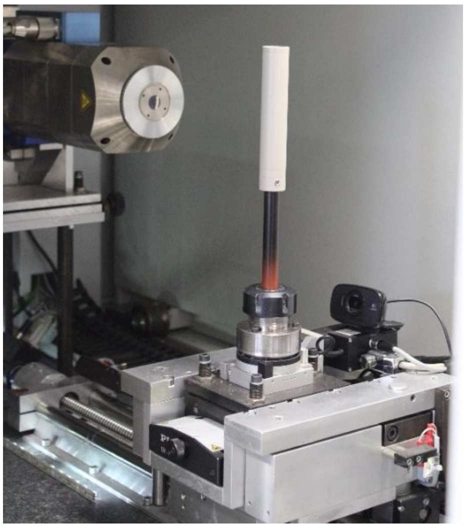

Figure B.1. µ-CT equipment.

Table B.1. X-ray tomography imaging parameters for samples.

Parameters	**Unit**	**Value**
Acceleration voltage	(kV)	40
Current	(µA)	120
Exposure time	(ms)	1000
Projections	(-)	1200
Voxel size	(µm)	18.7
Distance	(mm)	500

The processing of raw grayscale images of the compacted beds was performed using the ImageJ/Fiji software, developed by the National Institute of Health, Maryland, USA, and the Laboratory for Optical and Computational Instrumentation, Wisconsin, USA (Schindelin et al., 2012). Initially, the stack of raw grayscale images was cropped to the respective region of interest by removing the cylindrical container. The reconstructed volumes had a size of 350 × 350 × 350 voxels. Multiple radiographs were taken for each projection during each scan. The average of the radiographs was used to reconstruct a 3D volumetric image. The image analysis was conducted to determine the porosity and tortuosity of the bed. For this, the images were binarized after applying a median filter. The porosity and tortuosity were determined using MATLAB's image tools through the SEM Image Porosity and Pore Size and TauFactor applications, respectively.

Table B.2 summarizes the porosity and tortuosity values of the X-ray analyzed beds, while the reconstructed 3D images are shown in Figure B.2. It is observed that the porosity of the bed decreases in the presence of the fungus, as it fills some of the empty spaces. The porosity also reduces for drier particles or those that underwent the extraction process, as drying decreases the dimensions of the particles, and extraction can fragment them, facilitating a better fit in the container. Larger and more uniform particles tend to stack in a way that creates larger empty spaces between them, resulting in relatively high porosity. On the other hand, the tortuosity increases in beds containing fungus. According to Cunha et al. (2019), beds formed only by rice have a porosity of 0.464.

Table B.2. Porosity and tortuosity of beds made of different granular materials.

Material	**MC (kg-w/kg-ds)**	**ε**	**SD**	**λ**	**SD**
Cooked rice	0.667	0.679	0.032	1.685	0.092
Conidiated rice	0.667	0.532	0.009	2.175	0.078
	0.250	0.492	0.038	2.560	0.085
Conidiated rice after 4 hours of extraction	0.111	0.406	0.001	1.485	0.021
Conidiated rice after 4 hours of extraction	0.053	0.378	0.038	1.735	0.120

MC - moisture content; ε – porosity; λ – tortuosity; SD – standard deviation.

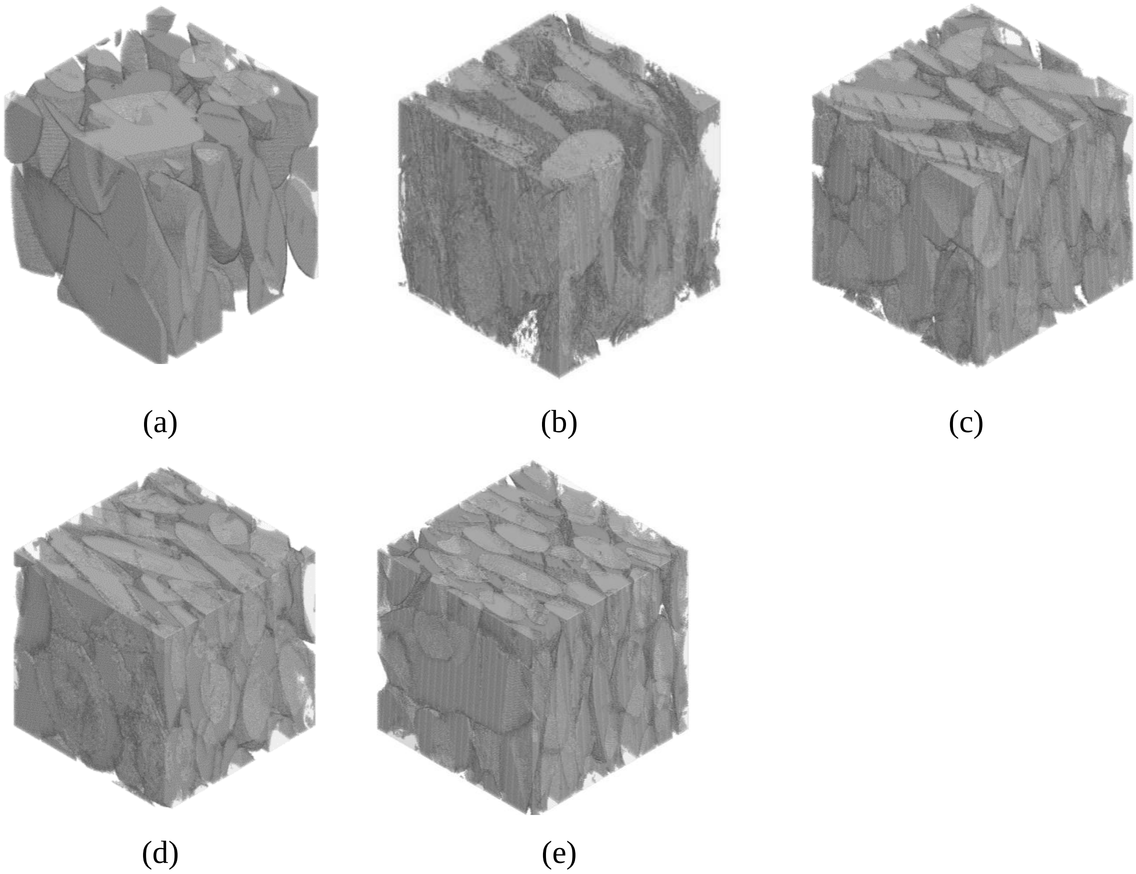

Figure B.2. X-ray images of (a) cooked rice, 0.667 kg-w/kg-ds; (b) conidiated rice, 0.667 kg-w/kg-ds; (c) conidiated rice, 0.250 kg-w/kg-ds; (d) conidiated rice after 4 hours of extraction, 0.111 kg-w/kg-ds; and (e) conidiated rice after 8 hours of extraction, 0.053 kg-w/kg-ds.

B.2. CENTESIMAL ANALYSIS OF EXTRACTED SPORES AND RESIDUAL RICE

The centesimal analysis of the material extracted in vibrating sieves and the residual rice was conducted using the official methodologies of the Adolfo Lutz Institute (2008), except for the analysis of carbohydrates and moisture. Moisture was determined by gravimetric difference using an infrared lamp scale MB45. Ash content was determined by the gravimetric method in a muffle furnace, heating 0.5 g of sample at 550°C for approximately seven hours until the ash turned completely white. This method is used to quantify the fixed mineral residue that remains after the complete combustion of organic matter. The Kjeldahl method was employed for protein determination. This is one of the most traditional and reliable methods for total nitrogen analysis, with the obtained value being multiplied by a specific conversion factor to estimate the protein content in the sample. Lipid content was analyzed by the Soxhlet method, which involves the continuous extraction of lipids from the sample using an appropriate solvent. This method is widely used to quantify lipids in biological and food samples, ensuring accuracy in measurements. Carbohydrate content was considered as total starch, with quantification performed using the Total Starch Assay Kit (AA / AMG) (Megazyme International Ltd., Bray, Ireland). This kit is a specific and effective tool for accurately and reliably quantifying starch, particularly useful in samples like rice grains. All analyses were conducted in triplicate. The centesimal composition of the extracted material, as well as the residue retained on the first sieve, is presented in Table B.3.

Table B.3. Centesimal analysis of residual rice and extracted material.

	Residual rice	**Extracted material**
Moisture content	18.38 ± 3.62%	13.35 ± 2.06%
Ash	1.03 ± 0.01%	3.38 ± 0.15%
Lipids	0.74 ± 0.07%	0.04 ± 0.03%
Proteins	10.25 ± 0.65%	63.99 ± 3.73%
Starch	61.73 ± 1.26%	2.63 ± 0.78%

The analysis of the moisture data presented in Table B.3 reveals important information about the behavior of the residue and the extracted material. Rice grains have an ash content ranging from 0.5 to 1% (Lopes; Lopes, 2008). According to Table B.3, the ash content found in the residual rice was 1.03%, which is consistent with the expected ash content for rice. The ash content of the extracted material is three times higher than that of the residue, indicating that the extracted material is composed of a significant amount of minerals, as ash is an inorganic residue resulting from the combustion process or the burning of organic matter in a sample, representing the total amount of minerals present in that sample (Figueiredo, 2007). Furthermore, the ash content found in the extracted sample helps us understand that rice residues may be detached during the extraction process and considered in the collected mass. However, no conclusions can be drawn about the quantity of rice particles contained in this agglomerated material, nor how much of this ash corresponds to these rice particles.

It is observed that the residual rice had a lipid content of 0.74%, which is consistent with the fact that rice has a very low lipid content, usually less than 1% (Lopes; Lopes, 2008). In contrast, the extracted material sample showed almost negligible lipid content. It is worth mentioning that spores are fungal particles, whose lipid quantity and composition are determined by the genetic makeup of each species and are strongly influenced by the composition of the medium (Sancholle; Lösel, 1995). Thus, it can be concluded that the low lipid content of the substrate used for cultivation, along with the specific characteristics of the

M. anisopliae fungus, led to the production of a biomass (mycelium + fungus) that is poor in lipids.

Regarding the protein content quantified in the extracted material, it is noted that this is the largest component. Thus, it is possible to conclude that the material is primarily composed of biomass (conidia + mycelium), which are mainly made up of proteins. It is known that at least 70 different proteins are synthesized in the mother cell and arranged around the spore, forming the spore's coat (Mckennhey et al., 2010). Therefore, the high protein content is associated with the protective structures of these organisms. Finally, knowing that the average protein content of white rice is 7.5% (Kennedy; Burlingame, 2003), the residue was found to have a protein content of 10.25%. This value is higher than that of raw rice, which can be attributed to the small fraction of conidia that remain attached to the rice particles.

Rice is a carbohydrate-rich food, mainly composed of starch. In polished white rice, the starch content is around 80% (Lopes; Lopes, 2008). When analyzing the residual rice, the value is lower. Since part of this starch is consumed during cultivation, the value found in this analysis is lower than that of raw rice. A value similar to the one found here is reported by Cunha (2020) after incubation, observing a starch content of around 67.5%. However, it should be noted that the analysis conducted by this author referred to rice that underwent a liquid extraction, which removes all conidia from the sample, reducing the protein content and consequently increasing the other components like ash, starch, and others.

On the other hand, the extracted material showed a starch content of 2.63%. This data confirms that there is a small fraction of fine rice particles that detach along with the spores during the operation. Thus, this extraction method enables the production of a virtually pure product for commercialization. Therefore, when examining the centesimal composition of the residue, it is noted that 7.87% of its composition was not characterized, likely representing the fiber fraction that was not analyzed. This may also apply to the extracted material, where 16.61% of its composition was not characterized. However, fiber analysis is required to confirm these hypotheses. The uncharacterized percentage may also include some sugars contained in these samples, as the analysis performed here only quantifies starch synthesized by α-amylase, not the entire carbohydrate content.

B.3 REFERENCES

CUNHA, L. P. et al. Production of conidia of the entomopathogenic fungus Metarhizium anisopliae ICB 425 in a tray bioreactor. **Bioprocess and biosystems engineering**, v. 42, p. 1757-1768, 2019.

FIGUEIREDO. Determinação de cinzas e conteúdo animal – cinzas. 2007. 30p. Available in:<http://www.pfigueiredo.org/BromII_5.pdf>. Accessed in: 10 of august of 2024.

INSTITUTO ADOLFO LUTZ. Procedimentos e determinações gerais. Métodos físicoquímicos para análise de alimentos. 1. ed. digital. São Paulo: Instituto Adolfo Lutz, 2008.

KENNEDY, G.; BURLINGAME, B. Analysis of food composition data on rice from a plant genetic resources perspective. **Food Chemistry**, v. 80, n. 4, p. 589-596, 2003.

LOPES, A. de M.; LOPES, M.F de L. Aspectos qualitativos e nutricionais do arroz. 2008.

MCKENNEY, P. T.; DRIKS, A.; EICHENBERGER, P.. The Bacillus subtilis endospore: assembly and functions of the multilayered coat. **Nature Reviews Microbiology**, v. 11, n. 1, p. 33-44, 2013.

SANCHOLLE, M.; LÖSEL, D. Lipids in fungal biotechnology. In: **Genetics and Biotechnology**. Berlin, Heidelberg: Springer Berlin Heidelberg, 1995. p. 339-367.